



Coexistence and Spectrum Sensing of
IEEE 802.11 Systems for Cognitive
Radio Applications

Jan-Willem van Bloem

Coexistence and Spectrum Sensing of IEEE 802.11 Systems for Cognitive Radio Applications

Jan-Willem van Bloem

Graduation committee:

chairman and secretary:

Prof.dr.ir. A.J. Mouthaan University of Twente

promotor:

Prof.dr.ir. C.H. Slump University of Twente

assistant promotor:

Dr.ir. R. Schiphorst University of Twente

referee:

Dr.ir. M. Nekovee British Telecom

members:

Prof.dr.ir. P.J.M. Havinga University of Twente

Prof.dr.ir. S.M. Heemstra de Groot Eindhoven University of Technology

Prof.dr.ir. B. Nauta University of Twente

Prof.dr.ir. G.J.M. Smit University of Twente

This research is financially supported by Agentschap Telecom, University of Twente, British Telecom and funding support from the European Union COST-TERRA projects COST-STSM-IC0905-9942 and COST-STSM-IC0905-9121.

CTIT

CTIT Ph.D. Thesis Series No. 13-250
Centre for Telematics and Information Technology
P.O. Box 217, 7500 AE
Enschede, The Netherlands.

Signals & Systems group,
EEMCS Faculty, University of Twente,
P.O. Box 217, 7500 AE Enschede, The Netherlands

Print: Wöhrmann Print Service
Typesetting: L^AT_EX₂
Cover design by Maarten van Bloem

© J.W.H. van Bloem, Enschede, 2013

No part of this publication may be reproduced by print, photocopy or any other means without the permission of the copyright owner.

ISBN 978-90-365-3516-8
ISSN 1381-3617 (CTIT Ph.D.-thesis series No.13-250)
DOI 10.3990/1.9789036535168

COEXISTENCE AND SPECTRUM SENSING OF
IEEE 802.11 SYSTEMS FOR COGNITIVE
RADIO APPLICATIONS

DISSERTATION

to obtain
the degree of doctor at the University of Twente,
on the authority of the rector magnificus,
prof.dr. H. Brinksma,
on account of the decision of the graduation committee,
to be publicly defended
on Thursday the 16th of May 2013 at 14:45h

by

Johan Willem Hermanus van Bloem
Born on the 29th of December 1982
in Almelo, The Netherlands

This dissertation has been approved by:

Promotor: Prof.dr.ir. C.H. Slump

Assistant promotor: Dr.ir. R. Schiphorst

To my parents

Samenvatting

Het merendeel van de hedendaagse draadloze communicatie voor korte afstand is gebaseerd op de IEEE 802.11 standaard, ook bekend als Wi-Fi, en is ontwikkeld voor data uitwisseling waarbij een zekere bandbreedte aan radio spectrum gebruikt wordt. Echter, veel van de huidige nieuwe technologieën, zoals Wi-Fi, zijn alleen toegestaan in vergunningsvrije radio banden aangezien spectrum schaars beschikbaar is en daarom efficiënt gebruikt moeten worden. Tegenwoordig opereert een overgrote meerderheid van de Wi-Fi systemen in de vergunningsvrije 2.4 GHz ISM band die echter steeds meer overbelast raakt door het toenemende gebruik van Wi-Fi. Daarnaast is er ook een groeiend aantal apparaten actief in deze band die niet op Wi-Fi technologie gestoeld zijn. In deze thesis wordt de co-existentie van Wi-Fi systemen behandeld voor het reduceren van congestie en interferentie in deze banden. De nadruk ligt hierbij op spectrum waarneming en detectie technieken, bedoeld voor cognitieve radio toepassingen, om de co-existentie te verbeteren van Wi-Fi systemen in de ISM band. De verbeteringen in co-existentie zitten enerzijds in de detectie van interferentie bronnen en congestie mechanismen voor een efficiënter spectrum gebruik. Anderzijds zitten de verbeteringen op het vlak van spectrum monitoring zodat het daadwerkelijke spectrum gebruik nauwkeuriger kan worden vastgesteld en waarbij de invloed van de meetapparatuur op de waarnemingen geminimaliseerd is.

Als eerste worden spectrum waarnemingstechnieken beschouwd voor het monitoren van draadloze technologieën met een kort bereik. We laten de meerwaarde zien van het gebruik van mobiel inzetbare spectrum waarnemingsapparatuur en resultaten worden gepresenteerd. In aanvulling hierop wordt de invloed van de automatische versterkingsregeling - een belangrijke element in spectrum waarnemingsapparatuur - onderzocht om de prestaties van het spectrum waarnemen te kunnen verbeteren. Hiertoe zijn technieken ontwikkeld en toegepast om de invloed van automatische versterkingsregeling te verwijderen uit de waargenomen spectrum data. Resultaten laten zien dat de verstoring door de automatische versterkingsregeling kan leiden tot een overschatting van het daadwerkelijke spectrum gebruik met 60% in de 2.4 GHz ISM band.

Ten tweede is de invloed van interferentie op Wi-Fi systemen onderzocht. Dit houdt in enerzijds interferentie als gevolg van externe niet op Wi-Fi gebaseerde apparaten en anderzijds interferentie veroorzaakt door overlappende Wi-Fi netwerken opererend op hetzelfde radio communicatie kanaal. Om de invloed van interferentie te kunnen vaststellen is speciale meetapparatuur ontwikkeld om op simultane wijze de veroorzaakte congestie als wel de veranderingen in spectrum gebruik te kunnen waarnemen. De meetresultaten laten zien dat het draadloze

medium inefficiënt wordt gebruikt als gevolg van een grote hoeveelheid transmissie overhead. In situaties met extreem veel congestie kan dit mogelijk leiden tot slechts 21% aan data t.a.v. het totaal mogelijke transmissie verkeer.

Ten derde is het gebruik van Wi-Fi systemen in de niet vergunningsvrije UHF/VHF banden onderzocht als alternatief om de ISM band te ontlasten en vanwege de significante hoeveelheid extra beschikbare bandbreedte. In deze banden opereren de Wi-Fi systemen naast de gebruikers met de primaire rechten voor deze banden (o.a. TV-stations) onder voorwaarde dat het secundaire gebruik van Wi-Fi systemen geen interferentie veroorzaakt ten opzichte van de primaire gebruikers. De Wi-Fi standaard voor deze band, 802.11af, maakt hiertoe gebruik van cognitieve radio om de beschikbare spectrum op een bepaalde locatie te detecteren voor secundaire exploitatie van de UHF/VHF banden. Om de co-existentie tussen 802.11af systemen en primaire gebruikers voor elke type omgeving te kunnen waarborgen is het van belang dat de cognitieve detectie ook functioneert in een gebied met veel terrein obstructies (o.a. hoge gebouwen, heuvels) hetgeen de ontvangst van het primaire signaal mogelijk kan verhinderen. Om de detectie van primaire signalen te verbeteren is een methode gepresenteerd waarbij een netwerk van samenwerkende cognitieve radio's gecombineerd wordt met toegang tot een centrale database. De detectie resultaten van deze hybride methode zijn vergeleken met een methode met alleen database toegang. Daarnaast is de hybride methode geoptimaliseerd, gebruikmakend van verrichtte metingen, om de detectie prestaties te maximaliseren.

Abstract

Most of today's short range wireless communication is based on the IEEE 802.11 standard, also referred to as Wi-Fi, which has been developed to exchange data using a certain portion of radio spectrum. However, many of today's new technologies, such as Wi-Fi, have been allocated to unlicensed spectrum bands while spectrum is scarcely available and therefore needs to be used efficiently. Nowadays, a vast majority of the Wi-Fi systems operates in the license-exempt 2.4 GHz ISM band that becomes more and more crowded due to the growing usage of Wi-Fi. On top of that, a growing number of non Wi-Fi technologies become active in this band as well. In this thesis the coexistence of Wi-Fi systems with other technologies is addressed to deal with congestion and interference issues. The focus is on spectrum sensing and detection techniques, that can be used by cognitive radio applications, to enhance the coexistence of Wi-Fi systems in the ISM band. The improvement in coexistence can be achieved through the detection of both interference sources and congestion mechanisms which in turn can assist in a more efficient usage of the radio spectrum. In addition, improvements can be made on the monitoring side to assess the spectrum usage better and thus more precisely by minimizing the influences of the measurement equipment on the observation data.

First, we investigate spectrum sensing for monitoring short-range wireless technologies. We show the value of using mobile spectrum monitoring equipment and results are presented concordantly. Additionally the impact of Automatic Gain Control (AGC), an essential building block in spectrum monitoring receivers, is investigated in order to enhance spectrum sensing performance. By doing so, techniques are developed and applied to remove the AGC influences from the monitoring spectrum data. The results show that interference due to the AGC could lead to an overestimation of the actual spectrum usage by 60% in the 2.4 GHz ISM band.

Secondly, the influence of interference on Wi-Fi systems has been investigated. This entails respectively interference due to non Wi-Fi technologies and co-channel interference due to overlapping Wi-Fi systems. A measurement tool has been developed to assess spectrum utilization and to measure the congestion simultaneously. The obtained results show the inefficient use of the wireless medium due to a large amount of transmission overhead which may lead to only 21% of actual data content transmitted in highly congested areas.

Thirdly, the alternative use of Wi-Fi communication in the licensed UHF/VHF bands has been investigated to alleviate the congestion and interference issues in the ISM band and to access the large amount of additional available bandwidth. The operation of Wi-Fi systems in these bands is considered to be allowed under

the condition of secondary use, i.e. avoiding interference to users with the primary rights (e.g. TV-broadcasting stations). Recently the IEEE 802.11af standard has been set up, based on cognitive radio, to provide Wi-Fi access by the detection of available spectrum in the UHF/VHF bands at a particular location for secondary exploitation. Paramount in order to guarantee the co-existence between licensed primary users and 802.11af systems is that cognitive detection operates properly in each type of geographical area, i.e., also for locations shadowed by large terrain obstacles (e.g. buildings, hills). To achieve this a novel collaborative sensing scheme with geolocation access to a central white-space database is presented and a comparison is made with the approach providing access to a central database only. Supported by measurements an optimization of the presented scheme is carried out in order to enhance primary detection performance in shadow fading environments.

Contents

Samenvatting	i
Abstract	iii
Contents	v
1 Introduction	1
1.1 Increasing 802.11 Demand	1
1.1.1 The 802.11 Standard and Coexistence Issues	3
1.2 Cognitive Radio: Enhancing 802.11 Coexistence	5
1.2.1 Coexistence Standards and Cognitive Radio for IEEE 802	7
1.3 Thesis Overview and Research Questions	9
2 Mobile Spectrum Monitoring to Assess Spectrum Occupancy	13
2.1 Introduction	13
2.2 Spectrum Usage Analysis	14
2.3 Results	15
2.4 Conclusion	20
3 Removing Non-Stationary Noise in Spectrum Sensing Using Matrix Factorization	23
3.1 Introduction	23
3.2 Background	24
3.3 Related Work	26
3.3.1 Research Objectives	27
3.4 Mobile Monitoring Equipment	28
3.4.1 Mobile Monitoring System	28
3.4.2 AGC Calibration	29
3.5 System Model	31
3.5.1 Notation	31
3.5.2 Singular Value Decomposition	32
3.5.3 Non Negative Matrix Factorization	33
3.6 Results	34
3.6.1 Validation of the Results	40
3.7 Conclusion	41

4	Spectrum Utilization and Congestion of IEEE 802.11 networks in the 2.4 GHz ISM Band	43
4.1	Introduction	43
4.2	Related Work on Monitoring QoS	44
4.2.1	QoS: Overlapping WLANs	45
4.2.2	Contributions	45
4.3	IEEE 802.11 Coexistence Mechanisms	46
4.3.1	Legacy IEEE 802.11	46
4.3.2	IEEE 802.11e	47
4.4	Interference Mechanisms	49
4.4.1	Setup	49
4.4.2	Experiments	51
4.4.3	Results	51
4.5	Live Measurements	56
4.5.1	Setup	56
4.5.2	Experiments	56
4.5.3	Results	57
4.6	Conclusions	60
4.6.1	Future Research	61
5	IEEE 802.11: Impact of Different Types of Interference Sources	63
5.1	Introduction	63
5.2	Monitoring Quality of Service	64
5.2.1	Performance Evaluation of 802.11 with Interference	64
5.2.2	Contributions	65
5.3	The 802.11 Interference Results in Controlled Environments	65
5.3.1	Measurement Setup	65
5.3.2	Results	67
5.4	The 802.11 Interference Results in Urban Environments	70
5.4.1	Measurement Results	71
5.4.2	Extrapolation of Results	75
5.5	Conclusion	78
6	Collaborative Sensing to Enhance TV White-Space Database Performance in Shadow Fading Environments	81
6.1	Introduction	81
6.2	Related Work	83
6.2.1	Geolocation Database	83
6.2.2	Cooperative Sensing	83
6.3	Theory: Performance and Analysis	84
6.3.1	Log-normal Shadowing	85
6.3.2	Collaborative Sensing	86
6.4	Model	87
6.4.1	Generic Model	87
6.5	Model Validation	89
6.5.1	Use Case: Sudbury TV-Station	89
6.5.2	Simulation	89
6.5.3	Field Measurements	93

6.6	Results	95
6.6.1	Model Validation: Performance	95
6.6.2	Extension of the Simulation Model	97
6.7	Conclusion and Future Work	98
7	Outlook	101
7.1	Recommendations	104
	Bibliography	107
	List of Publications	119
	Acronyms	121
	Acknowledgments	125
	Curriculum Vitae	125

Chapter 1

Introduction

1.1 Increasing 802.11 Demand

Over the years the growth of Wi-Fi has rapidly increased and is expected to continue at a very strong pace. Nowadays, Wi-Fi is a well-known concept and a very popular technology that allows an electronic device to exchange data. The term Wi-Fi is used in general as a synonym for “WLAN” (Wireless Local Area Network). However, Wi-Fi is actually a trademark owned by the Wi-Fi Alliance [1], a nonprofit international association, that has been set up to promote WLAN technology and to certify WLAN products. Further, the term Wi-Fi is used as the brand name for their WLAN products that are based on 802.11 standards as provided and defined by the Institute of Electrical and Electronics Engineers (IEEE).

The use of Wi-Fi is further encouraged by the rapid increase in popularity of wireless public hotspots that provide shared Wi-Fi access to multiple end-user devices in non-residential areas. As a result the number of public hotspots has expanded from the initial creation of small independent networks, which often covered only a single restaurant or hotel, to larger, service provider-owned networks designed to provide wireless access in highly crowded public locations. For example, among the first open Wi-Fi access providers is BT (British Telecom) rolling out a large-scale open Wi-Fi network in the UK in 2007 [2, 3] based on urban residential Wi-Fi where BT broadband customers share a portion of their bandwidth. Recently BT has announced that its hotspots numbers have hit a new high with 7.5 million across the world [4]; this is claimed as the currently biggest Wi-Fi network worldwide as according the BT press release in [5].

For the years to come the number of Wi-Fi hotspots in non-residential settings is expected to continue following this spectacular upward trajectory while consumers are more and more demanding ubiquitous network access since they are accustomed to use Wi-Fi when on the go. This trend has been investigated by comScore [6] showing that more than 37 percent of mobile phone traffic and more than 90 percent of tablet traffic is already transported over Wi-Fi in the USA [7, 8]. In line with this, according to Informa Telecoms & Media predictions [9] around 5.8 million public hotspots worldwide are expected in 2015 (shown in Figure 1.1(a)). Also a very strong growth in the number of private residential hotspots is predicted (see Figure 1.1(b)) that hits the 600 million hotspots in 2015. This explosive growth is driven by several

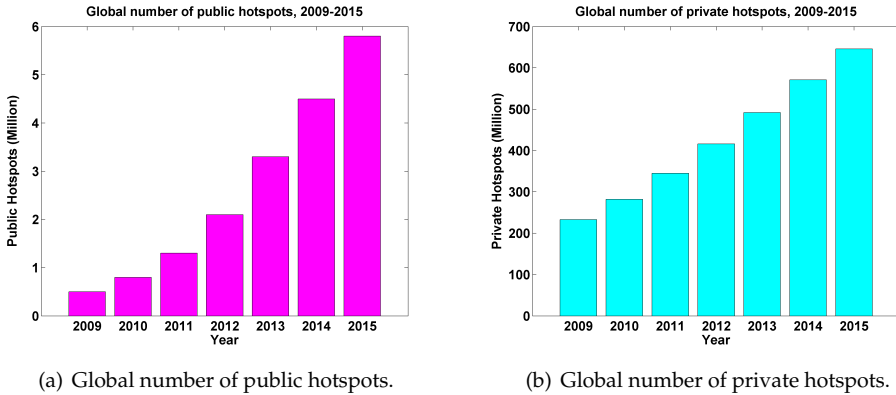


Figure 1.1: The number of global Wi-Fi hotspots in the period 2009-2015. Source: Informa Telecoms & Media.

factors [9, 10]: 1) ubiquity of Wi-Fi chipsets in mobile devices such as smartphones, laptops and tablets; 2) end-user demand for Wi-Fi connectivity over 3G and 4G for mobile devices; 3) widening support by service providers of Wi-Fi hotspots as a way to offload traffic from congested cellular networks and to enhance the end-user experience. The expansion of Wi-Fi into hundreds of millions of hotspots world-wide has established Wi-Fi as the most heavily-used wireless global technology in terms of the volume of data transmitted. Also the data usage over Wi-Fi connections accounts for an increasing portion of the total network access [11], from 41% in 2011 to 51% in 2016 (see Figure 1.2) as Wi-Fi integrated circuit (IC) sales and Wi-Fi product certification volumes continue to increase [7]. The latter is because of the decreasing manufacturing costs of integrating Wi-Fi chipsets which made it a must-have feature in every smartphone and tablet that comes to market.

Thus according to the above-stated trend Wi-Fi is today's preferred technology for domestic areas. However, for mobile data traffic in non-residential areas the use of 4G networks is considered more ideal due to its large area coverage and availability. This is particularly true for the emerging new LTE (Long Term Evolution) radio platform technology, universally marketed as 4G wireless service, which allows cellular network operators to provide increased capacity and speed over wireless data networks. Furthermore, for non-residential areas the LTE standard offers better mobility service, handover capability and QoS (Quality of Service) compared with Wi-Fi. This is because of the centrally managed architecture of LTE networks, whereas Wi-Fi relies on a network organized in a distributed fashion. However, the LTE performance varies depending on the network and the area (i.e. the number of end-users). This is especially the case in crowded areas where the surge of mobile data is likely to cause cellular traffic congestion. Note that the growth in mobile cellular data demand is rising and increases at an even higher pace than the Wi-Fi growth (see Figure 1.2).

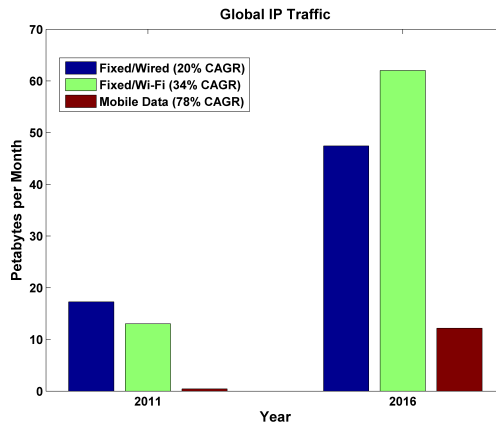


Figure 1.2: The increase in data traffic usage for different services in petabytes per month. Here CAGR represents the Combined Annual Growth Rate. Source: Cisco Visual Networking Index (VNI), www.cisco.com.

1.1.1 The 802.11 Standard and Coexistence Issues

A large part of 802.11's success can be contributed to its inherent compatibility with current 802 networks, in particular with the 802.3 wired Ethernet networks. The original 802.11 base-standard was adopted in 1997 and is different in many aspects from the standard that exists today. The base-version has undergone subsequent amendments that have led to new protocol standards, which are corrections and or extensions to the basic protocol, but are still part of the 802.11 family. For instance, popular standards are those defined by the 802.11a/b/g protocols providing amendments that mainly differ in the type of radio modulation. These standards were followed up by the 802.11n protocol, nowadays used on a wide-basis, which incorporates MIMO (Multiple Input, Multiple Output) antennas to achieve higher throughputs. Furthermore, the vast majority of 802.11 technologies is active in one of the following unlicensed radio spectrum bands:

2.4 GHz ISM band Refers to the Industrial, Scientific and Medical band; covers the radio frequency range of 2400 MHz - 2500 MHz. Typically a channel bandwidth of 20 MHz is used with a total of 13 channels (14 in Japan); this has been defined for the 802.11 b/g modes. In practice it turns out that Wi-Fi systems mainly use the non-overlapping channels 1, 6, and 11. This is often due to the manufacturer default channel settings. In addition, two adjacent 20 MHz channels are allowed to be merged for operation in double channel mode which is defined for 802.11n systems.

5 GHz U-NII band(s) Refers to the Unlicensed National Information Infrastructure band(s) and covers different frequency ranges in the radio spectrum from 5.15 GHz to 5.85 GHz. The operating frequencies vary from country to country and depend on the country-specific regulations. Mainly 802.11a technology is active in the U-NII band employing the 20 MHz non-overlapping channels. In addition, also 802.11n systems are allowed in this band using either the 20 MHz

or 40 MHz channel operation mode.

These frequency bands provide the total sum of available spectrum for 802.11 systems for over 30 years. However, due to the explosion in number of 802.11 systems coming to the market there has been an increase in utilization of Wi-Fi especially in the 2.4 GHz ISM band. Studies have pointed out that the ISM band has become very crowded [12] not only because of the increased number of Wi-Fi devices but also due to the high number of non-Wi-Fi devices active in this band such as: microwave ovens, cordless phones, Zigbee, Bluetooth, wireless sensor networks, Audio/Video (A/V) transmitters, baby monitors, garage door openers, etc. The crowded environment in the 2.4 GHz ISM band gave rise to many coexistence issues between 802.11 systems and other technologies. Hence, coexistence issues need to be addressed to avoid congestion and interference problems that in turn can cause performance degradation such as 1) reduction of wireless transmission speed, 2) connection problems, 3) reduction in coverage range.

On the other hand, one consideration would be to opt for the 5 GHz U-NII bands which is less crowded and faster due to the higher operating radio frequency. However, there are some drawbacks regarding the 5 GHz U-NII bands usage. First, the higher the radio frequency of a wireless signal the shorter its range, i.e. 2.4 GHz networks are able to cover a substantially larger range than 5 GHz wireless networks. Second, 5 GHz signals have difficulties penetrating solid objects such as walls and floors when compared to 2.4 GHz signals. This can limit the coverage area of a 5 GHz hotspot inside buildings like homes and offices where many walls may be situated between hotspot antenna and the client. Third, the 5 GHz equipment is not compatible with already installed 2.4 GHz equipment; this may give problems when upgrading a current large wireless network installation. Fourth, the 2.4 GHz products such as access points, antennas and network cards are more easily available and are less expensive compared to the 5 GHz products.

Most of the 802.11 systems are active and will be active in the 2.4 GHz ISM band because of the above-described drawbacks on the use of 802.11 systems in the alternative 5 GHz band. For this reason most of the challenges lie ahead in establishing proper coexistence between systems in the unlicensed 2.4 GHz ISM band. Furthermore, it turns out that most of these coexistence problems relate to interference issues between systems [12] in an one-to-one fashion; typical sources of interference are listed below:

- Interference between Wi-Fi clients of the same network.
- Interference between Wi-Fi networks on respectively the same radio channel (co-channel interference) or partly overlapping channels (adjacent channel interference)
- Bonded channel interference, due to incompatibility between the IEEE 802.11 b/g and IEEE 802.11n respectively
- Interference with IEEE 802 systems other than 802.11 systems, e.g. Bluetooth, Zigbee, etc.
- Interference with non IEEE 802.11 systems such as A/V systems, microwave ovens, cordless phones, etc.

Hence, it is paramount to address interference issues in order to improve 802.11 QoS and to enhance coexistence with other systems in license-exempt bands. One promising approach to tackle the above-mentioned issues is Cognitive Radio (CR) which is addressed in the following-up section.

1.2 Cognitive Radio: Enhancing 802.11 Coexistence

Over the years, with the development of digital radio technologies, the concept of "cognitive radio" came into play introduced by J. Mitola in 1998 (published in an article in 1999 [13]) for a form of radio that would change its performance by detecting its environment and changing accordingly with the purpose to enhance spectrum resource allocation and coexistence between radio systems. Furthermore, cognitive radio [14] has been defined by Mitola as: *"The point in which wireless personal digital assistants (PDAs) and the related networks are sufficiently computationally intelligent about radio resources and related computer-to-computer communications to detect user communications needs as a function of use context, and to provide radio resources and wireless services most appropriate to those needs."* Regulatory bodies recognized the inefficient use of the radio spectrum in which the utilization depends on both time and place. For this reason regulatory bodies, including the Federal Communications Commission (FCC) in the USA and Ofcom in the UK, have adopted the concept of cognitive radio and Dynamic Spectrum Access (DSA) to better use the spectrum [15, 16, 17]. In what follows, we use the definition used by FCC [18]: *"Cognitive radio: A radio or system that senses its operational electromagnetic environment and can dynamically and autonomously adjust its radio operating parameters to modify system operation, such as maximize throughput, mitigate interference, facilitate interoperability, access secondary markets"*. Note that in general two main types of cognitive radio exist [15]. One is Full Cognitive Radio (also known as Mitola radio [19]), in which every possible parameter observable by a wireless node (or network) is considered. The other is Spectrum-Sensing Cognitive Radio wherein only the radio-frequency spectrum is considered. Note that most of today's research and development focuses on the latter type of cognitive radio. Moreover, cognitive radio can be divided into two categories based on the type of spectrum being used:

Licensed-bands Radio spectrum has been assigned to licensed users having the primary rights to use these bands:

1. Bands already in use: Digital TV broadcasting bands (between 54 and 862 MHz) i.e. UHF (Ultra High Frequency) in the UK and the VHF (Very High Frequency) band in the USA. Also the 3.6 GHz band has opened up but in the USA only; the same holds for the 4.9 GHz band which is however also available in a few other countries.
2. Candidate bands: Radar bands (2700-3100 MHz, 5250-5850 MHz); aeronautical band for Distance Measuring Equipment (DME) in the frequency range of 960-1215 MHz; the 2360-2400 GHz band (aeronautical mobile telemetry, land mobile & services ancillary to program making / services ancillary to broadcasting, amateur radio services)

Unlicensed-bands These bands can be accessed on a license-exempt basis: e.g. the ISM bands and U-NII bands.

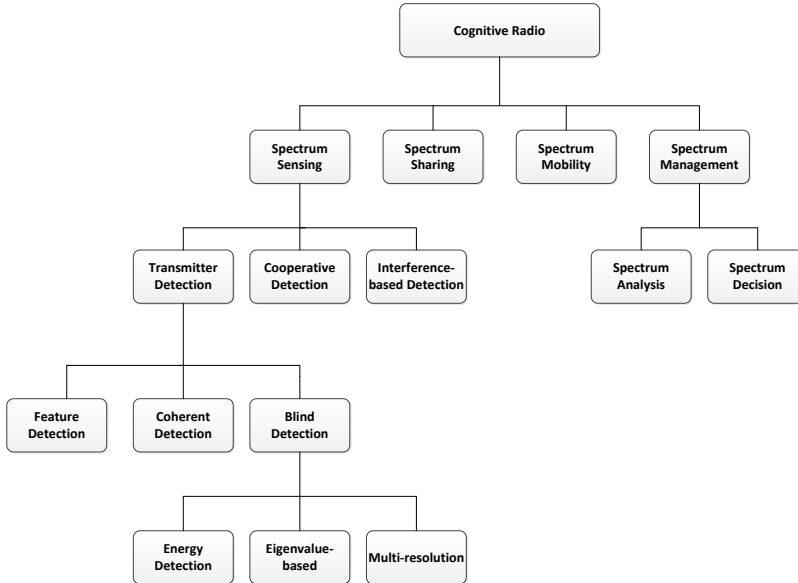


Figure 1.3: Classification of cognitive radio functions.

Among the main functions of cognitive radio is *spectrum sensing* (see Figure 1.3) which is defined while the spectrum needs to be sensed in order to avoid interference with incumbent systems and to determine the available portions of the spectrum [15, 16]. Based on the obtained sensing information the best available spectrum is captured so that the user QoS requirements can be fulfilled; this entails respectively the processes of *spectrum analysis* and *spectrum decision* (i.e. spectrum management functions). Furthermore, cognitive radio functions exist to assure coexistence with other users. This means on one hand *spectrum sharing* in order to coordinate access to this channel with other users, i.e. providing fair scheduling policies. On the other hand, cognitive radio needs to be flexible to give priority to licensed users, i.e. vacate the channel when a licensed user is detected (*spectrum mobility*). Note that in this work the focus is on respectively *spectrum sensing* and *spectrum management*. Doing so, first the *spectrum sensing* function is split up based on the type of detection used for sensing:

- Transmitter detection, i.e. whether the signal from a primary transmitter is locally present in a certain spectrum or not.
- Cooperative detection, i.e. a network of sensing devices been set up to enhance primary transmitter detection.
- Interference-based detection, i.e. measuring and identifying the interference sources.

Secondly, the *spectrum management* function is highlighted which can also be divided into respectively *spectrum analysis* and *spectrum decision*. The former is

defined as assessing the quality of the selected spectrum band by the channel characteristics, i.e. parameters such as the spectrum usage (time/place), interference level, channel estimation (e.g. SNR). Furthermore, the latter comprises the selection of the most appropriate operating spectrum channel for transmission; this is based on different decision rules using the channel characteristics from the *spectrum analysis* as input.

1.2.1 Coexistence Standards and Cognitive Radio for IEEE 802

The cognitive radio concept can be thought of as an evolution of IEEE 802 coexistence mechanisms which has been considered from the developing stage as early as 1999 [13, 20]. In particular for the unlicensed spectrum bands wherein a variety of unrelated protocols can be found, e.g. 802.11, 802.15 and 802.16. An overview of the evolution process towards cognitive radio can be found in Table 1.1. Further, the first generation of coexistence mechanisms were designed so that the unrelated protocols would coexist better [20]; for this purpose cognitive techniques such as Dynamic Frequency Selection (DFS) and Power Control (PC) were developed and standardized. These initial coexistence mechanisms were included in respectively 802.16a, 802.15.2 and 802.11h [20]. Doing so, the 802.16 amendment has specified DFS for WiMAX systems in license exempt bands whereas, in a similar way, IEEE 802.15.4 has included the Dynamic Channel Selection (DCS) mechanism which in turn can be viewed of as the DFS equivalent. Moreover, DFS features have also been developed for 802.11 systems to allow for military radar detection and the re-allocation of potential interfering 802.11 APs to other frequencies. The latter has been covered by the 802.11h standard which can be regarded as an early-stage unintentional (simple) cognitive radio standard [20, 21, 22]. Additionally, 802.11h has been integrated into the IEEE 802.11-2007 standard and provides DFS and PC capabilities to 802.11a systems for radar and satellite detection. This is to comply with the FCC rules requiring the secondary use of Wi-Fi systems in portions of the 5 GHz spectrum when additional channels were added to the available range in 2007.

Besides power control and frequency control algorithms also more general coexistence guidelines have been specified for 802 systems. One such standard is 802.15.2 that has been developed because of coexistence issues between Bluetooth and 802.11 systems and includes two classes of coexistence mechanism: 1) collaborative techniques e.g. Time Division Multiple Access (TDMA) and 2) non-collaborative techniques such as Adaptive Frequency Hopping (AFH). Based on the successes of 802.15.2 the technical working group 802.19 within IEEE has been set up to act as a coexistence advisory committee across all of IEEE 802. Additionally, the 802.11y standard has been defined which specifies a flexible spectrum management framework (e.g. by leveraging coexistence mechanisms from 802.11h) for operation with high power Wi-Fi equipment in the 3.65 GHz band. However, the 802.11y standard is not limited to the 3.65 GHz band only but has been designed to operate in any spectrum; promising candidates are the TV-bands for reuse of the spectrum. In the evolution towards cognitive radio the 802.11k and 802.11e extensions to the 802.11 standard have been of relevance mainly in the area of fair resource sharing [22]. Here 802.11k enables radio networks to collect information about other APs, about link quality of neighboring stations, measuring interference levels, and the traffic load of the air-medium. Further, the 802.11e

Table 1.1: The evolution of radio protocol standards towards full cognitive radio with dynamic spectrum access; the standards are listed for licensed and unlicensed bands separately.

	Unlicensed bands	Licensed bands
Cognitive Radio	IEEE P1900 802.16h-2010	802.11af ECMA 392 IEEE P1900 802.22
Fair Resource Sharing	802.11k-2008 802.11e-2005	
Coexistence	802.15.2-2003	802.19 802.11y-2008
DFS + PC	802.16a-2003 802.11h-2003 802.15.4-2003	

standard incorporates QoS support, e.g. by adjusting the amount of traffic load in highly-congested environments.

The above-discussed IEEE 802 standards already include cognitive radio capabilities or related building blocks and most of these evolved from coexistence activities. This has led to the two primary cognitive radio standards of today [16, 21, 23]: 802.22 and IEEE P1900 (developed by the IEEE DYSPAN standards committee and formerly known as IEEE SCC41). These cognitive radio standards are focused on protection of the licensed (primary) users and on dynamic channel access policies for the opportunistic use of licensed spectrum and less on coexistence between different protocol/technologies in the same band. The IEEE 802.22 standard is under development since 2004 and aims to use cognitive radio techniques to allow sharing of geographically unused spectrum allocated to television broadcasters [24]; this in order to bring broadband Internet access to rural low population density areas. Additionally, the network architecture of 802.22 including the protocol implementation has been derived from IEEE 802.16 WiMAX and a coverage range of around 100km can be reached concordantly. However, the development of the 802.22 standard slowed down the last years [24] and there is no final completion of the standard yet. Another cognitive radio standard for the TV bands is the emerging 802.11af technology [21, 25], also informally known as super-Wi-Fi or White-Fi, which would be the first Wi-Fi (802.11) standard active in these bands for white-space access. The superlatives used to describe 802.11af are mainly due to respectively the lower operating frequency that can be used in the TV bands

compared to the ISM bands which means that a higher coverage can be established [26], and the possible larger portion of bandwidth available in the TV bands. The 802.11af standard is under development and the first stable draft version has been released recently in September 2012. The high speed of 802.11af standardization is attributed, to a large extent, to the reuse of existing 802.11 infrastructure. In addition, 802.11af provides promising commercialization perspectives and low equipment costs as compared to other CR standards in TV bands e.g. 802.22. Note that the main difference with 802.22 lies in the medium access mechanisms [27], i.e., 802.11af uses a listen-before-talk protocol adopted from 802.11 whereas 802.22 employs Time Division Multiplex (TDM)-based access, that means, without any back-off procedures for channel access taking into account.

In contrast to the 802.22 and the 802.11af standards the IEEE P1900 protocols concentrate on the higher protocol abstraction levels which includes the development of architectural concepts and specifications for network management between incompatible wireless networks [20, 23], e.g. dynamic spectrum access policies for 3G/4G and Wi-Fi systems.

1.3 Thesis Overview and Research Questions

In this thesis several research topics are addressed related to cognitive radio and coexistence issues regarding 802.11 systems. In particular, each chapter covers one of these topics and in turn relates to specific publication(s). Furthermore, the research questions addressed in this thesis are listed below where each question relates to a specific chapter. Below, each chapter is briefly summarized followed up by its associated research question:

Chapter 2 deals with mobile spectrum monitoring to assess the spectrum utilization of short-range technologies in urban areas; this is needed while the fixed monitoring network is not sufficient, i.e. would require a very high density of fixed monitoring sites to achieve the above-described objective. Further, mobile monitoring entails space-time measurements in a particular frequency range but also database-infrastructure issues to efficiently query the vast amount of collected measurement data for a specific geographical area, frequency band, and time-period. Results are presented among which a comparison of spectrum utilization between rural and urban areas in specific licensed frequency bands.

Question *How do the radio spectrum observation results obtained from the mobile monitoring network compare for different type of areas, i.e., rural versus urban?*

Chapter 3 concentrates on spectrum monitoring equipment issues to enhance spectrum occupancy accuracy in case of blind spectrum sensing receivers. In particular, the focus is on the Automatic Gain Control (AGC) building block, present in lots of spectrum analyzers, that may distort spectrum monitoring to a large extent by adjusting signal levels and by lifting the noise floor; this in order to maintain a reasonable constant signal level for Analogue-to-Digital (A/D) conversion because of the limited dynamic range of the ADC. To remove the AGC effects from the monitoring data so-called matrix factorization

techniques are presented in combination with calibrations measurements and results are provided concordantly. For this purpose the spectrum analyzer, deployed for mobile monitoring in Chapter 2, has been used; the frequency band of interest has been the 2.4 GHz ISM band for which the proposed techniques were applied.

Question *What is the impact of the AGC on the performance of mobile spectrum monitoring and how can it be removed best?*

Chapter 4 deals with spectrum utilization and congestion issues of 802.11 systems in the 2.4 GHz ISM band. The impact of overlapping 802.11 networks (co-channel interference) has been investigated supplemented with live measurements in different types of environments, i.e., office room, city-center, and college-room. The QoS monitoring of 802.11 systems took place at the two lowest layers of the OSI protocol in parallel. For this purpose a specific packet sniffing software tool has been developed which is used in combination with spectrum analyzing equipment. This has been set up to assess and analyze the occurring interference mechanisms derived from the monitoring data.

Question *How is the QoS degradation due to overlapping Wi-Fi networks and what are the occurring mechanisms?*

Chapter 5 focuses on the impact of different sources of interference on 802.11 communication and the associated mechanisms. Here sources of interference refer to non-802.11 systems also active in the 2.4 GHz ISM band, i.e. among others, microwave ovens, audio/video senders and Bluetooth systems. The interference influence from these sources upon 802.11 has been investigated in a controlled environment by monitoring the two lowest layers of the OSI stack. In addition, the impact of interference in urban outdoor environments has been measured and analyzed. A model is presented to extend the results to a country/city-wide Wi-Fi coverage model incorporating the impact of interference on its coverage range. The work has been commissioned by BT to model Wi-Fi coverage in urban areas to investigate the economic feasibility of providing large-scale open Wi-Fi access in the UK.

Question *What are the mechanisms that indicate and/or cause performance degradation of 802.11 systems in the 2.4 GHz ISM band for different interference sources i.e. microwave ovens, A/V transmitters, and Bluetooth devices?*

Chapter 6 concerns the secondary use of 802.11af systems in the TV bands by means of dynamic spectrum access, herein addressing coexistence issues with licensed users (digital TV broadcasting) specifically in shadow fading environments (i.e. hidden node problem). A hybrid approach is presented based on cooperative sensing combined with geolocation access to a white-space database to enhance primary detection by 802.11af devices and herewith reducing the risk of interference upon licensed users. For this purpose a performance analysis of different algorithms has been carried out fusing the sensory data from the CR devices. Further, the detection performance of the hybrid scheme has been compared with the pure geolocation

database to show the possible gain. In addition, measurements were carried out to model the channel environment and to validate shadow fading simulations.

Question *What is the gain in detection performance of using white-space database-assisted collaborative CR-based sensing when compared with a method that uses geolocation access to a white-space database only?*

Finally, Chapter 7 contains the outlook of thesis wherein the summary of the answers to the above-posed research questions is provided and recommendations are provided concordantly. Further, the contents of each chapter (except the outlook) relates to the above-mentioned papers wherein the results were disclosed. Below, tag symbols have been assigned to these particular papers in order to relate them to the corresponding chapters. Doing so, journal papers are preceded by the **A** tag, conference papers by **B**, and book chapters by **C**:

- A-1** J. W. H. van Bloem, R. Schiphorst, T. Kluwer, C. H. Slump. "Spectrum Utilization and Congestion of IEEE 802.11 Networks in the 2.4 GHz ISM Band," in *Journal of Green Engineering Special Issue on Cognitive Radio*, vol. 2, no. 4, July 2012.
- A-2** J. W. H. van Bloem, R. Schiphorst, C. H. Slump. "Removing Non-Stationary Noise in Spectrum Sensing Using Matrix Factorization," in *EURASIP Journal on Advances in Signal Processing*, vol. 2013, April 2013.
- A-3** J. W. H. van Bloem, S. Kawade, R. Schiphorst. "Collaborative Sensing to Enhance TV White-Space Database Performance in Shadow Fading Environments," *submitted*.
- B-1** J. W. H. van Bloem, R. Schiphorst, T. Kluwer, C. H. Slump. "Interference Measurements in IEEE 802.11 Communication Links Due to different Types of Interference Sources," in *Proceedings of the 8th International Conference on Wireless Communications, Networking, and Mobile Computing (WiCOM'12)*, vol. 2, Sept. 2012.
- B-2** J. W. H. van Bloem, A. J. Hendrikse, R. Schiphorst, and C. H. Slump. "An eigenvalue approach to enhance energy detection in a mobile spectrum monitoring network," in *5th IEEE International Conference on Signal Processing and Communication Systems*, pp. 346–351, Dec. 2011.
- B-3** J. W. H. van Bloem, R. Schiphorst, and C. H. Slump. "Initial results of a new mobile spectrum occupancy monitoring network," in *17th IEEE Symposium on Communications and Vehicular Technology in the Benelux*, pp. 64–69, Nov. 2010.
- B-4** S. Kawade, J. W. H. van Bloem, V. S. Abhayawardhana, D. Wisely. "Sharing your Urban Residential WiFi (UR-WiFi)," in *63rd IEEE Vehicular Technology Conference, 2006. VTC 2006-Spring*, pp. 162–166, May 2006.
- C-1** J. W. H. van Bloem, S. Kawade. "Database-Assisted Collaborative Sensing," in *Quasar Deliverable 2.5*, chapter 3, July 2012.

Further, in Table 1.2 the relation between chapter and papers is visualized. In addition, the addressed topics per chapter are provided.

Table 1.2: The relation between subjects and thesis chapters, supplemented by the relation between papers and thesis chapters.

Subjects					
	Chapter 2	Chapter 3	Chapter 4	Chapter 5	Chapter 6
Coexistence			•	•	•
Energy Detection	•	•	•	•	•
ISM Band		•	•	•	
TVWS Band					•
Interference detection			•	•	•
Spectrum Occupancy	•	•	•	•	•
DSA					•
Cognitive Network					•
802.11g/n		•	•	•	
802.15.4				•	
802.11e			•		
802.11af					•
Monitoring Equipment	•	•	•	•	•
Publications					
A-1			•		
A-2		•			
A-3					•
B-1				•	
B-2		•			
B-3	•				
B-4				•	
C-1					•

Chapter 2

Mobile Spectrum Monitoring to Assess Spectrum Occupancy

2.1 Introduction

Traditional tasks of the spectrum regulator include minimizing interference and locating (illegal) interferers, such as FM radio pirate transmissions [28]. In many countries a fixed network infrastructure of monitoring sites is used to monitor the spectrum. In the Netherlands, the fixed network consists of 12 monitoring sites that measure the received power from 100 kHz to 1.3 GHz in a 25 kHz raster. However, modern communications require smaller service area per base station and also higher frequencies up to 6 GHz. The traditional methods for spectrum monitoring cannot meet these requirements and are therefore not fully qualified anymore. Hence, new tasks for the spectrum regulator arise to determine the spectrum usage in higher frequency bands. More about present-day spectrum governance can be found in [29, 30, 31, 32] where economical aspect are treated in [33, 34, 35].

To meet these new tasks, we propose a new method to efficiently monitor the spectrum usage using a mobile monitoring network. This network consists of vehicles, equipped with the RFeye system of CRFS [36] which is able to measure the frequency spectrum up to 6 GHz. The RFeye measurement equipment is designed to provide a cost-effective system that can provide continuous, 24/7 monitoring of the radio spectrum. The measurement data is stored and can be used for offline spectrum analysis.

The advantages of using mobile spectrum monitoring compared to the traditional approach are:

- The spectral usage in a particular geographical area and frequency band can be assessed. The areas of interest can be investigated in more depth by assigning monitoring vehicles to these areas.
- The (spatial) resolution of the monitoring network increases.
- The regulator can, according to the requirements, dynamically change the size of the geographical area for spectrum monitoring.

- In general the standard deviation of radio signals in place is much higher than in time. Using a fixed network would require a very high density of fixed monitoring sites. This suggests the use of mobile spectrum monitoring.

2.2 Spectrum Usage Analysis

Many days of spectrum measurements induce a huge amount of collected data. In this section we describe how to access and use the huge amount of collected data from the monitoring vehicles (see Figure 2.1).

To start with, the data is measured and collected in the following way. The RFeye system measurement equipment, mounted on a vehicle, yields the measurement data while driving through rural and urban areas in the Netherlands. The spectrum between 10 and 500 MHz is sampled using a step size of 19.5312 kHz, while a reduced sample rate is used for the spectrum between 500 - 2000 MHz and 2000 - 6000 MHz using respectively step-sizes of 78.125 kHz and 156.25 kHz. The measurements take place at a 2 second time interval and yield the frequency response data for the specified spectrum range. These values were chosen by the Dutch radio communication agency who performed the measurements.

As a next step, the CRFS measurement data is loaded to a local computer for further offline processing. Subsequently, the data is transferred from the local system to an external server so that a huge amount of data of many measurement days can be stored. At the server system a MySQL database is maintained in order to analyze

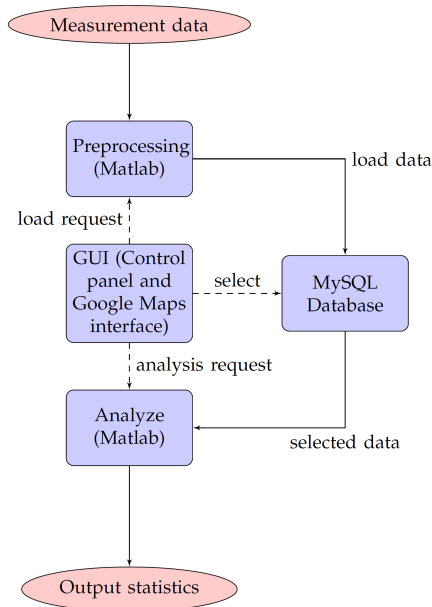
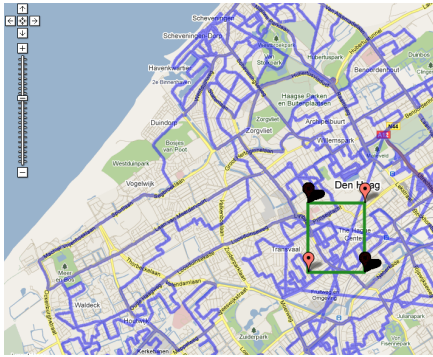


Figure 2.1: The process of loading, accessing and analyzing data from a MySQL database using Matlab. Dashed lines represent request commands.



(a) The selection tool: the area inside the green rectangle is selected. In this case an urban area.



(b) The measurement points in the selected area.

Figure 2.2: The selection tool using Google Maps, in order to select the area of interest graphically.

and access the data efficiently.

In Matlab, on a local machine, we access the MySQL database using a Graphical User Interface (GUI) tailored and built to meet the spectrum regulator's essential needs. Using this GUI, the geographical area and frequency band of interest can be selected. By using the Google maps API, the area selection takes place graphically which is shown in Figure 2.2. This provides us the spectrum traces for a selected geographical area, where each trace corresponds to a particular measurement time instant. Furthermore for each trace, the location information is retrieved and available by using GPS. Note that the data stored in the database is accessed through a MySQL interface in Matlab. This enables us to efficiently access and select data from the database using MySQL commands in a Matlab environment. The selected data in the database is downloaded to the local machine and is loaded to the Matlab workspace for further processing. For the measured data in the specified frequency band and geographical area, the accompanying histogram is computed leading to the Probability Density Function (PDF). In a similar way, the Cumulative Density Function (CDF) can be derived which is often more appropriate in spectrum usage analysis.

2.3 Results

In this section the results are shown for the GSM900 and GSM1800 downlink bands. To start with, the frequency sub-bands in the GSM900 are investigated. Table 2.1 lists for Dutch operators (KPN, Orange, Telfort, Vodafone)¹ in the GSM900 band the associated frequency sub-bands. The spectrum is analyzed per operator and per

¹The list with mobile network operators is based on the situation in the year 2006. At that time five operators were active in the GSM bands. Note, T-Mobile was at that time only active in the GSM1800 band. The situation is different now, due to the acquisition of respectively Orange by T-Mobile and Telfort by KPN. Hence, nowadays three mobile network operators are left in the Netherlands. This means that operator 1 and 2 are owned by the same operator. For that reason it is likely that the measured received power of these networks is less compared to the networks of operator 3 and 4.

Table 2.1: The sub-bands allocated to the various Dutch mobile telephone operators in the GSM900 band. Note that the operators, mentioned in this chapter, are labeled in this table in a different order.

	Operator 1	Operator 2	Operator 3	Operator 4
band 1 (MHz)	925.1 - 925.9	925.9 - 927.3	935.1 - 939.1	939.1 - 948.1
band 2 (MHz)	927.3 - 931.5	931.5 - 935.1	948.1 - 956.5	956.5 - 958.9

frequency sub-band. The outcome is shown in Figure 2.3.

Based on the results in Figure 2.3 it turns out that, for a specific operator, the spectrum occupancy differs significantly between distinct sub-bands. However, we merge the sub-bands per operator for respectively GSM900 and GSM1800. This in order to analyze the overall performance per operator. Besides, the spectrum occupancy for respectively the whole GSM900 and GSM1800 band is analyzed for two different geographical areas. The results are shown in Figure 2.4. The overall performance for GSM900 and GSM1800 shows the following outcome: the spectrum occupancy is significantly higher in urban areas compared to rural areas for each operator. Moreover, the cumulative density functions reveal higher activity, and thus higher transmit power, in the GSM900 band compared to the GSM1800 band. This corresponds with the results mentioned in the Singapore spectrum survey [37]. In addition, the performance of the operators are compared using the criteria stated in Table 2.2. Based on these field strength values, it follows that operator 3 provides the highest spectrum occupancy on average in the GSM bands.

To visualize the occupation results, Figure 2.5 shows the spectrum usage in the frequency band 948.1-956.5 MHz for many traces, respectively for a rural and urban geographic area. Note that the operator, assigned to the frequency band of interest, is

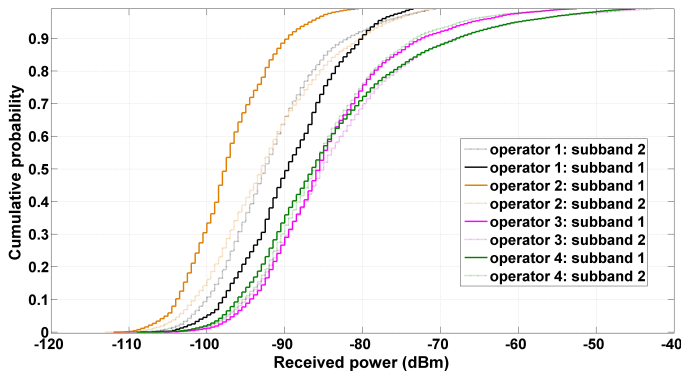


Figure 2.3: The cumulative probability density functions per sub-band in the GSM900 band for each operator active in the Netherlands, in a geographical rural area. The received power is expressed in dBm per frequency bin

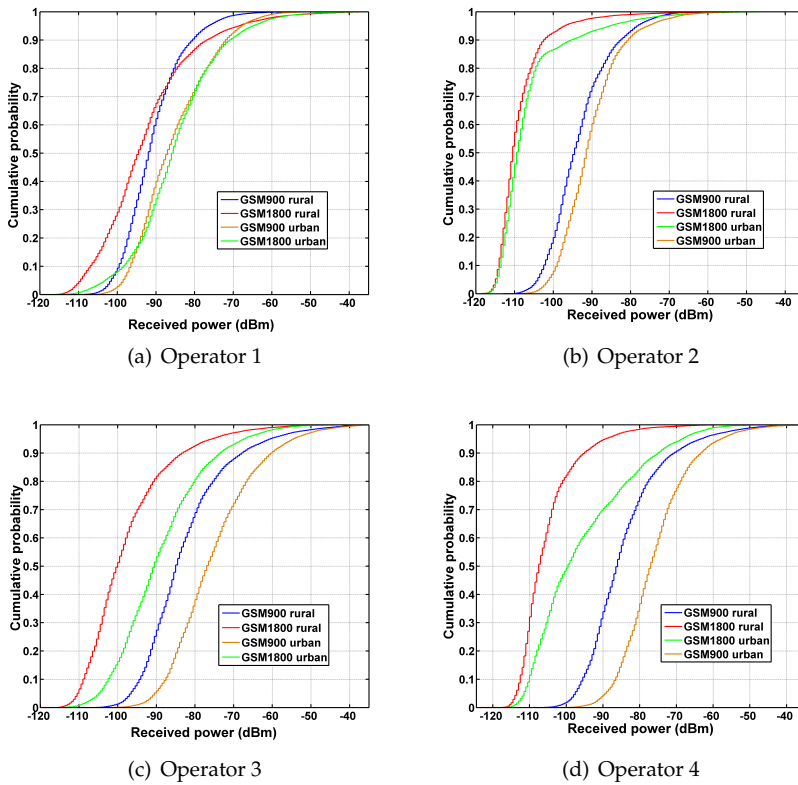


Figure 2.4: The cumulative density functions per operator in a rural and an urban area for respectively GSM900 and GSM1800, where the received power is expressed in dBm per frequency bin).

operator 3. The selected frequency band consists of several GSM downlink channels, each having an allocated bandwidth of 200 kHz, where a higher spectrum occupancy indicates a more congested network. As expected, the activity in this band, according

Table 2.2: As a quantitative performance measure, for each operator the field strength value is derived which separates the lower 10 percent of the frequency spectrum from the higher 90 percent for either the GSM900 and the GSM1800 band.

Operator	GSM1800 rural (dBm)	GSM1800 urban (dBm)	GSM900 rural (dBm)	GSM900 urban (dBm)
1	-107.0	-98.5	-99.5	-96.5
2	-114.0	-113.5	-102.5	-99.0
3	-109.0	-102.5	-94.0	-87.5
4	-112.0	-110.0	-95.5	-86.5

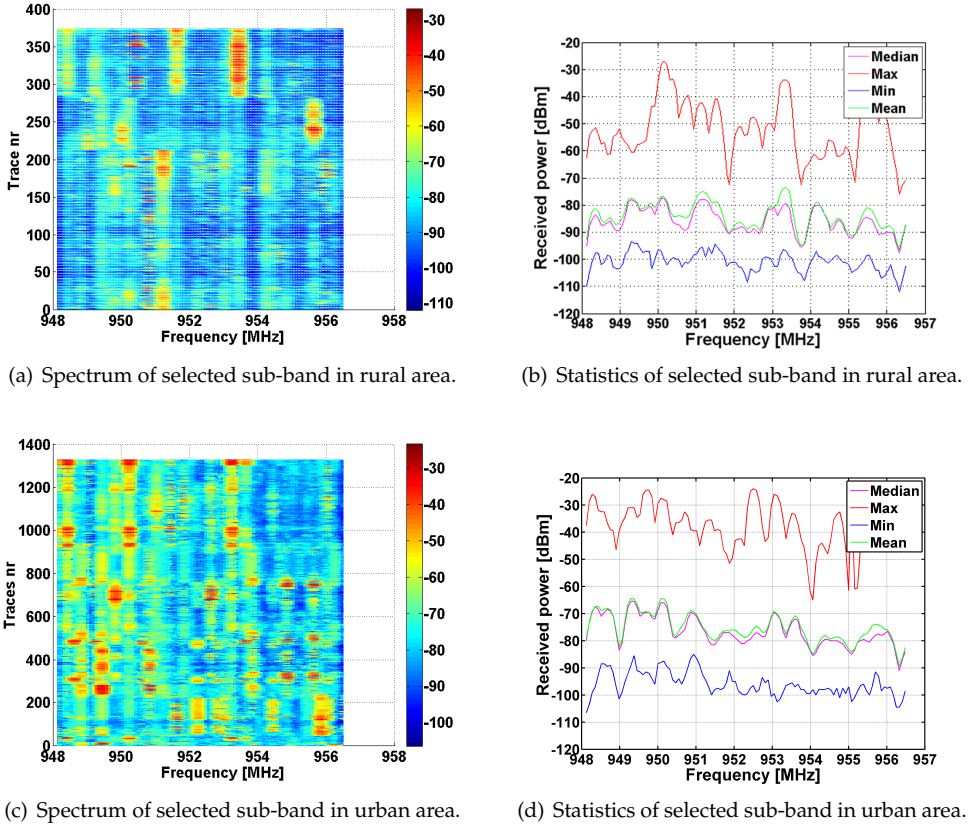


Figure 2.5: Frequency spectrum and statistics of operator 3 in the selected GSM900 sub-band, where the received power is expressed in dBm per frequency bin.

to GSM communication, is larger in the urban area. The data analysis yields respectively the mean, median, maximum and minimum field strength over time as a function of frequency. The results, associated with the selected geographical area, are depicted in respectively Figure 2.5(b) and Figure 2.5(d).

The statistics were based on measurements taken on many locations in a particular geographical area, which is different from what is reported in other papers regarding spectrum occupancy surveys. There the spectrum usage is measured at a fixed point [37, 38, 39, 40, 41, 42]. As a comparison, we aim to compute the deviation of the in-band spatial field strength variation in both GSM bands relative to the results of the fixed measurement set-up (e.g the Singapore occupancy survey [37]). For this purpose we compare the received power variation per band in different geographical areas for an arbitrarily chosen operator (in this case operator 4). The corresponding results are shown in Figure 2.6. Here the power variation on logarithmic scale, i.e. V_{dBm} , is computed based on the actual received in-band power for a particular trace. The latter is modeled as a random variable X , from which it follows that:

$$V_{\text{dBm}} = 10 \log X - 10 \log P \quad (2.1)$$

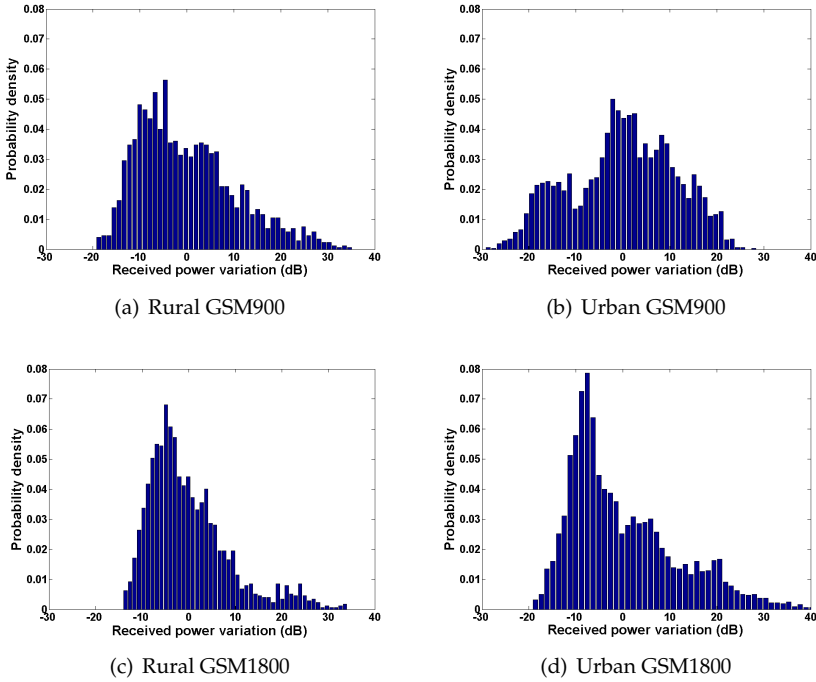


Figure 2.6: The received power variation of the selected operator 4.

where P stands for the derived mean power over time. The power variation results are shown in Figure 2.6. Based on these results it turns out that the in-band power in urban areas has a larger variation than in rural areas. Furthermore, the power variation for GSM900 surpasses GSM1800. We explain this as due to the higher GSM900 transmit power. Another thing that emerges from the power variation plots in Figure 2.6 is the shape of the distribution function. In the urban setting of GSM900, which happens to possess the highest signal to noise ratio (SNR), the probability density function exposes two peaks. One peak represents the in-band noise power whereas the second peak arises due to the received signal power. These two peaks are also present in the GSM900 distribution function for the rural area, however, the second peak is less strong compared to the peak in the urban environment's plot. Similarly for GSM1800, two peaks are displayed in the urban probability density function plot. This plot differs from the GSM900 case since the first peak, i.e. the received noise power, exceeds the second signal power peak. Moreover, due to the lower transmit power of GSM1800, the signal peak is hardly visible in the power variation plot of the rural measurement data. To analyze the distribution on a linear scale, the following conversion takes place:

$$V_{\text{linear}} = 10^{\frac{10 \log X - 10 \log P}{10}} = \frac{X}{P} \quad (2.2)$$

The results, plotted in Figure 2.7, show a relation between the SNR and the variation of the distribution function. As an example, the probability density function for

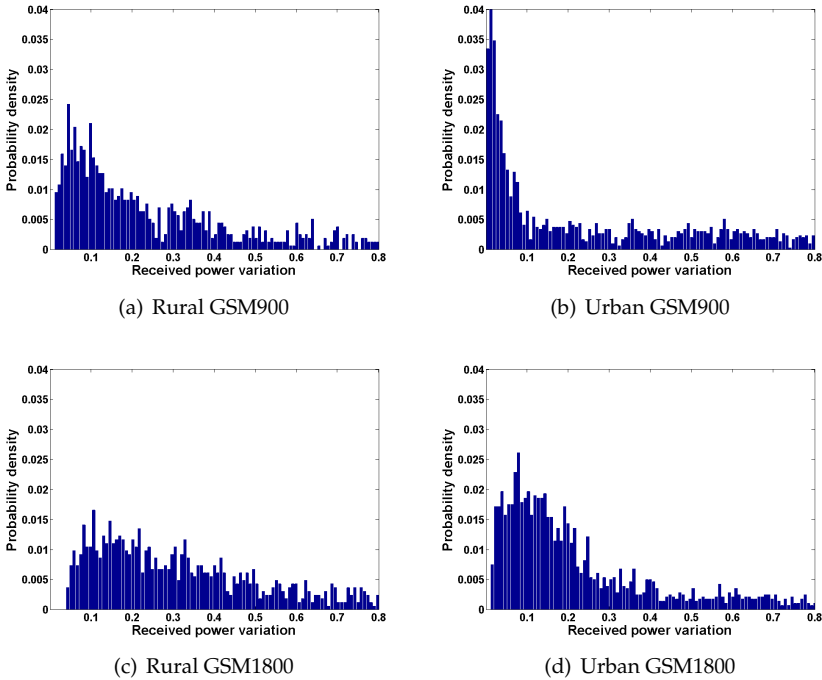


Figure 2.7: The received power variation of the selected operator 4 on a linear scale.

the rural GSM1800 situation is more widely spread on this interval compared to urban GSM900. Note that the histogram of these points tends to have a log-normal distribution. We consider it interesting to investigate this in more detail using a curve fitting approach.

2.4 Conclusion

In this chapter we present a new monitoring network for spectrum governance based on the RFeye system of CRFS [36]. A tool is built to effectively store and access the measured data on an external server system in order to determine the usage in a particular frequency band and geographic area. In addition, a method is described to analyze the data, and sample results are presented. The data analysis shows that sub-band usage varies per operator, where at the same time spectrum occupancy is significantly larger in urban areas compared to rural areas. In our set-up spatial field strength measurements are considered which we compared with the time varying field strength performed in the referred Singapore survey. There average occupancies for the GSM900 and GSM1800 frequency band are assumed. However, our measurements did show that the spectrum occupancy varies significantly in different geographical areas, which shows the importance of including spatial power variations. The distribution of the in-band spatial power variation tends to be a log-normal. It would be interesting for future research to investigate this in more

depth using curve-fitting methods in order to see which distribution, and scale parameters, fits best.

As expected, it appears from our measurements that the spectrum is more heavily used in urban areas compared to rural areas. Hence problems arise regarding the economical viability of opportunistic radio, i.e., you have more opportunity in rural, but most demand for spectrum in urban areas.

Chapter 3

Removing Non-Stationary Noise in Spectrum Sensing Using Matrix Factorization

3.1 Introduction

Nowadays the application of wireless technologies continues to grow, which requires the radio spectrum, a scarce resource, to be well-managed. Most of these modern wireless technologies take place in a frequency range from 200 MHz to 3 GHz and spectrum sensing is key to many applications. Several applications in this frequency range use spectrum sensing to identify white spaces (DSA applications) but also telecom operators use spectrum sensing to measure utilization and interference. An important part of these short range radio communication systems is active in the license-free 2.4 GHz ISM band, i.e. systems such as Wi-Fi (IEEE 802.11 b/g/n), Bluetooth, wireless sensor networks, wireless A/V links (e.g. wireless cameras).

In this chapter we have used this band as a test case. The applied techniques can be used for other bands as well. To monitor the radio spectrum usage in this band, we consider the RFeye mobile spectrum monitoring equipment of CRFS [36]. The mobile monitoring system can be built into vehicles to continuously measure spectrum usage on a country-wide scale while driving [43]. However, in a number of areas (very close to high power transmitters, e.g. UMTS stations) the detected input signals were significantly stronger than expected and measurements were affected as the Automatic Gain Control (AGC) system responded causing the noise floor in that particular band to be lifted. AGC systems are found in virtually all radio receivers, this means that the lifting effect is not limited to this specific equipment. In several cases, the AGC was fully engaged and the front-end of the receiver saturated, corrupting the data for that particular sweep [44]. The non-stationary noise caused by the AGC in the measurement data is the focus of this work. It is essential to remove the AGC noise from the measurement data, so that the in-band signals, and inherently the spectrum occupancy, can be assessed more accurately. Several methods are described in literature [45] to separate the noise and signal space. In

this chapter, we consider matrix factorization techniques, in order to detect and remove the noise from a block of data. This relates to the measurement equipment which outputs spectrogram data which includes AGC noise. This in turn requires techniques from principal component analysis [45, 46] and image processing in order to remove the noise from the spectrogram image.

The rest of the chapter is organized as follows. We first provide the background on AGC systems in Section 3.2. Next, in Section 3.3 a brief overview of related work in literature on spectrum occupancy is presented supplemented with the research objectives. In Section 3.4 we introduce the mobile monitoring network and measurements using the monitoring equipment to assess the AGC influence. Then the system model used for analysis, including the matrix factorization techniques, is provided in Section 3.5. In Section 3.6 we present the numerical results and a verification based on the analysis. Finally, the conclusions are drawn in Section 3.7.

3.2 Background

Nowadays, lots of radio systems and most of the spectrum analyzers are based on the super-heterodyne principle, i.e. by frequency mixing (or heterodyning) the received signal is down-converted to a fixed intermediate frequency. The conversion to an intermediate frequency is useful since filters can be set to a fixed frequency for which very sharp selective filters can be built. Furthermore, this makes them easier to tune and fewer stages for filtering are required when compared with the low-cost direct conversion (zero-IF) receivers which operate directly on the original radio carrier frequency. Due to this heterodyne principle the super-heterodyne radio comprises two stages: Radio Frequency (RF) and Intermediate Frequency (IF). Note that a super-heterodyne receiver can also be built of several IF stages to improve the radio reception; two or three IF stages are called double or triple conversion. However, these types of receivers are more costly and come at the expense of additional circuitry. Notice that each stage of the super-heterodyne receiver requires an AGC control loop in order to maintain the signal levels within an acceptable range.

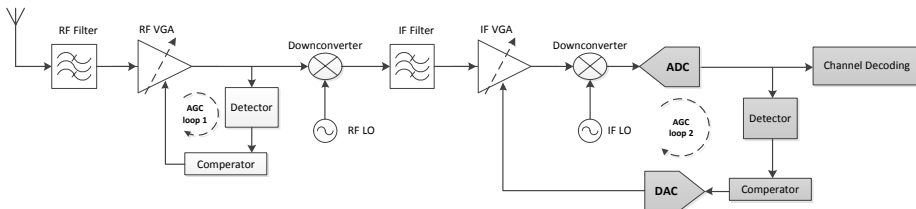


Figure 3.1: The super-heterodyne radio receiver with RF stage and one IF-stage. The first AGC loop operates in the RF stage in order to prevent the RF-amplifier (i.e. RF VGA circuit) from overloading the RF-mixer (downconverter). The second AGC loop operates in the baseband domain and sets the IF-gain of the IF-amplifier (i.e. IF VGA) to scale the signal input for the A/D conversion.

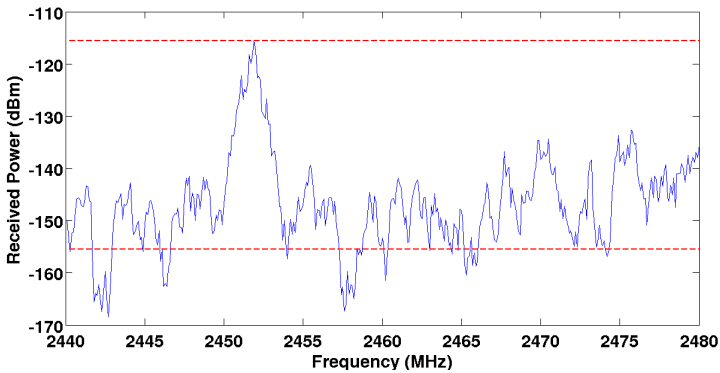


Figure 3.2: The second AGC loop entails respectively an upper and lower threshold. The upper-threshold can be set to the highest detected signal within a specific frequency range (typically tens of MHz) which depends on the AGC settling time. The lower threshold is defined on a fixed distance from the upper-threshold, i.e. in this case 40 dB. The signals below the lower-threshold are pulled up by the IF-gain.

Using AGC means that weaker signals receive more gain and stronger signals receive attenuation, i.e. an AGC system uses a high and low gain setting defined by respectively a lower and upper threshold. An outline of the heterodyne receiver and the AGC loops is shown in Figure 3.1 for a system with one IF-stage. Regarding the RF stage, an AGC loop is necessary to prevent strong RF signals from overdriving the RF amplifier and mixer. This would give rise to undesirable side-effects such as inter-modulation products and higher harmonics which degrade the sensitivity of the receiver and may mask the wanted signal. Here AGC control entails adjusting the RF-gain so that the RF-amplifier operates in its linear region, i.e. preventing the RF-amplifier from running into saturation (non-linear region) which causes the inter-modulation problems. However, as a drawback note that a reduction of the RF gain increases the Noise Figure (NF) of the system.

Used in the IF-stage a second AGC system operates to maintain a reasonable constant signal level for the Analogue-to-Digital (A/D) conversion because of the limited dynamic range of the ADC. This means that the signal input is required to be scaled properly for A/D conversion so that - despite large incoming signal variations - the average ADC output falls within the pre-set range. To scale the signals for A/D conversion the thresholds of the second AGC loop can be defined based on the highest detected signal (see Figure 3.2). Doing so, the upper-threshold can be set to the highest signal strength which in turn also defines the level for the lower-threshold based on this value (defined to be at a fixed distance from the upper-threshold). This means that due to strong incoming signals the noise floor will be lifted while the elevated lower-threshold causes an increased IF-gain. As a result, this improves the quantization of weak signals because smaller signal variations will toggle now more bits at the A/D conversion. Typically, note that an increasing IF-gain (AGC loop 2) can be used to scale the signals for A/D conversion whereas the preceding RF-amplifier adversely applied a reduced-gain (AGC loop 1) for handling strong signals [47].

Next, the AGC loop is described in more detail. First, note that for most applications an AGC system with closed-loop feedback is used to settle the desired output signal amplitude (for instance the AGC loops depicted in Figure 3.1); feed-forward loops also exist but are less common. In general the AGC loop consists of a Variable Gain Amplifier (VGA), a peak detector, and a comparator (using the defined thresholds) where both peak detector and VGA are non-linear components. Regarding the design of the AGC loop, the important parameters are the settling time, i.e. the loop response time, and the loop stability. Note that many AGC systems are required to have a constant settling time throughout the full dynamic range of input signal levels, which can be up to 80 dB; in order to achieve this an exponential gain for the VGA is employed, so that the AGC loop will behave as a first-order linear system in decibels (dB). Moreover, to accomplish loop stability the settling time is much slower than the input signal change, i.e. the AGC loop bandwidth must be significantly smaller than the bandwidth of the VGA.

For most heterodyne radio receivers the settling time of the AGC loop takes at least 0.5 ms for a fast loop implementation in mobile applications [48]. For super-heterodyne spectrum analyzers the principle is very similar to the above-described super-heterodyne radio receivers with the addition that the oscillators are driven by a ramp generator to sweep through the frequency range. Here, the slow settling time may corrupt the performance of the spectrum analyzer which carries out a full frequency sweep over many GHz typically within 100 ms. During the settling time period a wide range of frequencies is swept through (typically tens of MHz) for which the AGC gain is fixed and which in turn causes amplification of unwanted signals, i.e. thermal noise. This means that for the duration of AGC settling time the noise floor is lifted over a wide frequency range which scales non-linearly with the detected strongest signals in this range (see also Figure 3.2). This has been referred to as non-stationary noise and is of particular concern in receiver design because it decreases the sensitivity of the receiver's signal detection due to the higher noise level.

3.3 Related Work

In literature the AGC is described mainly from a RF point of view with focus on front-end design among which [49] is a classical paper on AGC design. The two basic topics of AGC in literature are the loop stability and the settling time and the basic theory can be found in [50] and [51]. In addition, the classical exponential constraint on the gain characteristic of the VGA to obtain constant settling time is discussed in [52, 53, 54]. However, achieving an exponential relationship in CMOS and other technologies is less obvious as discussed in [55, 56].

In recent years, many papers, among which [47] and [48], have discussed the digital AGC circuits in wireless communication systems which are primarily designed for mobile reception; such an AGC circuit is required to be fast in order to compensate for the strong signal variations introduced by Rayleigh fading. To cope with this type of small scale fading the design of AGC systems for super-heterodyne receivers is discussed in [48]. Moreover, it turns out that the optimal AGC settling time depends on the mobile speed as described in [57] and has the aforementioned value of typically at least 0.5 ms.

For spectrum sensing, three signal processing techniques are commonly used, including (a) energy detection [58, 59], (b) matched filtering [60], and (c) cyclostationary detection [61]. Both matched filtering and cyclostationary detection require *a priori* signal information. On the other hand, the energy detection method requires no knowledge of the signal to be detected which is an advantage. Note that this is the case for the obtained monitored spectrum data, where in most cases, no signal information is available (i.e. blind spectrum sensing). Energy detection works as follows: in a certain frequency band of interest, the received signal power is compared to a predefined threshold. In this light, the ITU (International Telecommunication Union) recommends a threshold placed 10 dB above the ambient noise floor for energy detection as stated in [62, p. 168] and [37].

However, there are some drawbacks regarding energy detection. First, the energy detection method relies on knowledge of the noise power level [63]. Secondly, the decision threshold is subject to fluctuations in the signal to noise ratios (SNRs). To overcome these limitations the so-called eigenvalue-based solutions were introduced in [64, 65]. They use the derived set of eigenvalues to find the threshold for spectrum sensing, by assigning the lower-ranked eigenvalues as noise contributions. The threshold is computed based on the ratio maximum to minimum eigenvalue $\lambda_{max}/\lambda_{min}$. In addition, they aim to find the related probability of false alarm and the probability of detection based on these eigenvalues. However, there is a drawback, since in practice it is hard to determine the minimum eigenvalue accurately, because it turns out that the lower eigenvalues are biased [66].

3.3.1 Research Objectives

To resolve the above-described spectrum monitoring problem, we are interested in matrix factorization techniques, e.g. eigenvalue-based, for a different purpose: aim to remove the dominant noise (the non-stationary AGC noise) in order to project out the signal space using the multi dimensional measurement data (i.e. the frequency, time and field strength dimensions). In this way the spectrum occupancy can be assessed more precisely using energy detection. To achieve this two state-of the art matrix factorization techniques are employed, i.e. Singular Value Decomposition (SVD) [45, 67, 68] and Non-negative Matrix Factorization (NMF) [69, 70, 71].

In line with this, recently in [72] the initial results on spectrum occupancy for different types of areas were presented by using solely SVD processing (for the UMTS band). Building upon this idea, we aim to enhance the research on AGC noise removal by using and comparing different matrix factorization techniques for the 2.4 GHz ISM band in conjunction with an experimental verification. To our knowledge this approach to remove AGC noise is novel and not found in literature.

3.4 Mobile Monitoring Equipment

3.4.1 Mobile Monitoring System

To analyze the effect of non-stationary AGC noise, we use the measurement data obtained from monitoring vehicles used by the Dutch regulator. These monitoring vehicles continuously perform full spectrum sweeps while driving in an particular area. As a test case we used the monitoring recordings from the 2.4 GHz ISM band, one of the most dense frequency bands. These measurements include many days of spectrum monitoring in the Netherlands, thereby employing the monitoring system of CRFS [36]. In our configuration the measurements take place at a 2 second time interval in which a frequency sweep is carried out (takes in total 100ms), using a step-size of 156.25 kHz, to sample the spectrum in the 2.4 GHz ISM band. The monitoring data, which results as output of the measurement equipment, is referred to as raw /unprocessed data. This means that for each frequency bin and time instant the received average power P_{rx} is stored per hertz of bandwidth.

The spectrogram of the raw data for a sample area is provided in Figure 3.3 and the corresponding statistics and data distribution in Figure 3.4. Here, the Wi-Fi channels can be identified from the monitoring results in the spectrogram because it entails most of the traffic in this band. Note that there are in total 13 overlapping channels which are actually in use, only in Japan there is a 14th channel. In practice it turns out that Wi-Fi systems mainly use the non-overlapping channels 1, 6, and 11 (often due to the manufacturer default settings).

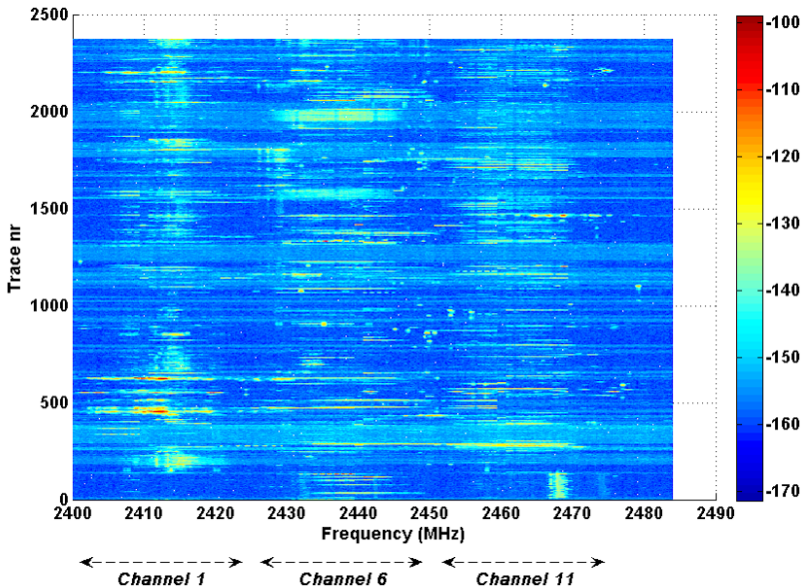
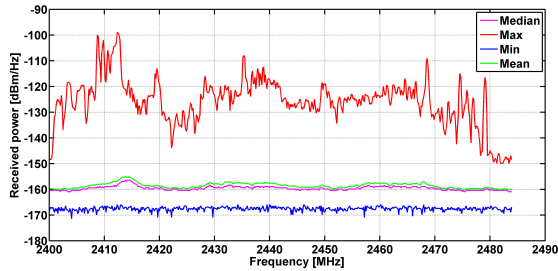
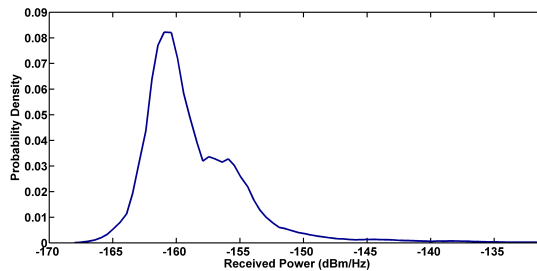


Figure 3.3: The spectrogram of the raw monitoring data (field strengths in dBm/Hz) w.r.t. the 2.4 GHz ISM band; the time instants are denoted as traces. Here, the main Wi-Fi channels are 1, 6, and 11 which correspond to center frequencies of respectively 2412 MHz, 2437 MHz and 2462 MHz; the bandwidth of each channel is 20 MHz.



(a) The mobile spectrum monitoring statistics (i.e. the mean, median, maximum and minimum signal levels). The latter corresponds with the thermal noise floor.

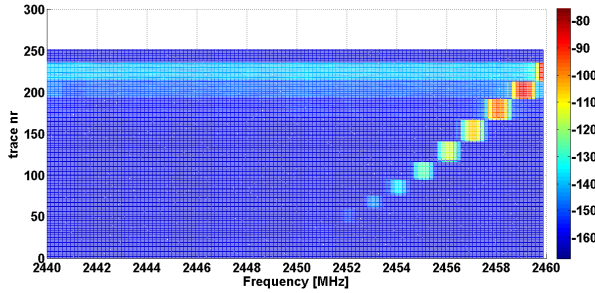


(b) The PDF of the signal levels of the raw monitoring data which includes the AGC noise components.

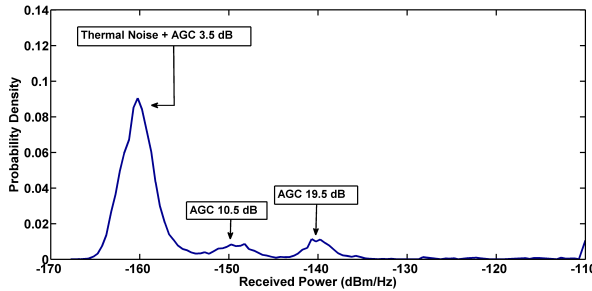
Figure 3.4: The statistics and PDF of the raw monitoring data in the 2.4 GHz ISM band from 2400 MHz to 2483.5 MHz.

3.4.2 AGC Calibration

The influence of the AGC on the measurement data is investigated in the remaining of this section; this is achieved by setting up an experiment. Note that the monitoring equipment uses the super-heterodyne principle and the associated AGC. Moreover, the equipment is able to log digitally both the IF-gain and the IF lower-threshold (scaled w.r.t. the thermal noise floor) while the second AGC loop operates in the baseband domain (see Figure 3.1); this means logging of increased gain values only (i.e. no attenuation). In addition, recall that the IF-gain is set to properly scale the input signals for A/D conversion. Furthermore, in what follows the IF-gain and IF lower-threshold will be meant when reference is made to respectively the AGC gain and AGC threshold. To investigate the influence of the AGC on the measurement equipment an experiment is set up in a controlled environment. Here the same configuration settings are used in a similar fashion as for the nationwide monitoring readings, i.e., using the same frequency sampling resolution, time observation interval, etc. In doing so, the transmission power of an unmodulated test signal is increased in a controllable way, in steps of several dBs, at the input of the monitoring equipment. Meanwhile spectrum monitoring is performed and the AGC threshold is stored for each time observation. Next, the frequency sweep results are shown in the spectrogram of Figure 3.5(a); the corresponding AGC threshold, the average AGC



(a) Spectrogram showing the AGC distortion (field strengths in dBm/Hz). The input signal increases in strength over time (traces) and is visible by the stepwise square-shaped signal.



(b) The distribution of the field strengths based on the spectrogram data in Figure 3.5(a).

Figure 3.5: To show the influence of the AGC, a power varying test signal is fed to the receiver input. The noise level is pulled up which results in wide-band artifacts in the spectrogram. In addition, the specification of the input signal power levels is listed in Table 3.1.

gain (G_{AGC}), signal field strength, and trace interval are listed in Table 3.1. Note that here the AGC gain is constant throughout the ISM band and scales with the highest detected signal which in turn causes the noise level to be lifted significantly. This effect is visible in the spectrogram of Figure 3.5(a), indicated by the horizontal strips which we refer to as wide-band artifacts. Furthermore, the Probability Density Function (PDF) of the measurement data is plotted in Figure 3.5(b). The PDF shows three distinguishable peaks. The leftmost distribution is a mixture of on one-hand thermal noise and on the other hand AGC noise contributions due to the lower AGC gain of $G_{AGC} = 3.5$ dB; here the dominant component is thermal noise (i.e. $G_{AGC} = 0$ dB which causes the Gaussian shaped distribution. In addition, the second and third peak are AGC noise contributions which correspond to the following AGC gain values: $G_{AGC} = 10.5$ dB and $G_{AGC} = 19.5$ dB. Finally, the signal contributions are present from -135 dBm/Hz onwards and are clipped at -110 dBm/Hz for the sake of clarity/visibility.

Relating the test measurement back to the mobile monitoring readings sheds light on the AGC distortion in the spectrogram of Figure 3.3. Here the wide-band artifacts stretch several hundreds of MHz, caused by the strong signals in nearby bands (e.g.

Table 3.1: The AGC recordings that result from experimental spectrum monitoring, tested by varying the power of the input signal. The maximum value of the input signal, for a particular time interval, is shown in the first column.

Input Signal (dBm/Hz)	Time Traces (nr)	AGC Threshold (dB)	G _{AGC} (dB)
-156.2	1 - 42	0	0
-150.7	43 - 59	0	0
-143.2	60 - 75	0	0
-134.7	76 - 94	0	0
-124.2	95 - 118	0	0
-115.2	119 - 140	0	0
-105.2	141 - 166	2	0
-95.2	167 - 191	12	3.5
-86.2	192 - 212	21	10.5
-75.7	213 - 235	31	19.5
-156.7	236 - 251	0	0

the UMTS band) due to high power transmitters in the vicinity. In the next section we propose a system model to remove the AGC noise components.

3.5 System Model

3.5.1 Notation

Let the unprocessed data be represented as $\mathbf{X} = [X(t, f)]$ in which $t \in \{1 \cdots N_t\}$ denotes the discrete time instants and where $f \in \{1 \cdots N_f\}$ denotes the frequency bins. Regarding \mathbf{X} , the number of rows N_t relates to the time-frame of monitoring, which in turn consists of a fixed number of t independent time instants (a.k.a. 'traces'). In addition, each recording at a given time instant is linked to a specific spatial coordinate. Similarly, N_f defines the total number of frequency bins, also referred to as frequency observations. Note that each element in matrix \mathbf{X} can either be classified as a signal (denoted by '1') or as noise (represented as '0'), based on a predefined threshold η . In line with this the *spectrum availability function* $\mathbf{X}_c = [X_c(t_i, f_j)]$ is defined through,

$$X_c(t_i, f_j) = \begin{cases} 1, & X(t_i, f_j) \geq \eta \\ 0, & X(t_i, f_j) < \eta \end{cases} \quad (3.1)$$

which represents the matrix of classifications where the time traces are associated with the matrix rows and the frequencies with the matrix columns. Now, a signal is detected if the measured field strength exceeds the threshold. Otherwise the data is classified as noise. As a result, the choice of threshold value is critical for proper signal detection. To analyze the distribution of the data, it is common use to look at

the second order statistics and at the covariance matrix which is defined by

$$\mathbf{C} = E \left[(\mathbf{X} - E[\mathbf{X}]) (\mathbf{X} - E[\mathbf{X}])^T \right] \quad (3.2)$$

where E denotes the expectation operator. Furthermore, $(\cdot)^T$ denotes the Hermitian transpose and \mathbf{x}_k represents the k^{th} column of \mathbf{X} . However, \mathbf{C} is not known beforehand and has to be estimated. For this purpose an unbiased estimate, i.e. sample covariance matrix $\hat{\mathbf{C}}$, is computed; the latter is derived based on samples of collected measurement data and is an approximation of the actual covariance matrix \mathbf{C} . Now, based on a given sample set consisting of N_f frequency domain observations of the N_t dimensional random variable $X \in \mathbb{R}^{N_t \times 1}$ (a $N_t \times 1$ column vector) an estimation of \mathbf{C} is defined through,

$$\hat{\mathbf{C}} = \frac{1}{N_f - 1} \sum_{k=1}^{N_f} (\mathbf{x}_k - \boldsymbol{\mu}) (\mathbf{x}_k - \boldsymbol{\mu})^T \quad (3.3)$$

as the sample covariance matrix, also referred to as the estimated covariance matrix. Notice that $\hat{\mathbf{C}}$ has $N_f - 1$ in the denominator rather than N_f in contrast to \mathbf{C} (see [66]). For a certain time instant t the mean received field strength is computed through integration of the corresponding N_f samples in the ISM band as follows:

$$\boldsymbol{\mu} = \begin{bmatrix} \mu_1 \\ \vdots \\ \mu_{N_t} \end{bmatrix} = \frac{1}{N_f} \sum_{k=1}^{N_f} \mathbf{x}_k \quad (3.4)$$

where the column vector $\boldsymbol{\mu}$ contains the mean received field strength for each time instant.

3.5.2 Singular Value Decomposition

Based on the covariance matrix, we apply a technique known as SVD, in order to project out the signal space. Note that the SVD technique is preferred over an alternative method, named eigendecomposition. This is because SVD is numerically stable, yielding always non-negative eigenvalues, unlike eigendecomposition.

As a first step the unbiased data matrix, denoted by \mathbf{M} , is defined in order to show how to decompose the sample covariance matrix into its sample eigenvectors and eigenvalues. Here $\hat{\mathbf{C}} = \mathbf{M}\mathbf{M}^T$ holds, where matrix \mathbf{M} is derived as

$$\mathbf{M} = \frac{1}{\sqrt{N_f - 1}} (\mathbf{X} - E[\mathbf{X}]) \quad (3.5)$$

Now, the singular value decomposition of matrix \mathbf{M} can take place, which leads to the following factorization:

$$\mathbf{M} = \mathbf{W}\boldsymbol{\Sigma}\mathbf{U}^T \quad (3.6)$$

where the diagonal entries Σ_{ii} of $\boldsymbol{\Sigma}$ are known as the singular values of \mathbf{M} . It is known, from the field of Principal Component Analysis (PCA) [45, 46], that the columns of \mathbf{W} (left singular vectors) are eigenvectors of $\mathbf{M}\mathbf{M}^T$ and the columns of

\mathbf{U} (right singular vectors) are eigenvectors of $\mathbf{M}^T\mathbf{M}$. Hence, it can be shown that the sample covariance matrix can be decomposed into its sample eigenvectors and eigenvalues:

$$\hat{\mathbf{C}} = \mathbf{M}\mathbf{M}^T \quad (3.7)$$

$$= (\mathbf{W}\boldsymbol{\Sigma}\mathbf{U}^T) (\mathbf{U}\boldsymbol{\Sigma}^T\mathbf{W}^T) \quad (3.8)$$

$$= \mathbf{W}(\boldsymbol{\Sigma}\boldsymbol{\Sigma}^T)\mathbf{W}^T \quad (3.9)$$

where $\mathbf{U}^T\mathbf{U} = \mathbf{I}$, due to the orthogonal column structure of matrix \mathbf{U} . Furthermore, \mathbf{W} denotes the sample eigenvector matrix of $\hat{\mathbf{C}}$. Thus, the sample eigenvalues and eigenvectors of $\hat{\mathbf{C}}$ are derived by computing $\text{SVD}(\mathbf{M}) = \mathbf{W}\boldsymbol{\Sigma}\mathbf{U}^T$. The sample eigenvalues can be computed, since the singular values of diagonal matrix $\boldsymbol{\Sigma}$ correspond to the square roots of the sample eigenvalues of matrix $\hat{\mathbf{C}}$. The obtained sample eigenvectors, contained in matrix \mathbf{W} , can be used to create a projection $\tilde{\mathbf{X}}$ of the measured data \mathbf{X} , containing solely the strongest signal space components:

$$\tilde{\mathbf{X}} = \sum_{i=1}^L \mathbf{w}_i \mathbf{w}_i^T (\mathbf{X} - E[\mathbf{X}]) + E[\mathbf{X}] \quad (3.10)$$

where \mathbf{w}_i are the column vectors of \mathbf{W} , i.e., the columns $\mathbf{w}_1 \cdots \mathbf{w}_L$ correspond to the first L principal components of \mathbf{X} . As a consequence, the principal subspace, $F = \{\mathbf{W}_i\}_1^L$, is spanned by the first L principal components of \mathbf{X} . Since mean subtraction, i.e. mean centering, is necessary for performing PCA, we get a corrected version of matrix \mathbf{X} , by adding $E[\mathbf{X}]$. As a drawback, the SVD method is not constrained to output non-negative data, which can result in a small percentage of outliers - negative valued field strength data - which causes numerical problems when translated back to logarithmic values. To overcome this problem, we manually map the negative data values to a fixed arbitrary small positive value.

3.5.3 Non Negative Matrix Factorization

Since SVD is not constrained to output positive valued data we investigate a second technique known as NMF [69] which is referred to as a dimension-reduction technique. The basic idea is the following: given the non-negative data matrix $\mathbf{X} \in \mathbb{R}_+^{N_i \times N_f}$ (i.e. the non-logarithmic representation is used) the NMF algorithm aims to construct a low-rank approximation of \mathbf{X} of rank L . Doing so, NMF opts to find two nonnegative matrices \mathbf{U} and \mathbf{W} such that $\mathbf{X} \approx \mathbf{U}\mathbf{W}$. Note that the latter expression holds with equality once the residual matrix \mathbf{R} is taken into account: $\mathbf{X} = \mathbf{U}\mathbf{W} + \mathbf{R}$. As such, the elements of the residual matrix \mathbf{R} can either be negative or positive valued. Recall that the NMF algorithm provides as factorization output the two matrices \mathbf{U} and \mathbf{W} which are nonnegative factors of \mathbf{X} and are defined as $\mathbf{U} = [\mathbf{u}_1, \cdots, \mathbf{u}_L]$ and $\mathbf{W} = [\mathbf{w}_1^T, \cdots, \mathbf{w}_L^T]^T$; here \mathbf{U} is a $N_i \times L$ matrix containing the basis vectors as its columns whereas \mathbf{W} denotes a $L \times N_f$ matrix containing the coefficients vectors. Now, by applying NMF a low-rank approximation of the feature space of \mathbf{X} can be achieved, i.e. the data matrix \mathbf{X} can be estimated by using a linear

combination of the basis vectors with the coefficients vectors through,

$$\mathbf{X} = \sum_{j=1}^L \mathbf{u}_j \mathbf{w}_j^T + \mathbf{R} \quad (3.11)$$

where rank L are the number of independent principal components present in the constructed lower-ranked approximation of \mathbf{X} . Thus, $L \leq \min(N_t, N_f)$ is required to establish the desired rank-reduction. Next, in order to carry out the factorization of matrix \mathbf{X} a cost function $D(\mathbf{X}, \mathbf{UW})$ needs to be defined to quantify the quality of the approximation. Such a cost function can be constructed using some measure of distance between \mathbf{X} and the product \mathbf{UW} . Examples of such measures [70, 73, 74, 75, 76] include Euclidean distance and Kullback-Leibler (KL) divergence. Henceforth the KL measure is used as cost function since the advantage of KL compared to other cost functions lies in the guaranteed convergence to a fixed point. This occurs at the expense of lower processing speed, i.e. many iterations are needed. However, this is not a limitation for AGC noise removal due to the off-line processing possibilities. The optimization problem is now defined as follows:

$$\min_{\mathbf{U} \in \mathbb{R}_+^{N_t \times L}, \mathbf{W} \in \mathbb{R}_+^{L \times N_f}} [D(\mathbf{X}, \mathbf{UW})] \quad (3.12)$$

where the cost function $D(\mathbf{X}, \mathbf{UW})$ equals

$$\sum_{i=1}^{N_t} \sum_{j=1}^{N_f} \left(\mathbf{x}_{ij} \log \frac{\mathbf{x}_{ij}}{(\mathbf{UW})_{ij}} - \mathbf{x}_{ij} + (\mathbf{UW})_{ij} \right) \quad (3.13)$$

The objective function is convex in \mathbf{U} , and in \mathbf{W} , but not convex in both simultaneously. Therefore an algorithm cannot guarantee to converge to a global optimum. Using an iterative update algorithm, such as gradient search, will therefore find a local optimum of the objective function. In fact, the NMF problem does not have a unique global minimum. Fortunately, it turns out that the achieved feature extraction (i.e. rank reduction) with only local minima has been shown to be of significant quality for many applications [74]. Finally, note that the most important difference between NMF and other matrix factorization methods, such as SVD, is that the data is described by using additive principal components only. The reason therefore are the non-negative constraints on \mathbf{U} and \mathbf{W} .

3.6 Results

This section illustrates the application of the matrix factorization techniques, i.e. SVD and NMF, to remove the AGC distortion and to assess spectrum occupancy more accurately for monitoring applications in the 2.4 GHz ISM band. To start with, a performance evaluation of both techniques is carried out in order to find out which technique suits best for further analysis. Basically, both techniques can be employed for the following: a decomposition of the unprocessed monitoring data into independent principal components to project out the signal space from the noise space. Let $L = 300$, and $N_t = 2400$; for both NMF and SVD the corrected

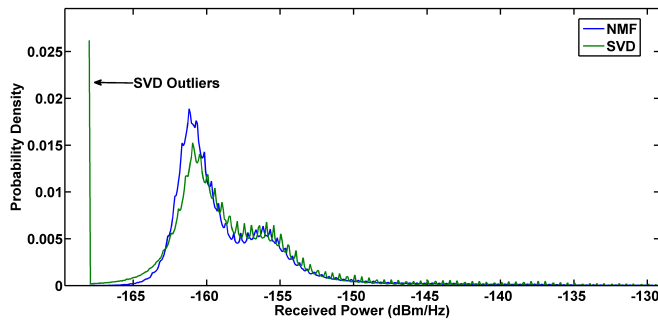


Figure 3.6: A performance comparison: NMF versus SVD. Here, the SVD curve displays an instant peak which is due to the outliers i.e. non-negative values. This is not the case for NMF which shows a curve without an instant outlier peak. Both algorithms ran with the same number of principal components: $L=300$.

spectrograms are derived and the associated PDFs are depicted in Figure 3.6. As a result it turns out that the SVD produces negative valued data (outliers) which in turn distorts the spectrogram and causes problems whilst applying the required logarithmic conversion. Here, the instant peak in the PDF of Figure 3.6 corresponds with the probability mass of the negative valued outliers which were mapped numerically to an arbitrary small positive valued number, as referred to in Section 3.5.2. Furthermore, Figure 3.6 shows that NMF provides similar results as SVD but without the outliers, i.e. no instant peak. Thus, in fact NMF outperforms SVD and in what follows NMF is set as the preferred matrix factorization technique for spectrum occupancy assessment in the 2.4 GHz ISM band.

For projecting out the signal space, it is essential to select the proper number of principal components L so that the non-stationary (AGC) noise components can be removed from the spectrogram without removing signal components. This is possible since it is known from literature that the lower ranked principal components

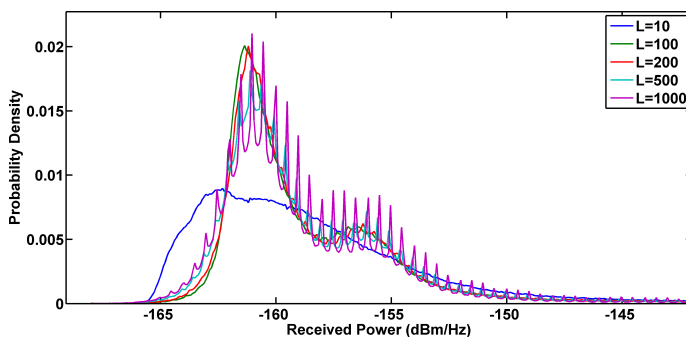


Figure 3.7: PDF curves of the monitoring data obtained from several NMF sessions which ran with different values of L , i.e. the number of independent principal components (field strengths in dBm/Hz).

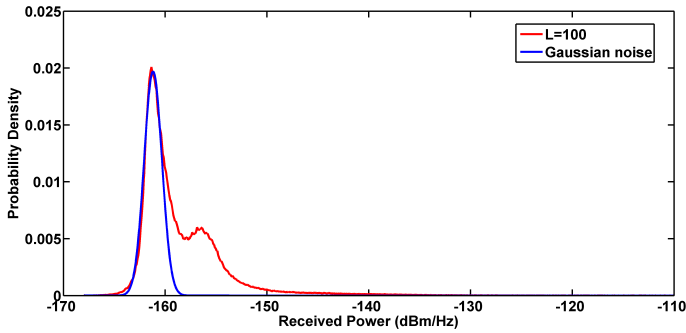


Figure 3.8: The best fit, taking the Gaussian distribution as the reference, turns out to be $L=100$.

contribute to the noise space [64]. To achieve this NMF is applied to the monitoring data for values of L in the range of $\{1, 2400\}$ and the corresponding PDF curves are depicted in Figure 3.7. The interpretation of the PDFs for different values of L is the following: a value of $L > 500$ for instance contains many noise components, indicated by its non-smooth character; on the other hand, the PDF curves for $L < 50$ are smoothed out and no threshold can be defined based on its shape. To derive the optimum number of principal components a performance metric is required; the performance metric in this case is the thermal noise which is distributed according to a Gaussian distribution and is provided by the calibration measurements. By fitting the Gaussian curve with the NMF curves for different L values the corresponding fitting errors can be derived; the results show that the optimal solution, i.e. minimal fitting error, is expected for $L \in \{50, 500\}$. Note that for instance the $L = 10$ curve shows no resemblance with the Gaussian metric curve and yields a high fitting error. In addition, it turns out that the best fitting result is obtained for $L = 100$, which is depicted in Figure 3.8.

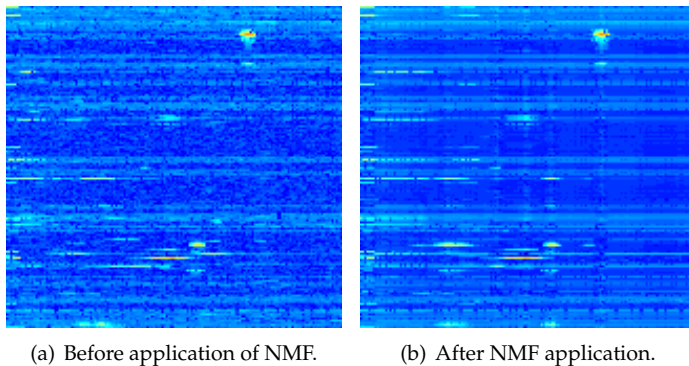
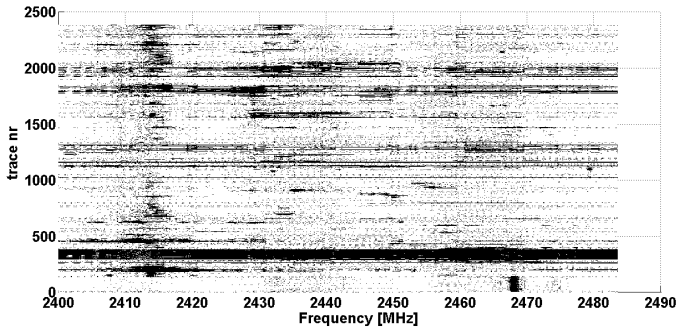
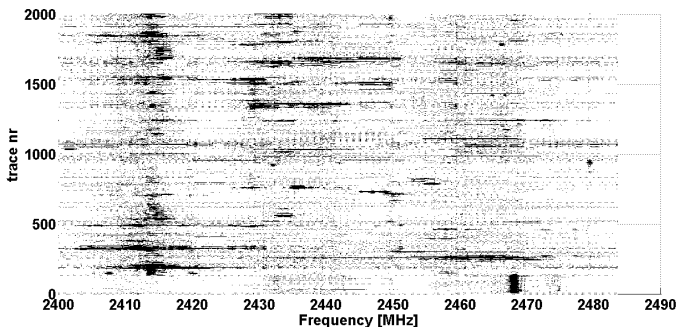


Figure 3.9: Applying NMF ($L=100$) on the monitoring data yields a corrected version of the spectrogram. The spectrogram before applying NMF is depicted in Figure 3.9(a); the corrected version after applying NMF is depicted in Figure 3.9(b).

Next, applying NMF ($L = 100$) to the monitoring data in Figure 3.9(a) provides the corrected data in Figure 3.9(b). The latter is smoother since only the main principal components are left over. Furthermore, by applying NMF the AGC noise is removed in the range $P_{rx} = \{-160, -157\}$ dBm/Hz and this shows the importance of choosing a good threshold value. Note that the AGC noise, present in the spectrogram as small random variations, is not covered by the first $L = 100$ principal components that mainly span the signal space. In line with this, recall that the PDF of the corrected spectrogram, as depicted in Figure 3.8, shows more contrast and follows a bimodal distribution which arises as a mixture of two unimodal distributions. Here, the threshold is required to be chosen at the lowest field-strength in between the two peaks (see Figure 3.8). Moreover, it turns out that the derived threshold is around the same value for each selected geographical area. This is the optimal threshold value while according to the performed calibration experiment the first peak is classified as a thermal noise distribution and the second peak as containing both (Wi-Fi) signal and AGC noise contributions. Note that the latter is caused by very strong signals in nearby bands (e.g. UMTS signals) that in turn triggers the AGC to lift up the thermal noise to values in the range $P_{rx} = \{-156, -152\}$ dBm/Hz. This is indicated in the binary occupancy spectrogram of



(a) Before the final AGC removal step.



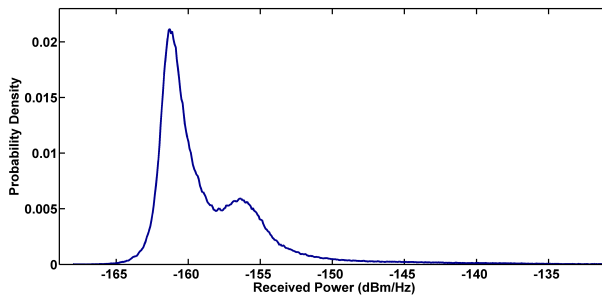
(b) After the final AGC removal step.

Figure 3.10: Occupancy plots after thresholding: black denotes used spectrum and white denotes unused spectrum.

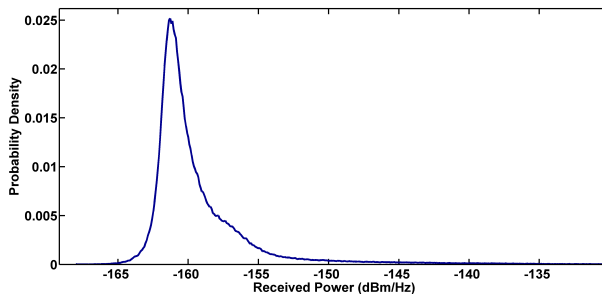
Figure 3.10(a) by the wide-band artifacts .

To reduce the influence of AGC the wide-band artifacts are removed from the spectrogram, i.e. the traces with more than 80 percent in-band occupancy are selected and deleted. In the sequel, this step is referred to as the second AGC removal step. Notice that NMF has set the stage for the second AGC step by smoothing the wide-band artifacts which also enhances their identification for removal (thus is referred to as AGC removal step 1). In Figure 3.10(b) the resulting binary occupancy map is depicted *after* the wide-band artifacts removal; in addition the corresponding PDFs are derived and shown in Figure 3.11; here the PDF of the spectrogram for NMF $L = 100$ is depicted in Figure 3.11(a) and the PDF of the spectrogram after removing the wide-band artifacts is shown in Figure 3.11(b); a significant decrease is demonstrated in probability mass for the second distribution whereas the thermal distribution retains its shape; based on this it turns out that the second distribution primarily contained AGC contributions.

Next, the spectrum occupancy is computed using the AGC removal algorithm and the outcome is compared with the energy detection method (using the ITU recommended threshold [62]). Here, the spectrum occupancy is assessed in a straightforward manner by placing a threshold 10 dB above the thermal noise floor and by applying energy detection accordingly, i.e. a threshold of $\eta = -158$ dBm/Hz is used. The occupancy results are listed in Table 3.2 for the ISM band, i.e.



(a) After AGC removal step 1.



(b) After AGC removal step 2.

Figure 3.11: A comparison of the field strength distributions: before and after applying the final AGC removal step respectively depicted in Figure 3.11(a) and Figure 3.11(b).

Table 3.2: The occupancy results for the 2.4 GHz ISM band (from 2400 MHz to 2483.5 MHz). The results show that the occupancy based on the energy detection (ITU recommended threshold) method provides an overestimation of the spectrum usage.

	Energy Detection (ITU-based)	AGC removal (step 1)	AGC removal (step 2)
2400 - 2483.5 MHz	34.92%	32.77%	21.85%
Channel 1	37.36%	35.02%	24.53%
Channel 6	37.45%	35.00%	23.79%
Channel 11	37.13%	35.17%	24.46%

2400 – 2483.5 MHz (Wi-Fi band), and for the non-overlapping default channels 1, 6 and 11. These results show that after each processing step the spectrum occupancy decreases. Remarkably it shows that the Wi-Fi band is 40% less occupied than one would expect based on the energy detection method (with the ITU recommended threshold). The other way around, the occupancy based on energy detection overestimates the spectrum usage by 60%. In addition, the results in Table 3.2 show that the occupancy of the default channels is always higher than the overall Wi-Fi band occupancy, indicating in line with the expectations that the default channels convey more Wi-Fi traffic than the other channels. Furthermore, Figure 3.12 depicts the spectrum occupancy of the 2.4 GHz ISM band (from 2400 MHz to 2483.5 MHz) to illustrate graphically the difference in spectrum usage estimation between the energy detection method (using the ITU recommended threshold) and the AGC removal algorithm (i.e. after AGC removal step 2).

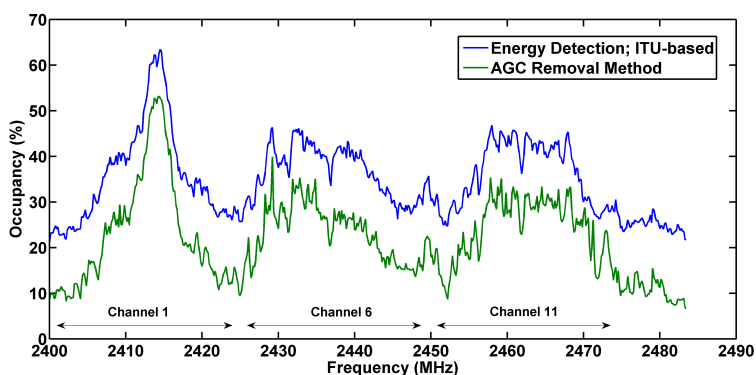


Figure 3.12: The occupancy of the 2.4 GHz ISM band (from 2400 MHz to 2483.5 MHz) for the area of interest. The blue curve represents occupancy according to the energy detection (ITU-based) method whereas the green curve denotes the occupancy computed by the AGC removal algorithm (step 2 in Table 3.2).

3.6.1 Validation of the Results

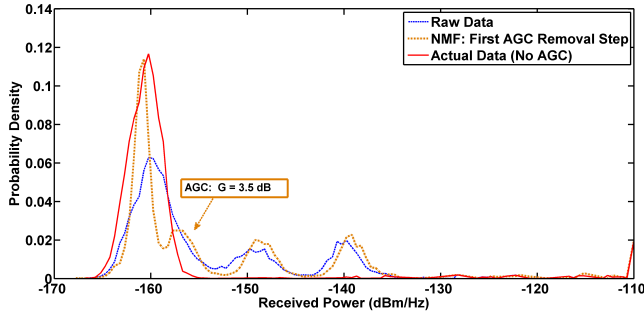


Figure 3.13: The PDF after AGC removal step 1 versus the PDFs of the field-strengths of the raw data (with AGC) and the actual data (without AGC). The focus is on the leftmost distribution peak which is in the field-strength range of $P_{rx} = \{170, -155\}$ dBm/Hz. For the actual field-strength data this corresponds to only thermal noise whereas for the raw data also AGC noise is included. As a consequence the difference in width between these two leftmost peaks equals the AGC noise contribution. Due to NMF the thermal noise and the lower AGC contribution ($G_{AGC} = 3.5$ dB) become separated and are visible as distinguishable distributions.

A validation of the above-described results is provided to verify the removal of exclusively AGC noise components from the raw field-strength data. For this purpose the data from the experiment described in Section 3.4.2 is used for which the AGC was turned on. However, note that for the same experiment also the spectrum data without AGC noise is available which allows the validation of the proposed AGC removal algorithm. Here, the verification covers both stages of the AGC algorithm. Regarding step 1, NMF is applied to the raw field-strength data as obtained from the calibration test experiment (with AGC distortion). The corresponding PDF is shown in Figure 3.13 alongside respectively the PDFs of the raw field-strength data (with AGC distortion) and the actual field-strengths (without AGC distortion). The figure shows the AGC noise distribution (i.e. $G_{AGC} = 3.5$ dB) which becomes visible after application of NMF and can be clearly distinguished from the thermal noise distribution.

This is key for the second AGC removal step while the AGC noise contributions can be properly removed now by deleting the smoothed wide-band artifacts. The PDF of the field-strengths after application of AGC step 2 is depicted in Figure 3.14 which turns out to consist of solely thermal noise while it resembles the PDF of the actual field-strengths. Finally, the spectrum occupancy values are provided; here the energy detection method (with the ITU recommended threshold) is used for respectively the raw field-strength data and the actual received power. Table 3.3 lists the corresponding spectrum occupancy results and indicates a large estimation error when the occupancy is computed based on the (unprocessed) raw field-strengths values. Furthermore, Table 3.3 shows that the AGC removal algorithm is very accurate (i.e. small estimation error) and able to effectively remove exclusively the AGC noise which provides a reliable estimate of the spectrum occupancy.

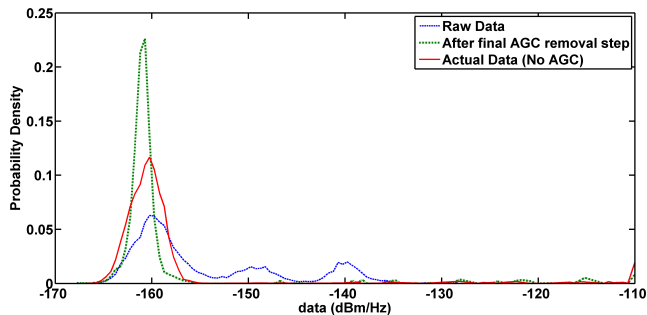


Figure 3.14: The PDF after application of AGC removal step 2 versus the PDFs of the field-strengths of the raw data (with AGC) and the actual data (without AGC). In this step the wide-band artifacts can be removed due to the pre-work of the NMF operation. After the final AGC removal step the PDF contains primarily thermal noise. Due to NMF the thermal noise distribution is compressed whereas the probability mass remains the same (see Table 3.3).

3.7 Conclusion

In this work we have presented a novel approach based on matrix factorization techniques to improve spectrum sensing significantly by eliminating AGC noise. To verify our method we used measured monitoring data in the 2.4 GHz ISM band. As we know from AGC test experiments the AGC lifts the thermal noise by a few dBs. We showed that by applying matrix factorization techniques, i.e. SVD and NMF, this part of the AGC noise can be removed; moreover, it turns out that NMF outperforms SVD. In addition, we employed a curve fitting approach to find the optimal number of components to be included by NMF; the resulting PDF follows a bimodal distribution and shows more contrast compared to the PDF of the raw monitoring data. This is due to the fact that a large part of AGC noise is centered around the threshold. Furthermore, NMF sets the stage for the final AGC removal step in order to delete the remaining AGC noise contributions (visible as wide-band artifacts in the spectrogram). Regarding the ISM band, by removing the AGC noise from the spectrogram we have demonstrated a reduction in spectrum usage of around 40% as when compared to spectrum occupancy assessment using the energy detection method (with the ITU recommended threshold). Further research

Table 3.3: The validation experiment: the spectrum occupancy and the estimation error compared with the actual spectrum occupancy i.e. without AGC noise (corresponds with an occupancy of 4.36%)

	Spectrum Occupancy	Estimation Error
Energy Detection	35.98%	31.62 %
AGC Removal Algorithm	4.70%	0.34%

could focus on the real-time implementation of AGC removal techniques and on its application to different frequency bands.

Chapter 4

Spectrum Utilization and Congestion of IEEE 802.11 networks in the 2.4 GHz ISM Band

4.1 Introduction

Commodity wireless broadband, e.g., Wi-Fi technology, plays a major role in society thanks to its widespread availability, ease of use and low cost. Many new applications have emerged for such technologies, Intelligent Transportation Systems (ITS), Dynamic Spectrum Access (DSA) systems and offloading of traffic from cellular networks. Because the role of Wi-Fi technology is becoming increasingly important, its long term viability in terms of capacity and ability to share spectrum efficiently, must be assured. Current practice shows already that Wi-Fi technology is not very efficient and there is a risk of collapse in certain scenarios, like high density video and data off-load from cellular networks.

In this chapter we focus on the crowded 2.4 GHz ISM band. The number of wireless devices (smartphones, laptops, sensors) that use this band is rapidly increasing. In many urban areas not only many WLAN networks can be found, also other systems such as Bluetooth, Zigbee and wireless A/V transmission systems use this band. On the other hand there is only a limited amount of spectrum available. So it is very likely that interference between systems in this band will occur. Due to the rapid increase of wireless devices, interference is expected to become even more important. In this chapter we address this issue by providing a setup to measure the service level - i.e. can all devices fulfill their communication needs - in this band with focus on WLAN systems based on the IEEE 802.11e standard. The IEEE 802.11e is an extension of the 802.11 Wireless Local Area Network (WLAN) standard and is developed to enhance Quality of Service (QoS) support. Furthermore, note that IEEE 802.11e has been incorporated into the current published IEEE 802.11 standard to which we refer - with slight abuse of notation - as IEEE 802.11e. On the other

hand, we refer to the traditional IEEE 802.11 technology without QoS support as legacy IEEE 802.11 systems.

The service level measurements can be split into two parts: utilization and congestion. Utilization or spectrum sensing means how much of the 2.4 GHz ISM band is in use for a certain area. When the utilization has been measured, it is still unknown what the quality is of the wireless connections i.e. degradation cannot be measured; a measure for quality is congestion. Basically it analyzes the frame types transmitted through the wireless medium. Congestion occurs if the retry frame rate or the number of control frames is high. WLAN systems often use these frames to mitigate interference from other WLAN networks. Measuring the service level is an crucial parameter to assess the efficiency of the WLAN networks on other wireless networks and to identify coexisting issues. For the coexistence of competitive 802.11e networks the available resources have to be shared by overlapping and competing WLANs with high offered traffic load. Measuring and assessing the QoS of competing overlapping 802.11e compatible WLANs is the main topic of this work.

The chapter is organized as follows. First in Section 4.2 the related work on monitoring QoS is highlighted. Next, in Section 4.3 the 802.11(e) coexistence mechanisms are presented. In Section 4.4 the influence of overlapping 802.11e WLANs on the same radio communication channel is investigated based on measurements set up in a controlled environment. In Section 4.5 the monitoring results, taken in real environments without control, are presented. Section 4.6 concludes the chapter.

4.2 Related Work on Monitoring QoS

The OSI protocol stack of the IEEE 802 standard consists of five layers where the lower two layers involve the wireless aspects of communication, i.e. the Physical (PHY) layer and the Medium Access Control (MAC) link layer. To assess the overall Wi-Fi QoS the monitoring must take place at these lower two layers. At the PHY layer this entails a threshold-based approach to determine spectrum occupation. This value can be used to assess utilization of the band. On the other hand, at the MAC link layer the total frame rate and retry frame rate have been found to be good parameters for quantifying the level of utilization and network degradation [12]. In addition, monitoring of the proportions of the different MAC link frame types can be used to assess the overhead in a Wi-Fi network, i.e., data, management and control (e.g. Clear-to-Send(CTS), Request-To-Send (RTS), and (Block) Acknowledgment (ACK) frames. Much of the papers discuss the QoS on the MAC link layer only, i.e. in [77, 78] the performance evaluation of 802.11 WLAN systems is provided and in [79, 80, 81, 82] the 802.11e MAC link layer QoS. The advantage herein lies in the broad range of MAC link layer specific aspects and protocols which can be modeled and compared. Notice that in this work we use both RF spectrum and MAC link layer monitoring in order to address the overall QoS.

Not much related literature has been found on overall QoS. First, a description of the overall Wi-Fi QoS monitoring is provided in *Estimating the Utilization of Key License-Exempt Spectrum Bands*, Final report, issue 3, April 2009 by Mass Consultants Limited commissioned by the British regulator Ofcom [12]; here monitoring takes place at various locations in the UK and live readings are obtained. In the latter

report the QoS is assessed at the MAC link layer level but is only monitored at the highest abstraction level, i.e., whether the type of frame is data, management or control; this means that no deep packet inspection is carried out (e.g. ACK, RTS, CTS, etc) so that a description of the occurring mechanisms cannot be provided thoroughly. Furthermore, in [83] the total QoS is assessed of WLAN systems in live environments using a cognitive radio approach. Regarding monitoring QoS, the impact of overlapping WLAN interference is not addressed in the above-provided papers.

4.2.1 QoS: Overlapping WLANs

The problem of overlapping WLANs is for legacy 802.11 systems mainly focused on co-channel interference. Note, in this work we do not cover adjacent channel interference (e.g. see [84, 85]) for the sake of brevity. Elaborating on co-channel interference simulation based studies - using game theory models - are provided e.g. in [86, 87], and experimental studies in [88, 89, 90]. This entails MAC link layer performance models for assessing QoS; mainly the 802.11 interference impact on concurrent data throughput is investigated. For instance, it is shown in [90] that the throughput remained nearly constant irrespective of the distance between the 802.11 Access Points (APs), indicating that distance does not have an effect on the throughput as long as the APs are in the carrier sensing range. In addition, in [89] the performance of a particular AP in a highly congested environment is evaluated, i.e. many concurrent WLAN networks. Here the live recordings show that in case of bad link quality the AP becomes inactive for a while, i.e. the AP operates in cycles of respectively activity and inactivity. Furthermore, the related problem of 802.11 hidden node issues and the impact of the RTS/CTS mechanism are addressed in [91]. However, a drawback of the above-mentioned studies is that 802.11e is not taken into account.

Regarding 802.11e, stochastic simulations on overlapping 802.11e WLANs are provided in [80, 92, 93, 94]. This entails a 802.11e MAC link layer investigation using respectively the aggregate data throughput and data packet delay as performance metrics. Another simulation study on the related problem of hidden node terminals in the vicinity of 802.11e WLAN is given in [95]. Note that the advantage of [80, 92, 93, 94, 95] lies in the thorough theoretical research of overlapping 802.11e networks. However, the experimental work and the overall QoS are beyond the scope of their work.

4.2.2 Contributions

To assess the overall QoS for 802.11 systems - in highly congested environments with overlapping WLANs - an experimental validation is required. In line with this the main contributions of this work are:

- A measurement setup to measure the congestion in the 2.4 GHz ISM band. The setup is able to analyze three WLAN channels in parallel. In addition, the setup allows to identify which frame types (and subfields) are transmitted, useful to identifying congestion (This setup is an extension of the work by Mass Consultants [12]).

- Reporting the results of measurements in a controlled environment where the interference of a second WLAN network is measured. From these results one can conclude that the RTS/CTS mechanism found in the WLAN standard (used for the hidden node problem) is one of the main sources of congestion. WLAN networks often identify interference as a hidden node.
- Reporting the experimental results of devices that use the new 802.11e extension.
- Reporting the results of measurements in a live environment (college room, office room, city center). The results reveal that for a college room only 21% are actual data type frames. Almost 70% are control frames.

4.3 IEEE 802.11 Coexistence Mechanisms

In this section a short overview of legacy 802.11 mechanisms is provided to access the shared medium; subsequently the mechanisms of its enhanced version 802.11e are highlighted. It is important to know these coexistence mechanisms to analyze the experimental results.

4.3.1 Legacy IEEE 802.11

The legacy 802.11 WLAN technology is characterized by its best-effort service (no guarantee of any service level to users/applications). In legacy 802.11 WLAN the PHY layer comprises 13 channels in the 2.4 GHz ISM band where each channel has a bandwidth of 20 MHz.

On the other hand, legacy 802.11 MAC link layer defines two procedures for 802.11 stations to share a common radio channel [96], i.e., Distributed Coordination Function (DCF) and Point Coordination Function (PCF). Here the mandatory DCF is based on Carrier Sense Multiple Access with Collision Avoidance (CSMA/CA) and operates in a listen before talk fashion; DCF is designed for time-bounded services. Compared to DCF, the optional PCF is a contention-free scheme using a central controller to schedule channel access [97]. Note, in the sequel only DCF is

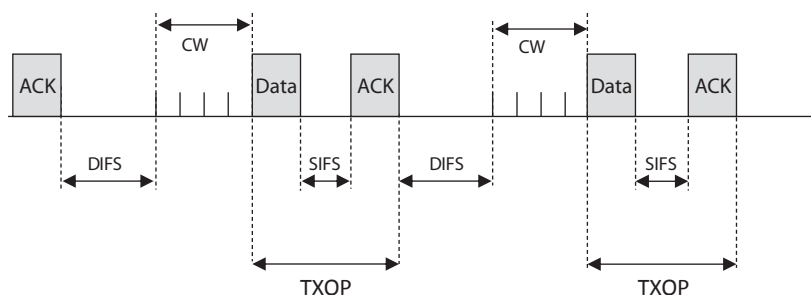


Figure 4.1: The 802.11 DCF protocol timeline. For each data frame transmission a back-off period precedes. The bounded time interval reserved for transmission is denoted as Transmission Opportunity (TXOP) using the 802.11e terminology.

highlighted as most of the current 802.11 technologies operate in DCF mode only. The timing of the DCF scheme is depicted in Figure 4.1. Essential for DCF is the so-called Contention Window (CW) which is maintained at each station. Based on the size of the CW a Back-off Counter (BC) is determined as a random integer drawn from a uniform distribution over the interval $[0, CW]$. Note, a station is allowed to transmit a frame if the channel stays idle during the so-called DCF Interframe Space (DIFS) time interval and if it subsequently remains idle during the followed-up back-off process. In addition, for each successful frame reception the receiving station immediately sends an ACK frame. Note that the ACK frame is transmitted after a Short IFS (SIFS), which is shorter than the DIFS, i.e. $DIFS = SIFS + 2 * Slottime$. To mitigate congestion the following mechanisms occur as part of DCF: a transmission failure causes the CW to increase in an exponential fashion; the other way around, the CW is decremented linearly in case of successful transmission (i.e. ACK reception).

4.3.2 IEEE 802.11e

Occurring 802.11e Mechanisms without Communication Errors

To support QoS the IEEE 802.11 Task Group E has defined 802.11e [98, 99] as an enhancement to the above-described legacy 802.11 technology. In addition, the current 802.11 standard (with 802.11e amendments) allows 20/40 MHz mode protection at the PHY layer in order to be compliant with legacy 802.11 systems [100] and entails automatic channel switching possibilities between channels. A maximum bandwidth width of respectively 22 MHz and 42 MHz is tolerated due to the extra 1MHz on each end that the channel is allowed to attenuate. At the 802.11e MAC link layer the Enhanced Distributed Channel Access (EDCA) protocol is defined to provide priority-based distributed channel access [101]. The EDCA is controlled by the HC (Hybrid Coordinator) - resided in the AP - and is developed to be compatible with the legacy 802.11 MAC protocol. Note, in literature [81] EDCA is also referred to as Enhanced (DCF), i.e. EDCF; moreover, according to the 802.11e terminology a data packet needs to be denoted as *QoS Data*. Under the EDCA, each channel access does not result necessarily in a single data frame transmission but more data frames are allowed in burst transmissions [102]. This

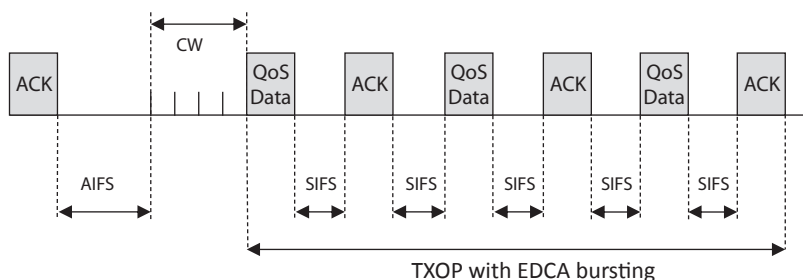


Figure 4.2: The 802.11e EDCA timeline. Using the 802.11e terminology, the MAC data units are denoted as *QoS data frames*.

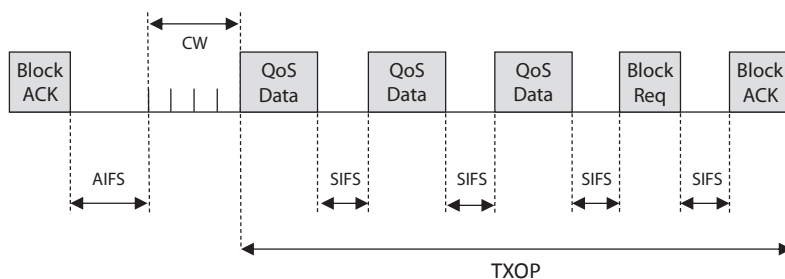


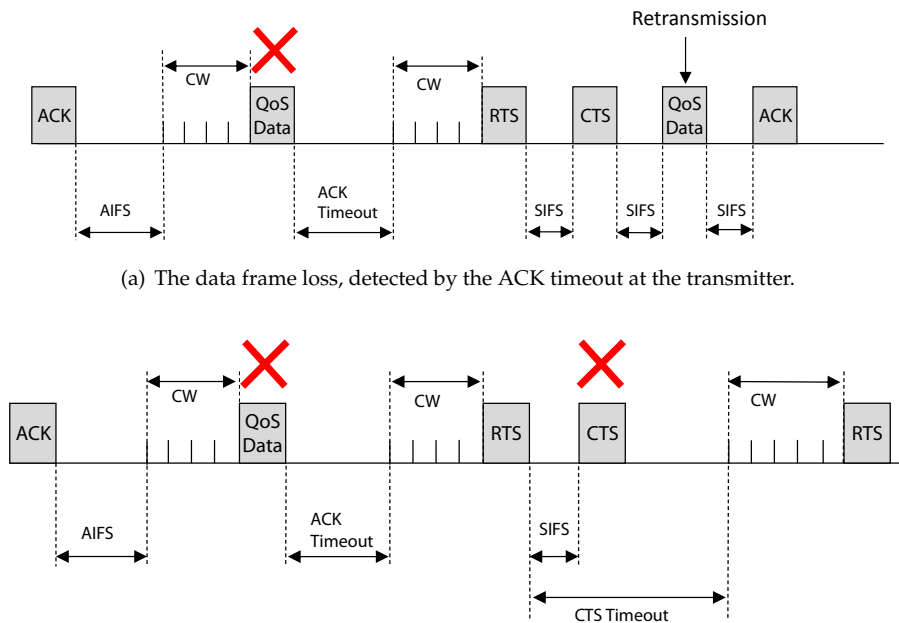
Figure 4.3: The IEEE 802.11e Wireless LAN with Block Acknowledgments. After a burst of consecutive data frames a Block Request frame is sent by the transmitter which in turn is acknowledged with a Block ACK frame by the receiver. The block ACK acknowledges the correctly received data frames from the preceding block.

means that a particular station - with gained channel access - has the right to initiate transmissions during the granted Transmission Opportunity (TXOP) time interval [103, 104, 105, 106]. In addition, another 802.11e parameter is defined: Arbitration Interframe Space (AIFS). Here AIFS is the legacy 802.11 DIFS equivalent, but its size depends on the frames/packet priority (note that AIFS is at least DIFS). Furthermore, in EDCA-TXOP mode the CW size is made significantly smaller than that for 802.11 DCF. The timeline of 802.11e communication in EDCA-TXOP mode is depicted in Figure 4.2. As a consequence, the higher throughput of EDCA-TXOP can cause jamming interference to other systems operating in the 2.4 GHz ISM band [107].

In highly congested wireless environments the 802.11e devices are allowed to switch transmission mode in order to increase throughput and reduce overhead, but this is not obligatory [108, 109, 110]. This is achieved by acknowledging several consecutive data frames with one response, i.e. a block ACK. The decision on the mode of transmission is made by the AP, and this can be set up within an ongoing TXOP transmission. The 802.11e block ACK feature is explained in Figure 4.3.

Occurring 802.11e Mechanisms with Communication Errors

The operation of 802.11e - with RTS/CTS protection enabled - in response to channel errors is the following. First the data frame losses are discussed which is depicted in Figure 4.4(a). A possible failed data transmission is detected by the sender due to the ACK timeout which in turn triggers a new back-off period. If the channel is sensed idle a RTS/CTS exchange is initiated which is followed up by the actual data retransmission. However, in a highly congested environment a subsequent RTS packet collision loss is not unlikely. The sender detects this by means of the CTS timeout mechanism so that another RTS packet can be queued for transmission. This in turn can lead to a number of consecutive RTS frames transmitted over the channel as illustrated in Figure 4.4(b).



(b) The RTS packet loss, detected by the CTS timeout mechanism. In a highly congested environment this can lead to a number of consecutive RTS frames.

Figure 4.4: The 802.11e features in conjunction with RTS/CTS to cope with channel errors.

4.4 Interference Mechanisms

The interference between 802.11e WLANs sharing the same radio channel is highlighted in this section. This is important before measurements in a live environment can be made in order to identify the interference mechanisms better from the live recordings. Interference mechanisms are investigated by performing measurements in a controlled environment. In order to determine the mechanisms that lay behind this type of interference a cross-layer approach is introduced comprising monitoring at both the PHY and MAC link layer.

4.4.1 Setup

The measurement setup consists of two 802.11e WLANs with network load, respectively denoted as the main network (first network) and the interfering network (second network). The measurements are set up in a controlled environment, i.e. a quiet environment without any nearby devices active in the 2.4 GHz ISM band.

To assess the interference influence of the second network on the main network RF monitoring and MAC link layer packet capturing take place simultaneously (see figure 4.5). In this setup we use passive methods for monitoring, i.e. the measurement setup only receives signals. The two networks are characterized in general terms as follows:

1. Main 802.11e WLAN network: a client streaming data from a server system at

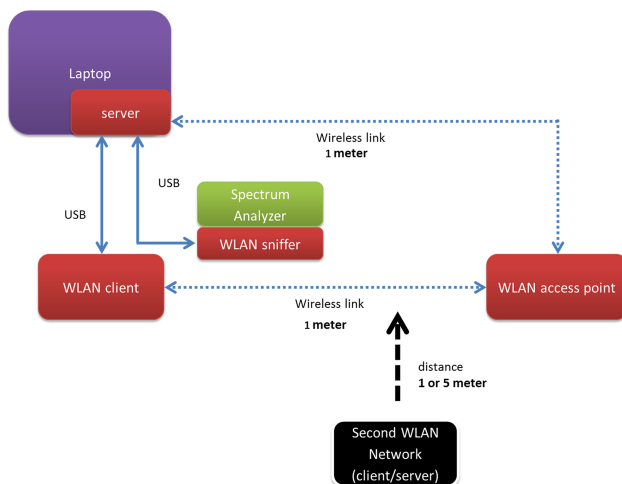


Figure 4.5: Measurement setup to assess the influence of an interfering network in a controlled environment

a fixed rate via the AP of network 1.

2. Interfering 802.11e WLAN network: positioned in range of the main network; data transmission takes place between a client at server through the AP of network 2 on the same WLAN channel as the main network.

The measurement equipment is located in the main network close to the client/server devices, since the influence of the interfering network on the main network needs to be assessed. The measurement equipment consists of:

- Packet sniffer: to capture raw packets on MAC link layer level.
- RF monitoring equipment: spectrum analyzer tuned to the 2.4 GHz ISM band.

Furthermore, to assess the level of interference certain performance metrics are required to determine service level degradation. At the MAC link layer level the following metrics are used: packet frame rate, retry rate (only defined for data and management frames), and subfields (e.g. RTS/CTS/ACK etc). In addition the measurement parameters associated to the setup are listed below:

- In the WLAN network the client, AP and server are within a radius of 1 meter.
- The AP (with 802.11e QoS support) operates at a maximum rate of 300 MBits/sec with 20/40 MHz protection mode enabled.
- The WLAN channel is set to channel 11: 2452 – 2472 MHz.
- Spectrum Analyzer: CRFS RFeye equipment [36].
- The field strengths are measured and depicted in dBm/Hz. The spectrum analyzer measures the spectrum every 200 ms at a frequency resolution of 4 kHz. For each frequency bin the instantaneous peak power is recorded.

- The packet sniffing software is custom-made, tailored to the specific monitoring needs.
- The sniffer application filters the frames by (destination) MAC address. So it allows to measure both the frames transmitted by the client and server.
- Data is transferred using the Unix network tool Iperf, and a session is set up between server and client devices.

Note that in this setup both server and client are connected to one laptop using virtualization software. In Iperf the UDP (User Datagram Protocol) mode has been selected instead of TCP (Transmission Control Protocol), because it allows to study the WLAN interference better. The reason for this is that TCP is supplemented with control algorithms that set back the frame rate to a lower level when the packet loss increases. This is not the case regarding the UDP mode - which is connectionless - and therefore gives a better understanding of the involved interference mechanisms.

4.4.2 Experiments

Using the measurement setup of Figure 4.5 two experiments are carried out. The conducted experiments are set up in order to investigate the impact of distance between two overlapping WLANs w.r.t. the service level. Here, in both 802.11e WLANs the QoS data rate between server and client is fixed to 170 frames/sec.

- Experiment 1: the interferer 802.11e WLAN at 1m distance.
- Experiment 2: the interferer 802.11e WLAN at 5m distance.

For both experiments the interferer traffic load is high, i.e. 424 frames/sec. In perspective, the maximum packet rate for IEEE 802.11g is around 2200 frames/sec.

4.4.3 Results

Experiment 1: WLAN interferer network at 1m

Regarding PHY layer, the monitoring results are depicted in Figure 4.6(a) (RF spectrum) and Figure 4.6(b) (RF occupancy). On the other hand, the MAC link layer monitoring results are shown in respectively Figure 4.7(a) (transmitted frames with destination client), Figure 4.7(b) (transmitted frames with destination server), and Figure 4.7(c) (transmitted frames from the interfering 802.11e WLAN). During the experiments no parameters have been changed, so the figures show behavior in time. Note that the that the occupancy has been determined by placing the threshold several dBs above the noise floor at -155 dBm/Hz.

- 0 – 20 seconds: the server data rate is at a normal level, i.e. 170 frames/sec. This also holds for the client with a similar ACK frame rate. The retry rate is nearly zero. The amount of QoS data load in the interferer network is very low.
- 20 – 80 seconds: period of congestion. The QoS data rate at the server drops gradually from 170 frames/sec to 50 frames/sec. The RF activity increases to occupancy values above 50%. In addition, there is an increase in the

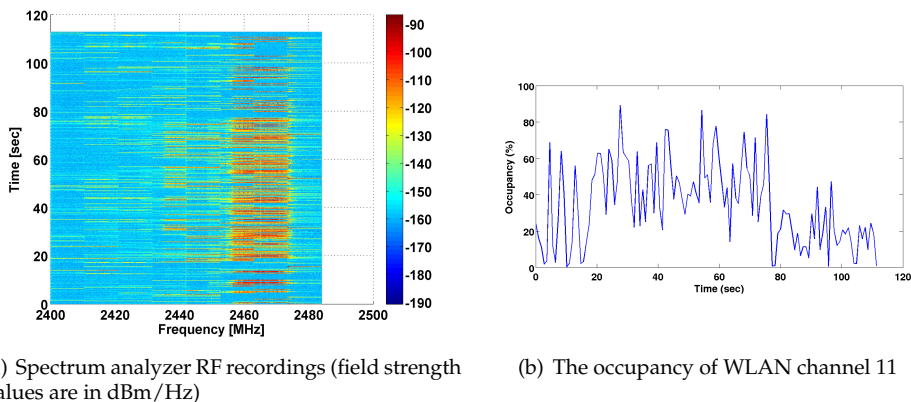


Figure 4.6: The RF spectrum monitoring results for experiment 1 with nearby interfering 802.11e WLAN at 1m. A rise in RF field strengths is visible during the period of high interferer activity, i.e. 20-80 seconds. Moreover, the extra bandwidth channel is visible in the spectrogram due to the 20/40 MHz protection mechanism.

number of retry frames in conjunction with a very strong drop of detected ACK frames to nearly zero. Besides, no RTS/CTS frames have been injected in the wireless medium by the server of the main network. However, a rise of RTS/CTS activity is measured coming from the interferer network (see Figure 4.7(c)). Thus it is likely that the interferer AP has initiated the RTS/CTS mechanism in order to mitigate interference; this according to the described 802.11 coexistence mechanisms in Section 4.3 , i.e. the main 802.11e WLAN network has been identified as hidden node. In a similar fashion an increase of (duplicate) 802.11e Block ACK frames is measured. However, the recorded amount of QoS data load in the interferer 802.11e WLAN remains nearly zero.

- 80 – 110 seconds: this period starts with a short peak (at 80 seconds) of QoS data in the main 802.11e WLAN which sets back to a rate of 170 frames/sec subsequently. In addition, the retry rate falls back to a minimum together with a low RF activity level of around 35%. The recorded QoS data rate of the interferer WLAN remains very low.

From the above-presented figures it can be concluded that the co-channel interference of a nearby second 802.11e WLAN network (at 1m) occurs in cycles of respectively activity and inactivity. This is in accordance with the experimental live results in [89] where the impact of overlapping WLANs on the aggregate AP throughput is recorded. During the active period this entails an initial strong increase of RTS/CTS frames. Next, the number of RTS/CTS frames falls back exponentially during this interval. This can be explained by the high number of occurring collisions with frames coming from the main network which in turn triggers the CSMA/CA mechanism of the interferer network to back off. However, the amount of traffic load from the interferer 802.11e WLAN is very high and has a jamming character which can be explained by the shorter CW interval due to the EDCA-TXOP transmission mode of 802.11e [98]. This is in line with the observations

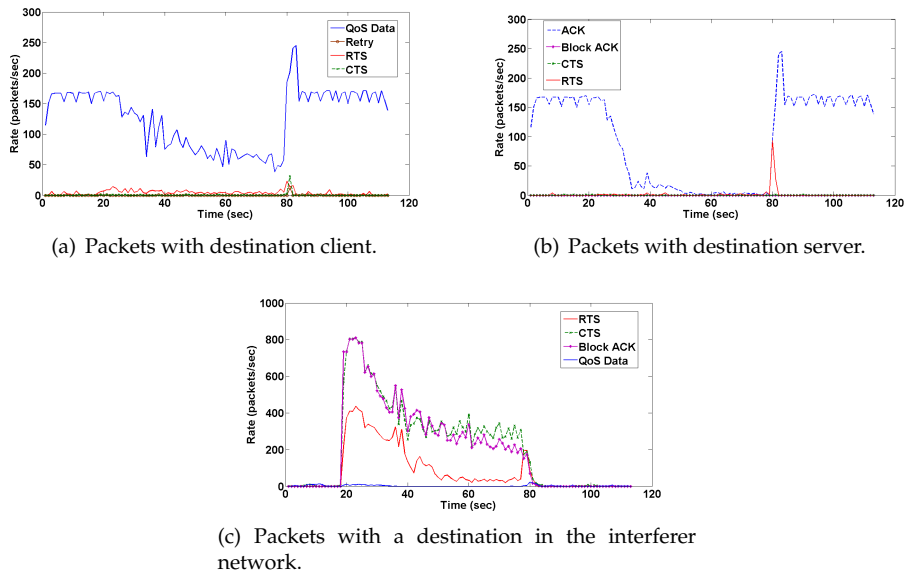


Figure 4.7: The MAC link layer monitoring results from experiment 1 with the interfering 802.11e WLAN at 1m. The impact of the interference network is visible mainly in the period 20-80 seconds. Here, the CTS and Block ACK frames in the interferer network are counted twice by the sniffer application because these frames are retransmitted by the AP and are not filtered as such.

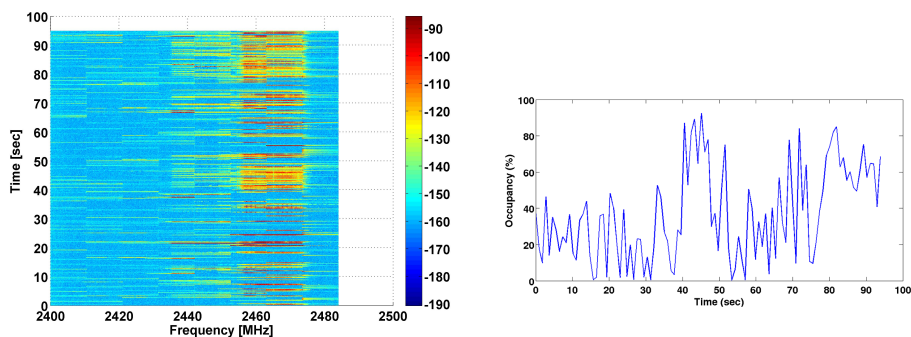
in [107] where the jamming impact of 802.11e is assessed.

During this period of congestion a strong increase of RF occupancy is observed in the spectrum occupancy plot in Figure 4.6(b) in conjunction with the use of an extra channel which leads to a total bandwidth of 40 MHz; this in contrast to the single 20 MHz channel mode employed in the cycle of interferer inactivity. However, according to [100] the 20/40 MHz protection mechanism has been developed to operate differently, i.e. switch to single channel 20 MHz mode in case of detected interference. In addition, there seems to be a second mechanism active, i.e. in the main network the retry rate increases due to the high load of RTS, CTS and Block ACK frames coming from the interfering network. This in turn triggers the CSMA/CA mechanism to back off which leads to a decline of QoS data injected by the server of the main network (see Section 4.3 describing the coexistence mechanisms).

Finally, it is observed that a period of high congestion can be identified by the high amount of respectively RTS, CTS and duplicate Block ACK frames. It turns out based on this experiment that Block ACK frames are a sign of congestion for 802.11e systems.

Experiment 2: 802.11e WLAN interferer network at 5m distance

In this experiment the 802.11e WLAN interferer network is positioned at a larger distance from the main network, i.e. at 5m distance. The configuration settings are



(a) Spectrum analyzer RF recordings (field strength values are in dBm/Hz)

(b) The occupancy of WLAN channel 11

Figure 4.8: Experiment 2: the RF spectrum monitoring results with interfering 802.11e WLAN at 5m. Two periods of congestion are visible, i.e. between 40-50 seconds and 80-95 seconds, by the higher level of RF field strength values.

similar to those in experiment 1. First, the PHY monitoring results are depicted in respectively Figure 4.8(a) and Figure 4.8(b), i.e. the RF spectrum and the spectrum occupancy of channel 11. Second, the MAC link layer monitoring results are shown in Figure 4.9(a) (packets with destination client), Figure 4.9(b) (packets with destination server), and in Figure 4.9(c) (packets with a destination in the interferer network).

- 0 – 40 seconds: the transmitted frame rate at the server is around 170 frames/sec in normal transmission mode; the same holds for the client rate (ACK frames). The average RF occupancy is below 40%. The packet loss in the network, i.e. retry rate, is negligible low.
- 40 – 50 seconds: the first period of congestion. A rise of RTS, CTS and Block ACK frames from the interferer 802.11e WLAN. At the start of this congestion period there is a peak in the number of RTS frames at the server. Subsequently the QoS data rate in the main network drops in conjunction with the ACK rate at the client site. In addition, the retry rate remains very low. Regarding the PHY layer, the RF activity is very high (> 80%) and an extra 20 MHz channel is visible in the spectrogram of Figure 4.8(a).
- From 50 – 80 seconds: QoS data frame rate at a normal level in the main network; the same holds for the ACKs at the client site. The number of RTS, CTS and Block ACK frames drops - compared to the preceding period of congestion - but is still present at a significant high level (peak rates: 150-200 frames/sec). In addition, it is observed from the data readings that the recorded QoS data - injected by the server of the interfering 802.11e WLAN - occurs in EDCA-TXOP block burst mode. Regarding PHY layer, there is a decline in RF activity but the occupancy level is significantly higher compared to the period 0 – 40 seconds.
- From 80 – 95 seconds: the second period of congestion. A rise in the number

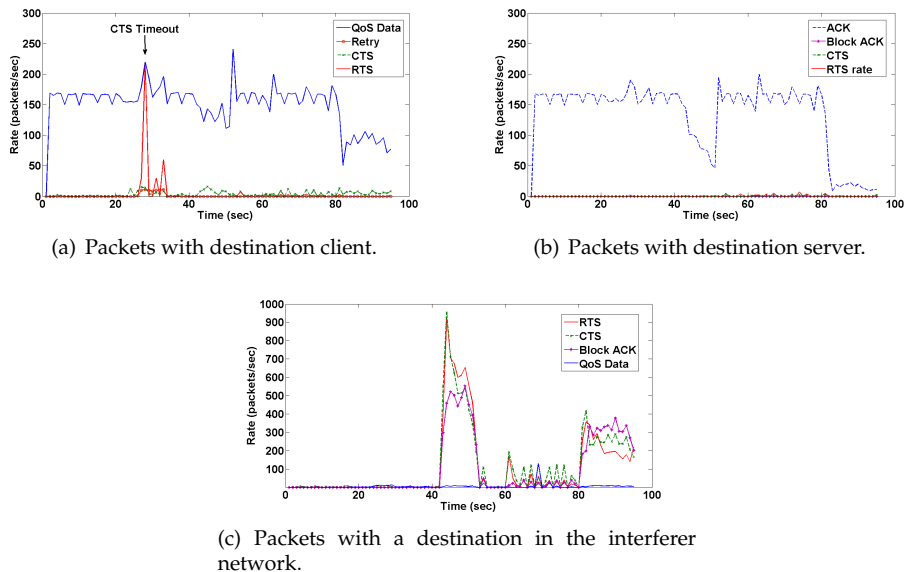


Figure 4.9: The MAC link layer monitoring results from experiment 2 with the interfering 802.11e WLAN at 5m. The impact of the interference network is visible mainly in the periods 40-50 seconds and 80-95 seconds. Here, the CTS and Block ACK frames in the interferer network are counted twice by the sniffer application because these frames are retransmitted by the AP and are not filtered as such.

of RTS, CTS and Block ACK frames occurs in the interferer 802.11e WLAN up till a level of 500 frames/sec. However, this is half the amount compared to the first period of congestion. On the other hand, the decline in QoS data and ACK frames is more significant compared to the first period of congestion. The RF occupancy is in the range of $\{50\% - 80\}$, i.e. significantly lower compared to the first congestion period.

In general, the impact of an overlapping co-channel 802.11e WLAN at 5m distance is comparable to the 1m case. Similarly, the interference network shows cycles of respectively activity and inactivity for the aggregate AP throughput. During these active cycles the service level of the main network degrades to a lower level, i.e. the QoS data rate drops by half the amount. This is in line with [90] where experiments show that the impact on the aggregate throughput is irrespective of distance as long as the WLANs are in carrier sense range of each other.

In accordance with the analysis of coexistence mechanisms in Section 4.3, the experimental results show the CTS timeout mechanism which occurs at the start of the congestion period as depicted in Figure 4.9(a). Additionally, according to the experiments the influence of interferer distance on the service level is limited but still perceptible. Key is that due to higher separation distance, i.e. 5m instead of 1m, the channel is more often sensed idle. This means that more timeslots are available to initiate transmissions for the interferer 802.11e WLAN. This is visible in the period $\{50 - 80\}$ seconds where the level of RTS/CTS frames - injected in the

network by the interferer 802.11e WLAN - is higher compared to the 1m case. In addition, to capture channel access the 802.11e block burst transmission mechanism becomes active at the interferer AP. Note that the moderate level of RTS/CTS packets from the interferer does not harm the QoS data rate during this interval. However, the moderate RTS/CTS load causes the CW to be adjusted to a larger size for both WLANs. As a consequence, in the subsequent period of congestion the interferer network injects RTS and CTS packets at a lower rate into the wireless medium. Note that this is also the case for the amount of QoS data injected by the server of the main network, i.e. visible as strong steep drop of QoS data in Figure 4.9(a).

4.5 Live Measurements

In this section the setup and the results are presented of measurements in a live environment.

4.5.1 Setup

A modified measurement setup has been used compared to the setup employed in the interferer measurements. Three WLAN sniffers are used in parallel to analyze the packets on channel 1, 6 and 11. The setup is shown in the Figure 4.10. Compared to the interference measurement modifications have been made to monitor all packets and distinguish between packet types (data/management/control). Besides, the monitoring system runs for a longer period of time to obtain a better estimate of the packet type statistics at a particular location. In addition, the measurement setup is installed in a live environment, i.e., no controlled conditions.

4.5.2 Experiments

Three live situations have been evaluated: college room, office room and city center. The first location, a college room, was selected because it is a very crowded place

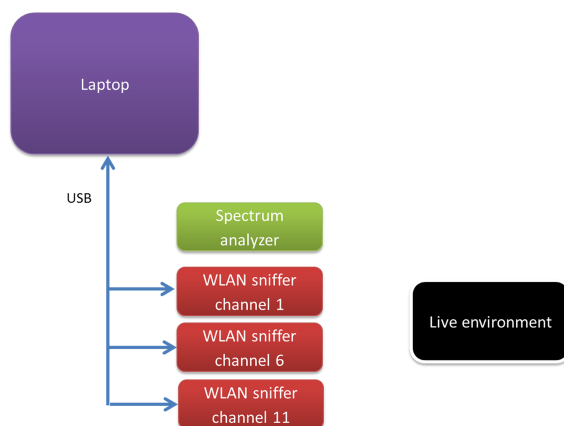


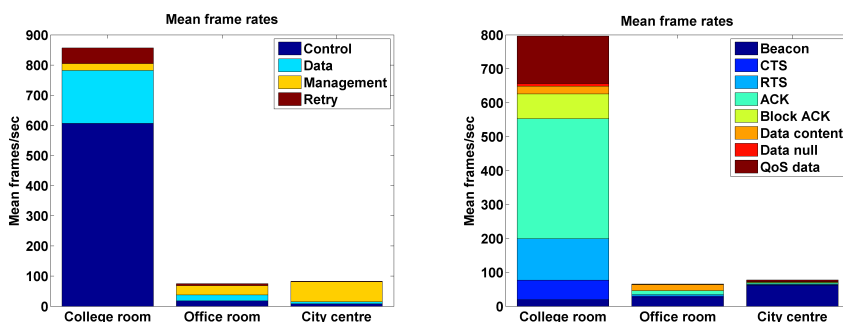
Figure 4.10: The measurement setup for the live recordings

with a large population of WLAN devices in one room. Furthermore, in the college room also experiments take place of which some of them use Bluetooth and/or WLAN connections. The second location, an office room, is selected as this is a location which consists of managed WLAN access points, similar to the college location. Finally, the third location, the city center, was selected as this is a place with unmanaged WLAN access points. Moreover, the place is known for WLAN problems on certain channels.

4.5.3 Results

Figure 4.11(a) shows the mean number of frames per second per location. It has been split up into management, control, data and retry frames. First of all the results show that the college room location has most of the traffic which is due to measurements that were carried out during a college with 75 to 100 students. Secondly in this location about 70% of the traffic are control frames and roughly 21% is actual data traffic. Figure 4.11(b) depicts the same locations, but here the frames are split up into the most important subfields. Retry frames and less frequent subfield packets are omitted from this figure. This figure reveals that most of the control frames are ACK and Block ACK packets. Note that the results are in line with the conducted experiments in Section 4.4.3; here high amounts of Block ACK frames are detected for 802.11e WLAN systems in times of high congestion due to overlapping WLANs.

In addition, Figure 4.11(b) reveals that only 21% are actual data packets, which is in line with the research conducted by [12]. Moreover, we observe that most of the data frames are QoS frames (16%). This type of frame indicates the use of 802.11e WLAN communication which is more dominantly present compared to the legacy 802.11 WLAN systems (indicated by the regular data content type). Also the figure shows that almost 20% of all traffic are RTS/CTS frames. This means that there is significant interference, probably due to the many WLAN devices. This is also depicted by the retry frame rate (7%) in Figure 4.11(a). At the office location the mean frame rate is much lower, the actual data frame seems to be similar to the college location, but there are almost no ACK frames. Also the beacon rate is about



(a) The occurrence of the different type of packets (b) The occurrence of the different subtype of packets

Figure 4.11: Results for live measurements on three different locations.

twice the rate as at the college location. One explanation for this is that in the office location more WLAN networks were active. In the city center, most of the traffic consists of beacon frames.

College Room Location. The measurements carried out in the college room are most interesting and highlighted below in more detail. These measurements were performed during a college which ended around 1400 seconds. Figure 4.12 shows the RF spectrum. This is followed by figures showing the occupancy in Figure 4.13(a), the subfield type versus time in Figure 4.13(b), and the figure showing the cumulative probability curves for the different types of frames in Figure 4.13(c). The figures are depicted for channel 1 where during the measurement 119 WLAN devices were identified. The other channels show similar behavior, and for brevity these results are omitted.

From Figure 4.13(b) it can be seen that the WLAN traffic is very spiky as expected. Interesting enough, when the college ends (at 1400 seconds) a sharp downwards transition is observed in the RF channel occupancy of Figure 4.13(a). Moreover, at this particular moment the occupancy drops from values around 65% to 20%. The RF monitoring results are supported by the experimental results in Figure 4.13(b) which shows high traffic in the first monitoring interval (i.e. 0 – 1400 seconds) and a significant lower traffic load in the second monitoring interval of 1400 – 2100 seconds. The first interval entails high amounts of RTS and Block ACK frames which is not the case for the second interval. Another observation is that the amount of legacy 802.11 data packets is more strongly present during the second monitoring interval in Figure 4.11(b). However, the amount of ACK frames seems to be steady throughout the entire monitoring session (0 – 2100 seconds). Interesting, the results in Figure 4.13(b) roughly indicate that most of the traffic in the highly congested first interval comprises 802.11e traffic which tends to capture channel access. On the other hand, the second interval shows a rise in the legacy 802.11 traffic whereas the portion of 802.11e QoS data and RTS/CTS is considerably low.

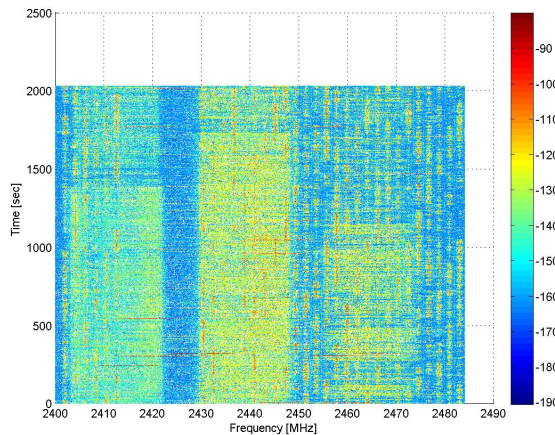
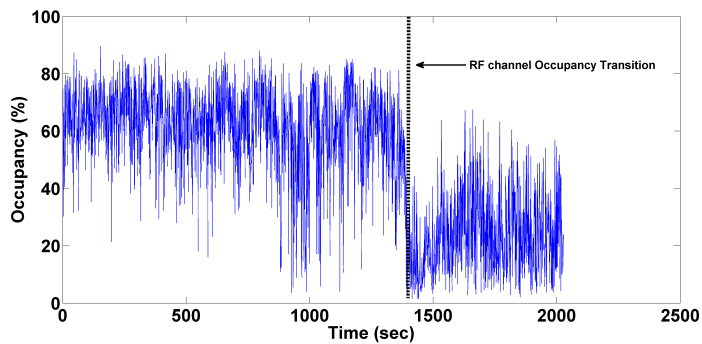
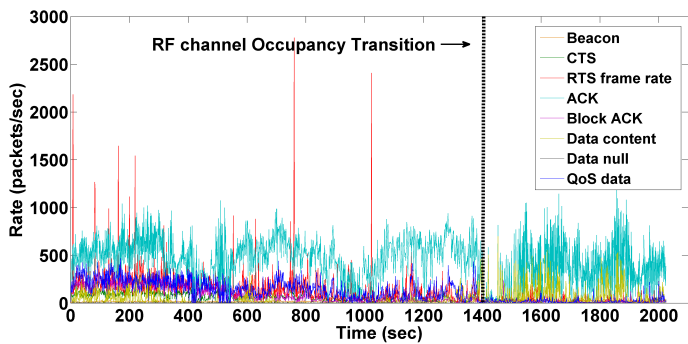


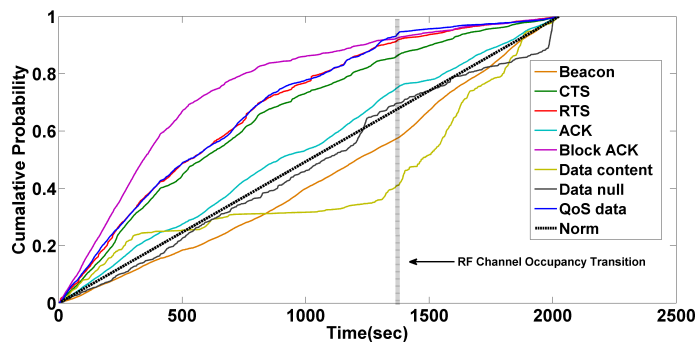
Figure 4.12: RF monitoring results for live measurements in a crowded college room (Field strength values in dBm/Hz).



(a) Occupancy of channel 1. At 1400 seconds a significant drop in RF occupancy occurs which is marked by the *transition landmark*.



(b) Individual packet rates on channel 1.



(c) The CDF curves for the different packet subtypes on channel 1.

Figure 4.13: Results for live measurements in a crowded college room on channel 1. The college ends at 1400 seconds. In the first interval of high congestion ($\{0 - 1400\}$ seconds) most of the traffic load is associated with 802.11e WLANs which comprises RTS, QoS data, and Block ACK frames. In the second interval ($\{1400-2100\}$ seconds) most of the traffic entails the legacy 802.11 type of frames, i.e. data content and ACK frames.

To give more insight in the time characteristics the Cumulative Density Function (CDF) curves in Figure 4.13(c) are provided. Here, as a comparison metric, the norm curve represents the situation of constant offered traffic load over time. This figure shows that the QoS data, RTS, CTS and Block ACK CDF curves are constantly positioned above the norm curve. Moreover, the cumulative probability of these packet types is above 80% at the 1400 seconds landmark. On the other hand, the legacy 802.11 data CDF curve displays a flat characteristic during the first interval of high congestion together with a cumulative probability of only 35% at 1400 seconds. However, a steep increase of this type of data packet is observed in the second interval. Thus in line with [107] it seems that 802.11e QoS stations capture the wireless medium in case of congestion, i.e. many WLAN stations. Moreover, this coincides with high amounts of RTS/CTS and Block ACK packets which are therefore good indicators of 802.11e induced congestion. This is confirmed by the sniffer readings which show that the QoS data packets are transmitted in blocks bursts.

4.6 Conclusions

In this chapter we have analyzed the spectrum utilization and congestion of 802.11 networks in the 2.4 GHz ISM band. It can be concluded that it is possible to assess the service level. This approach can be applied to other frequency bands where 802.11 technology is deployed such as the 5 GHz band. A cross-layer approach is provided to measure the spectrum utilization and congestion in this band. For this purpose it turns out that packet sniffing allows to identify congestion and that on the other hand spectrum sensing allows to identify utilization. Two situations are investigated using the latter techniques for monitoring.

First, results are presented on the impact of interference between 802.11e WLAN networks sharing the same radio channel in a controlled environment. The results show that the interfering network leads to severe congestion on the wireless medium which in turn occurs in cycles of respectively inactivity and activity. The situation of interferer activity, i.e. congestion, is caused by the RTS/CTS mechanism since the 802.11e WLAN networks often seem to identify each other as hidden nodes. Finally, the conducted experiments in a controlled environments show that the impact of overlapping 802.11e WLANs is relatively irrespective of distance, as long as the WLANs are in the carrier sense range of each other.

Secondly, monitoring sessions in real uncontrolled environments illustrate that only a small portion is actual data traffic. For instance, the live recordings taken in a college room - a location with up to 100 people - indicate that a significant number of packets is classified as control packets (e.g. RTS/CTS), where in turn the number of actual data content packets is quite low (less than 21%). This is in line with the conducted experimental results of the controlled environment, showing that RTS/CTS significantly degrades the performance when two networks are in range of each other; in addition, Block ACKs are identified as a good indicator of congestion in 802.11e WLAN environments. Moreover, the live readings show that 802.11e WLANs typically capture channel access over legacy 802.11 systems, e.g. by using data block burst transmissions. At two other locations, i.e. an office room and a city center site, the traffic mainly consists of management packets and

control packets. It can be concluded that the WLAN devices cannot properly handle interference of other IEEE 802.11(e) networks, which leads to very inefficient use of the radio spectrum. Thus there is room for more efficient use of the radio spectrum. Further research is needed how this commodity wireless standard can be made more efficient.

4.6.1 Future Research

It turns out that interference mechanisms are complex and often unexplored in practical situations. Therefore the following topics are interesting for further research. First it is interesting to look at the mechanisms causing interference between WLAN clients of the same network due to packet collisions. Secondly, many open questions remain regarding the interaction between 802.11e and legacy 802.11 systems with respect to for instance overlapping WLANs, e.g. the high amount of Block ACKs and the 20/40 MHz protection mode operation. Moreover, additional research could aim at many WLAN networks on the same channel, and interfering WLAN networks on adjacent overlapping WLAN channels. Thirdly, it is interesting to investigate how the packet rate on the MAC link layer and the spectrum utilization are related and whether an analytical expression can be provided. The analysis may take into account the different packet sizes that are possible (e.g. an ACK packet is in general significantly smaller than a data content packet). Finally, to improve on the 802.11(e) standard we recommend adjustments w.r.t. to the RTS/CTS protocol in order to cope with the high amount of RTS/CTS packets once two APs are in range of each other. In line with this, we recommend further inspection of the CSMA/CA protocol so that neighboring APs could share the channel more fairly including improvements on the back-off procedure.

Chapter 5

IEEE 802.11: Impact of Different Types of Interference Sources

5.1 Introduction

The number of wireless devices (smartphones, laptops, sensors) that use the 2.4 GHz ISM band is rapidly increasing. In many urban areas not only many Wi-Fi networks can be found, also other systems such as Bluetooth, Zigbee, microwaves and wireless A/V transmission systems use this band. On the other hand there is only a limited amount of spectrum available. So it is very likely that interference between systems in this band will occur. Due to the rapid increase of wireless devices, interference is expected to become even more important. In this chapter we address this issue by providing measurement results where the performance degradation of a Wi-Fi communication link due to a nearby interferer source has been measured. For this purpose we have implemented a setup to analyze both the spectrum (physical layer) and data packets (link layer) in the Wi-Fi communication link. Spectrum sensing can be used to measure the utilization of a Wi-Fi channel. Moreover each wireless communication standard has its own RF signature, so spectrum sensing can also be used to identify the interferer source. Although the utilization of a band can be analyzed it is still unknown what the quality is of the wireless link. To measure the quality and to know if there is congestion, data packets have to be analyzed. Here the retry rate and the number of control frames, used to manage the wireless link, can be used for this purpose. In addition, the interference models are extrapolated town-wide to assess the performance of WLAN technology rolled out in urban areas.

The chapter is organized as follows. First, Section 5.2 provides theoretical background and related work on monitoring Quality of Service (QoS). In Section 5.3 the measurements setup for experiments in a controlled environment is described and the associated monitoring results are presented for both PHY and link layer. In addition, in Section 5.4 interference results for an urban environment are provided with an extrapolation model to assess the QoS of 802.11 technologies on a town-wide scale incorporating interference. Finally, Section 5.5 concludes the chapter.

5.2 Monitoring Quality of Service

The OSI protocol stack of the IEEE 802 standard consists of five layers where the lower two layers involve the wireless aspects of communication, *i.e.* the PHY layer and the link layer. In addition, at the link layer all WLAN technologies are based on Carrier Sense Multiple Access (CSMA) which in turn can rely on different implementations of the Clear Channel Assessment (CCA) detection algorithm, *e.g.* energy detection; as a drawback CCA algorithms are typically not designed to handle interference [111]. This makes WLAN link layer in particularly vulnerable to interference, *i.e.* packet transmissions can be deferred if the interference signal adequately resembles a WLAN signal. To assess the overall Wi-Fi QoS the monitoring must take place at the lower two layers as these layers are responsible for the wireless link. At the PHY layer this entails a threshold-based approach to determine spectrum occupation. On the other hand, at the link layer the total frame rate and retry frame rate have been found to be good parameters for quantifying the level of utilization and network degradation [12]. In addition, monitoring of the proportions of the different link frame types can be used to monitor the overhead in a Wi-Fi network, *i.e.*, data, management and control (*e.g.* Request To Send (RTS), Clear To Send (CTS), and Acknowledgment (ACK)) frames.

Not much related literature has been found. First, in [12] a description of the overall Wi-Fi QoS monitoring is provided by Mass Consultants commissioned by the British regulator Ofcom; here monitoring takes place at various locations in the UK and live readings are obtained. Furthermore, in [83] the total QoS is assessed using a cognitive radio approach. However, the impact of interference and coexistence issues are not addressed in [12, 83].

5.2.1 Performance Evaluation of 802.11 with Interference

Much of the literature on coexistence issues is focused on Bluetooth interference only addressing interference mitigation in the 2.4 GHz ISM band. Here, the basic mechanism to mitigate interference between Bluetooth and other technologies is Frequency Hopping Spread Spectrum (FHSS). This entails Bluetooth transmissions to take place in an ad hoc fashion using frequency hopping (1600 hops/sec) between 79 channels of 1 MHz each. However, coexistence between Bluetooth and IEEE 802.11 remains an important issue and because of its relevance the IEEE 802.15 Working Group has set up the Task Group 2 (TG2), which is engaged in the development of coexistence mechanisms [112]; here two classes of coexistence mechanisms have been defined: on one hand collaborative techniques *e.g.* Time Division Multiple Access (TDMA) and on the other hand non-collaborative techniques such as Adaptive Frequency Hopping (AFH). Here, collaborative in the sense that interfering entities are required to explicitly exchange information to attain mutual coordination. Furthermore, note that owing to the AFH mode the degradation of Wi-Fi systems due to Bluetooth is expected to be lower when compared to systems lacking such mechanisms (*e.g.* A/V transmitters). A performance analysis of Bluetooth interference without AHF on IEEE 802.11b/g/n systems is provided in [113, 114, 115] showing packet losses up till 25%. An extensive evaluation of Bluetooth interference in AFH mode on IEEE 802.11g systems is described in [116] with packet losses up till 7%.

Another important source of interference are microwave ovens introducing wide-band interference throughout the 2.4 GHz ISM band. Experimental studies are conducted on microwave oven interference in [115, 117, 118, 119] describing mainly the spectrum characteristics and detection/mitigation issues on the PHY layer. In [114] a theoretical framework is provided including a microwave simulation model; here it is shown for instance that a 600W microwave produces worse case up till 10% packet loss for a Wi-Fi traffic load of $\lambda_w = 0.1$.

There is another important interference source classified as jamming [111, 120], *e.g.* A/V transmitters. Experimental studies show the severe impact of jamming as a 3 dB increment in signal interference power causes an increase in Packet Error Rate (PER) from 0% to 30%. The jamming interference is a continuous narrow band signal which deteriorates the Orthogonal Frequency-Division Multiplexing (OFDM)-modulated symbols of the IEEE 802.11g/n systems but on the other hand also leaves many carrier frequencies intact. However, the performance of the connection degrades very quickly and the different coding rates and modulation methods show no effect on the jamming tolerance. Furthermore, in [111] the interference power levels are incremented so that jamming terminates the Wi-Fi connection at a Signal-to-Jammer Ratio (SJR) of -1 dB for OFDM.

5.2.2 Contributions

The main contributions are:

- A measurement setup to assess the congestion and spectrum utilization of the 2.4 GHz ISM band by simultaneously monitoring on both PHY and link layer; this setup is novel, not found in literature. Moreover the tool can be applied to any interferer source.
- The behavior of the PHY and link layer mechanisms in a controlled environment under different interference conditions, *i.e.* A/V transmitter, microwave and Bluetooth.
- The performance of 802.11 technologies in an urban environment for different interference sources; the measurement result are extrapolated on a town-wide scale to determine the performance of 802.11 technologies once rolled out in urban areas.

5.3 The 802.11 Interference Results in Controlled Environments

5.3.1 Measurement Setup

In this setup we use passive methods to monitor the influence of an interferer source (see Figure 5.1) in a controlled environment. Passive means that the measurement setup only receives signals. For the experiments a connection is set up between Wi-Fi client and Access Point (AP) to start with; the same holds for the Wi-Fi server and AP. In addition, a network load is applied in the network between server and client. Next, monitoring is activated which entails on one hand logging Wi-Fi packets

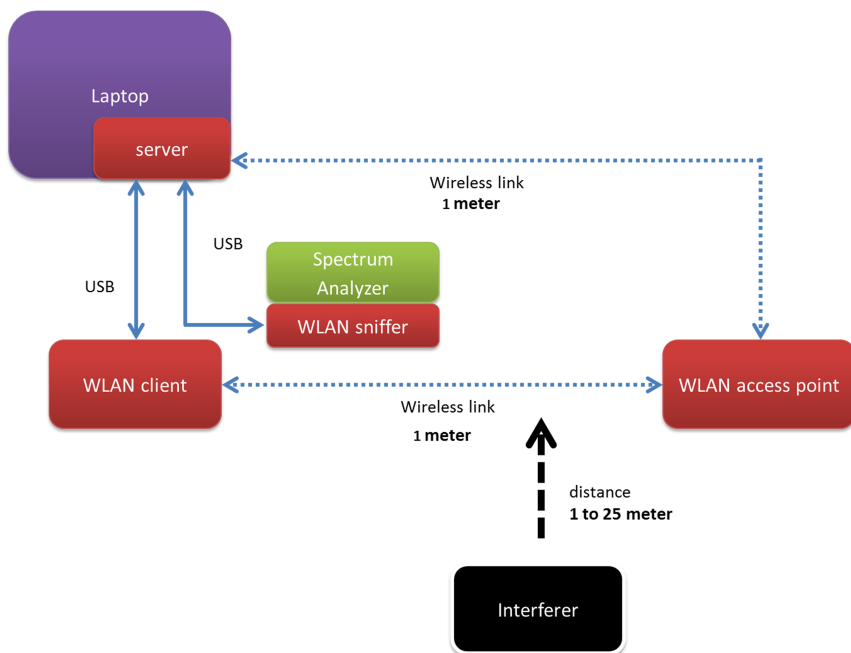


Figure 5.1: The measurement setup for simultaneously monitoring PHY and link layer performance.

by applying packet sniffing software and on the other hand - simultaneously - monitoring the 2.4 GHz ISM band by employing the CRFS spectrum analyzer. While monitoring is ongoing the influence of the interference source can be investigated; this is an extension of the UK survey [12]. The influence is assessed for three different interference sources using this setup, *i.e.* A/V transmitter, microwave, and active Bluetooth devices. The details regarding the measurement configuration are listed below:

- The measurement setup is deployed in a quiet controlled environment (*i.e.* abandoned building in remote area) without any nearby devices active in the 2.4 GHz ISM band.
- In the Wi-Fi network client, AP and server are within a radius of 1 meter.
- The AP transmits in 802.11g mode.
- The field strengths are measured and depicted in dBm/Hz. The CRFS equipment measures the spectrum every 200 ms.
- The sniffer application filters the packets by link destination address. So it allows to measure both the raw packets transmitted by the client and server. The sniffer software is specially developed for this purpose.
- To generate the Wi-Fi traffic data between client-server the Iperf open source tool is used.

- CRFS settings: a frequency sweep between 2400 – 2483.5 MHz with a resolution of 4 kHz.
- Wi-Fi channel 11: 2452 – 2472 MHz is used.

Note that in 802.11g mode a typical throughput of 3.1 Mbyte/sec is possible for the user. This results in around 2100 data frames/sec. In our experiments we offered Wi-Fi traffic load of around 10%. Moreover, as transport layer protocol UDP mode was chosen instead of TCP, because it allows to study the Wi-Fi interference better. The reason for this is that TCP has control algorithms that set back the frame rate to a lower level, when the packet loss rate increases. Moreover, UDP is connectionless and the PER could be easily measured. It should be noted that both UDP and TCP packets will be retransmitted when they are lost.

5.3.2 Results

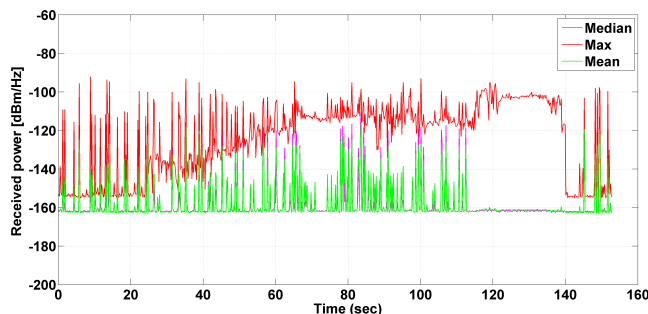
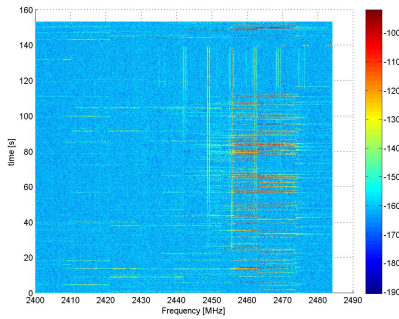
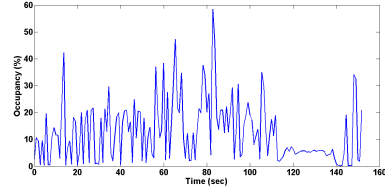


Figure 5.2: The mean (green curve), median (purple curve), and maximum signal strengths (red curve) as function of time. Here the maximum curve corresponds with the A/V transmitter signal's power, whereas the median and mean curves relate to the Wi-Fi signal power.

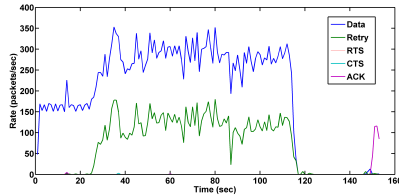
A/V Transmitter Interference. Using the described measurement setup the A/V transmitter interference (*i.e.* jamming) experiment is carried out. To investigate the Wi-Fi QoS as function of interference source power the A/V transmitter is first positioned at large distance (25m) from the client/AP; in a gradual continuous manner the A/V transmitter is moved in direction of the client/AP. Note that due to the indoor structure of the measurement environment the interference power level is used as performance metric for monitoring QoS instead of distance. To start with the A/V transmitter is turned on after 20 seconds of monitoring which is visible in the RF statistics plot depicted in Figure 5.2. From that point onwards the A/V transmitter is approaching the client/AP and this is visible in Figure 5.2 by the slope of the maximum received power curve indicating an increase from -155 dBm/Hz to -100 dBm/Hz. After 115 seconds of monitoring the nearby A/V interferer enforces the Wi-Fi connection to breakdown at a SJR of -1 dB due to the high level of jamming interference power of almost -100 dBm/Hz (at a distance of around 10m). A period of Wi-Fi inactivity follows until the A/V transmitter is manually turned off (at 140 sec) which triggers the Wi-Fi network to automatically



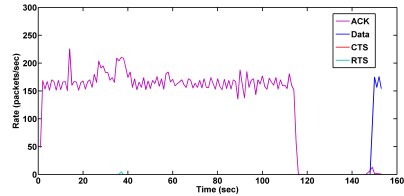
(a) PHY layer: spectrogram (received power in dBm/Hz).



(b) PHY layer: spectrum occupancy of WLAN channel 11



(c) Link layer: the transmitted packets with destination client.



(d) Link layer: the transmitted packets with destination server.

Figure 5.3: The A/V transmitter interference experiment: PHY and link layer monitoring results carried out in parallel. In the spectrogram the A/V transmitter signals are visible as narrow-band vertical artifacts

restore the connection after 142 seconds of monitoring. The RF monitoring results depicted in the spectrogram of Figure 5.3(a) and its corresponding occupancy plot in Figure 5.3(b) provide the following information: the active A/V transmitter can be identified in the spectrogram by narrow-band artifacts in vertical direction starting at 20 seconds; furthermore the figures clearly show Wi-Fi activity on channel 11 till the moment of network breakdown. According to the link layer observations in Figure 5.3(c) and (d) both server and client communicate at a rate of 170 frames/sec in normal transmission mode; in addition, whilst the A/V transmitter is turned on the retry rate increases to a level of 150 frames/sec and inherently the data frame rate increases by the same amount as shown in Figure 5.3(c). On the other hand, the ACK packet rate remains solid around a rate of 170 frames/sec (see Figure 5.3(d)) which indicates the eventual successful transmission of data frames. This process continues till network breakdown indicated by a sharp downwards transition of data frame rate in Figure 5.3(c). The results are compared with the experiments conducted in [111] which show a connection breakdown at a SJR of -1 dB and the similar narrow-band artifacts are observed in the RF spectrum. However, the Wi-Fi QoS at the link layer is beyond the scope of [111] and cannot be compared.

Microwave Oven Interference. In this experiment a microwave oven is used as interference source which is placed at one meter distance from the client/AP whilst it heats up a glass of water. Similar as for the A/V transmitter experiment the

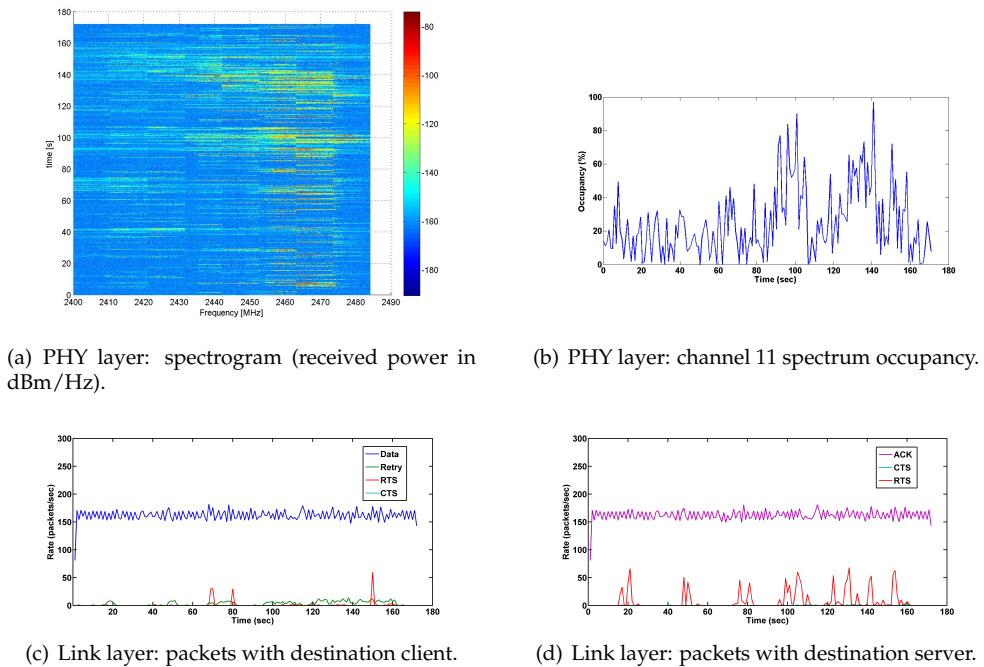
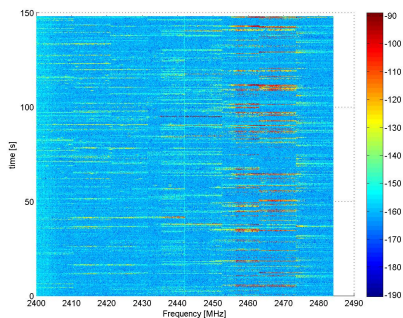


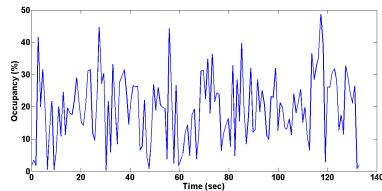
Figure 5.4: Monitoring results using the microwave oven as interference source. In the spectrogram the increased level of microwave interference is visible by the rise in wide-band signal level as function of time.

Wi-Fi QoS is assessed as function of interference power level, *i.e.* the mode of the microwave is shifted up from mode 1 to 5 (till 700 Watt). The microwave influence is displayed by the lifted levels of signal strengths throughout the 2.4 GHz ISM band depicted in the spectrogram of Figure 5.4(a) and in the occupancy plot of Figure 5.4(b). This effect is best illustrated for the two highest modes (from 82 - 110 seconds and from 110 - 160 seconds). Regarding link layer monitoring, Figure 5.4(c) shows the microwave impact during the two highest modes of interference, *i.e.* the retry rate is at a significant higher level of 6.95% (amount of packet loss). Furthermore, Figure 5.4(d) shows peaks in the RTS/CTS curve - occurs irrespective of the mode - once the microwave oven is activated. The Wi-Fi QoS monitoring results at the link layer are in line with the simulation model in [114] under comparable conditions, *i.e.* a 600W microwave at 0.5m, $\lambda_w = 0.1$.

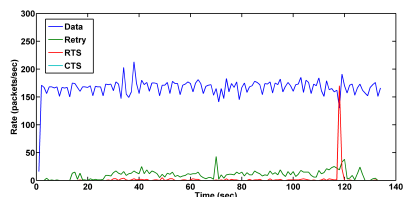
Bluetooth Interference. The influence of an active Bluetooth connection is tested in an experiment where an unidirectional data transfer at 1 Mb/sec between two v2.0 Bluetooth devices; both devices are within 1 meter of each other. Interference experiments are carried out with Bluetooth interference at distances ranging from 1m to 15m and monitoring results show distance independent characteristics (see [113]); for this purpose one particular experiment is highlighted, *i.e.* Bluetooth device communication at 1m distance from client/AP. Here Bluetooth is switched on from 15 seconds to 130 seconds of monitoring. Regarding the RF spectrum readings, artifacts are visible scattered throughout the spectrum in Figure 5.5(a) once Bluetooth



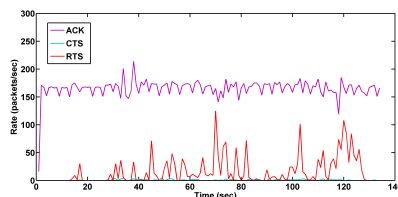
(a) PHY layer: spectrogram (received power in dBm/Hz).



(b) PHY layer: channel 11 spectrum occupancy.



(c) Link layer: packets with destination client.



(d) Link layer: packets with destination server.

Figure 5.5: Monitoring results for Bluetooth interference. In the spectrogram the Bluetooth interference is visible by the scattered artifacts due to the FHSS hopping mechanism

is turned on, *i.e.* frequency hopping becomes active and deploys the entire 2.4 GHz ISM band. However, the channel occupancy of the active Wi-Fi channel is low (*i.e.* less than 50 percent) and thus is affected only to a small extent by the ongoing Bluetooth communication as shown in Figure 5.5(b). This is in line with the link layer results in Figure 5.5(c) which show a low retry rate and an unaffected data frame rate; note that Figure 5.5(d) shows a rise in RTS/CTS traffic once Bluetooth becomes active. Regarding the link layer, the 7% average packet loss (*i.e.* retry rate) is identical to the experiments in [116] where an experiment is carried out with an AFH-enabled Bluetooth interference source positioned at 1m distance. Note that the focus in [116] is not on overall QoS, thus the other monitoring results cannot be compared.

5.4 The 802.11 Interference Results in Urban Environments

In what follows, the impact of interference on 802.11x technologies is investigated in an urban environment instead of in a controlled environment. This means that radio measurements are performed in a representative street environment to validate and refine the theoretical RF model which entails the performance evaluation of different 802.11x technologies for different devices. The influence of both Adjacent Channel Interference (ACI) and Co-Channel Interference (CCI) has been measured

for different interference sources such as Bluetooth, video senders and WLAN devices. Further, as performance metric the data frame rate is used while omitting the different types of packets for monitoring QoS. However, note that the 802.11e extension was not included in the full 802.11 standard at the time the measurements were conducted. Following up, the description is provided regarding the test environment measurements. First, tests recordings for data and video services were carried out using Dell/Sony laptops and Toshiba PDAs, 02 XDA II. The services tested on these devices were browsing, FTP upload/download and video streaming. Voice service was tested using HTC Tornado mobile phones and PDAs with the Skype application. Belkin and Netgear kits were used for evaluating the performance of 802.11 pre-n with Multiple Input Multiple Output (MIMO) antenna technology, while Cisco Aironet 1200 kits were used to evaluate 802.11g/a. D-link class 2 Bluetooth USB dongles and Philips video senders were used as external interference sources along with other WLANs.

5.4.1 Measurement Results

In the test setup, the AP was placed inside the house. Capacity and coverage tests were performed both indoors and outdoors for respectively 802.11 pre-n, 802.11a and 802.11g. Based on the measurements it was found that 802.11 pre-n technology outperforms 802.11g and 802.11a. Figure 5.6 shows that the outdoor range of 802.11 pre-n is around 70m as compared to 30m and 25m for 802.11g and 802.11a respectively. Here 802.11 pre-n provides excellent indoor bandwidth of around 25Mbps and outdoor bandwidth of 6-8 Mbps as compared to the 2-5 Mbps for 802.11a/g technology. High throughputs were available for all three technologies

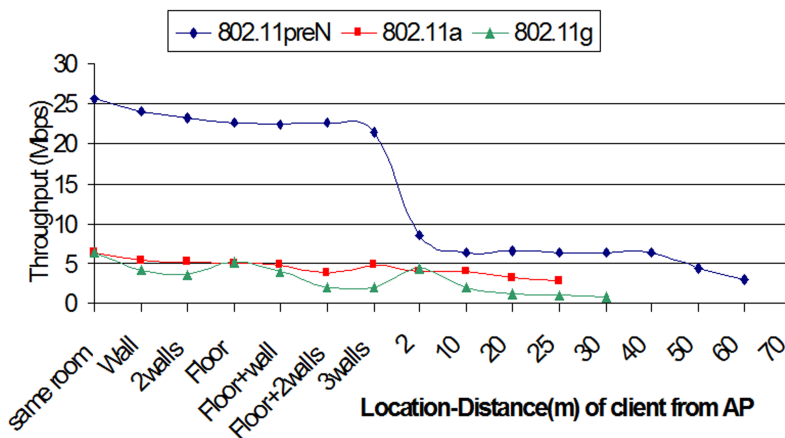
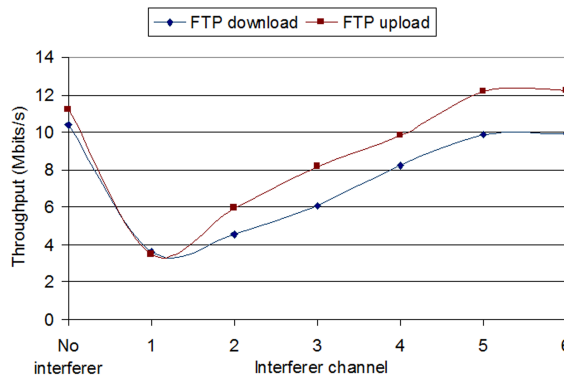


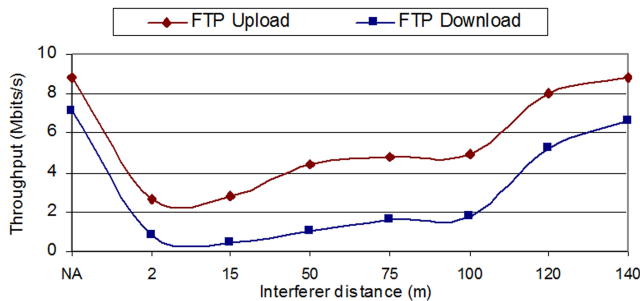
Figure 5.6: The coverage and throughput for different 802.11 technologies for which a FTP session has been set up between server (inside the house) and client (both indoors and outdoors). Here the throughput is depicted as function of distance. The graph shows that 802.11 pre-n outperforms 802.11g/a for both capacity and coverage. The performance of 802.11g and 802.11a are comparable, with the marginal note that the throughput of 802.11a is slightly better compared to 802.11g.

with the client positioned within few meters of the AP. One key finding has been the significance of AP placement in the house. Measurement results showed that a sub-optimally installed AP severely degrades the outdoor coverage. Reduction of about 50% of the original outdoor cell size was observed when an AP is placed in a middle room instead of outer room, i.e. the room closer to the street. Note that in many cases the selection of installation point would be beyond the control of the operator and sometimes beyond the control of the owner as well, hence the need of repeaters is recommended in such situations. It was further found that the cell size for video and audio services was approximately 70% of the data cell size for all three technologies.

Among others in [12] it has been stated that interference poses a serious problem for Wi-Fi technologies in urban environments while the 2.4 GHz ISM band is crowded with a growing number of devices. The degradation of QoS is mainly due to interference issues which also affects the service level agreements with the



(a) Impact of adjacent channel interference: the interferer is a 802.11g client nearby the interferer AP and at 8 meter distance from the client in the main network.



(b) Impact of co-channel interference.

Figure 5.7: The impact of WLAN interference on FTP throughput between AP-client in the main network. The client (802.11 pre-n) in the main network is at 6 meters distance from the AP (main network) while running a FTP download session on channel 1.

client base. The two possible types of interference are taken into account for the measurements: ACI and CCI. Recall that ACI is the interference caused by adjacent channels that have spectral overlap in the frequency domain of the client channel where the client is the device whose performance is being measured in presence of interference. In the test setup, the two WLANs were set up in neighboring houses of a terraced environment, one acting as the interfering WLAN. The client AP and interference AP were located inside the houses. The client was running outside the house on channel 1. First, the performance of the client was monitored without the interferer being active. Second, the interferer was switched on at a street distance of 12m away from the client on channels 2 to 6 (in an one-by-one fashion). Now, the impact of ACI is shown in Figure 5.7(a). Note that the client throughput was about 10-12 Mbps without interference but degraded to 5-6 Mbps when the interferer was occupying the next adjacent channel. The results were repeated for different distances between client and interferer but the results are not shown here while the results are in line with the latter observations.

Recall that CCI has been defined as the interference caused by nearby WLANs using the same channel or frequency as the client channel. In the test setup the two adjoining WLANs were set up on channel 1, one acting as interfering WLAN. The client was at a street distance of 20m from its connected AP. The performance of the client has been measured with the interferer being moved away from the client at a distance of 2m to 140m. Figure 5.7(b) shows the impact of CCI where the throughput degrades to about 1/3rd from 7- 9Mbps to 2-3Mbps but on the other hand improves with increasing interfering distance. Other sources of interference on 802.11 systems, such as Bluetooth and video senders, were studied as well. In addition, performance degradation of 802.11 due to the near-far effect has been investigated. The key findings are presented below.

First, video senders are classified as devices that interconnect the audio/video source such as cable, DVD, VCR to TV sets wirelessly in a home environment. It operates in the 2.4 GHz ISM band. In the test setup a video sender and a receiver

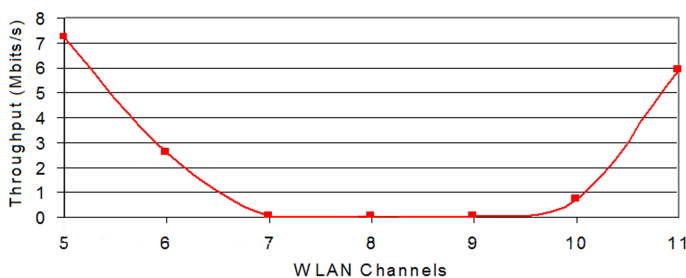


Figure 5.8: The impact of TV-sender interference where 2 in-house televisions were connected wirelessly. The throughput is monitored at a laptop client using both 802.11 pre-n and 802.11g for a FTP data download session. It turns out the interferer causes a break down of WLAN server-client communication on 4 channels i.e. no data throughput.

were installed in two rooms connecting two TV sets. The results w.r.t. TV-sender interference are depicted in Figure 5.8. Here, a WLAN was operational on the same channel as TV-sender. It was found that when the TV-sender was switched on the throughput of the operational WLAN dropped to zero. The outdoor range of the video sender can be up to 10m and hence may affect neighboring WLANs as well. Though there are 4 channels on the TV sender it still reduces the frequency reuse factor while performing channel management for blanket WLAN deployment.

Secondly Bluetooth, in a test setup three class-2 Bluetooth interferers were transferring data files within 5 meters from an AP. The AP throughput was degraded by 2-3 Mbps due to Bluetooth interference.

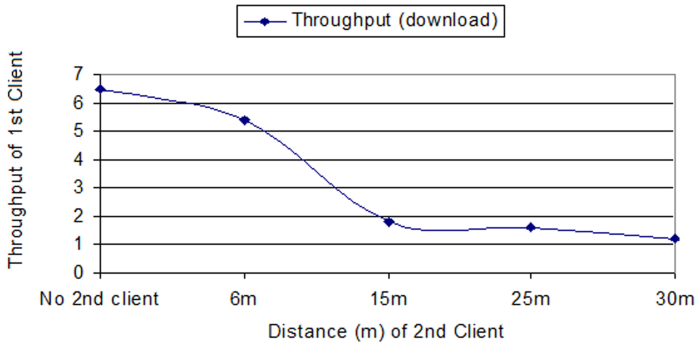


Figure 5.9: Near-Far effect

Thirdly the Near-Far effect: this may occur when clients on the street (i.e. on the public network) connect to UR-WiFi APs which in turn may affect the in-house users (i.e. private network), hence it is important to understand its impact. In the test setup 2 clients, each from respectively a private and public network, are connected to an UR-WiFi AP. The public network client is moved from 6m to 30m away on the street and the performance at the private network client is measured. Figure 5.9 shows the performance of an in-house client for which the throughput degrades from 6 Mbps to 1.5-2 Mbps as the public network client connects at increasing distance from the AP. This is due to increased time slots needed for the far-away client to send its data at a particular bit error rate and also because of the lower-order modulation being used. This results in non-uniform sharing of the air channel that in turn brings down the performance of nearby clients. This problem can be addressed by taking care of the UR-WiFi AP configuration settings so that the QoS of in-house clients can be guaranteed.

Summarizing, the measurements in an urban environment have shown that 802.11 pre-n performs better than 802.11g/a on various fronts and is the first recommendation.

- The 802.11 pre-n coverage is far better than 802.11a which is a key factor for rolling out urban Wi-Fi.
- 802.11 pre-n performs better than 802.11g in the presence of WLAN interference i.e. for both ACI and CCI; this also holds for the impact of Bluetooth interference.

- 802.11 pre-n performs better than 802.11a/g for both video and audio services and also handles jitter well.
- 802.11a technology is not affected by the interference problem as it uses the 5.2 GHz band, i.e. there are 13 non-overlapping channels as compared to 3 in 2.4 GHz ISM band.
- The coverage range and throughput of 802.11a is comparable to 802.11g (at the time in the year 2005/2006).

On the other hand, note the downside of 802.11a kits which are more expensive. Moreover, there are some regulatory concerns about the maximum permissible power at which it can operate in Europe. This in contrast with 802.11g for which the coverage and interference problems are severe but comes with lower expenses as compared to 802.11 pre-n, 802.11a, and 802.11b. For this reason 802.11a is not considered for further evaluation and also because of its limited capacity for urban Wi-Fi services. Other findings from the measurements are that the outdoor cell radii are approximately 75m, 30m and 25m for respectively 802.11 pre-n, 802.11g and 802.11a. Furthermore, it turned out that interference due to both ACI and CCI poses significant problems to urban Wi-Fi services. In addition, also the impact of the near-far effect is shown to be significant while it affects the performance of Wi-Fi in urban areas to a large extent.

5.4.2 Extrapolation of Results

Modeling the Urban Street Environment

An urban residential environment constitutes of different house types such as bungalows, semi-detached, detached, flats, etc. A theoretical propagation model is defined for an urban street environment. In the model, the performance of the WLAN was analyzed inside the house, in neighboring houses and along the street in the presence of other WLAN deployments. An appropriate radio propagation model, based on the Mixed Indoor-Outdoor model [121] and Multi-Wall-Floor(MWF) model [122], is developed and used for link budget analysis. A theoretical model is set up in which the pathloss between outdoor transmitter and indoor receiver [121] is calculated as

$$L = L_{micro} + L_{OW} + \sum_i k_{w_i} \cdot L_{w_i} + a \cdot R \quad (5.1)$$

where, L_{micro} is the micro cell pathloss based on the UMTS 30.03 Outdoor to Indoor and Pedestrian Test Environment pathloss model, L_{OW} is the outdoor wall penetration loss in [dB], R is virtual transmitter-receiver separation given in meters, k_{w_i} is the number of penetrated walls of type i , L_{w_i} is the loss of wall type i , and a is the attenuation in [dB/m] which takes a constant value of 0.8 dB/m. The RF model takes into account the non-linear relationship between the cumulative penetration loss and the number of penetrated floors and walls and is given by [122]:

$$NL = L_s \cdot n_s^{\frac{n_s+5}{n_s+3}-b} \quad (5.2)$$

where, NL is the non-linear wall loss in dB, L_s is the Loss per wall in dB, n_s is the number of walls of the same type, and b is the empirical constant equal to 0.5. A general estimation of the street coverage and capacity was made based on the theoretical model.

The Urban Environment: Simulation Results

The findings of the test measurements are extrapolated to show coverage at the town or city level. The town database is assumed to have information about household density, house layouts, streets, railway lines and rivers. With different towns having different densities the representative exemplar towns are chosen and modeled for urban-WiFi coverage. The test results are extrapolated to a town area with a tool written in MapBasic/MapInfo software [123]. MapInfo is a desktop software to perform mapping and geographical analysis. It includes features for raster and vector database support, map creation, report and graph creation. MapBasic software is a programming and application development environment on top of MapInfo.

Figure 5.10 shows a top view of a town area. The red lines indicate road edges while the dark brown rectangular objects indicate the outline of the houses in the area. In the example shown the total town area is 10.935 sq km and the area covered by houses is around 0.638 sq km i.e 5.8% of the total town area. A random number (0 to 1) is assigned for each house/building in the town. A WLAN adoption rate, or takeup, of 1% is chosen for the town which means that all houses with a random number less than the adoption level (0.01) are activated and marked with red squares. The channel distribution was based on actual site surveying results done in five different areas of the town. For the active cells a circular coverage with appropriate radius and channel is plotted. Furthermore, the coverage radius is based on the measurement results; for example 50 meters on average for the 802.11 pre-n technology. The overlapping coverage areas are merged so that the aggregate coverage of active cells can be computed. Here, the circular green shaded zones shown in Figure 5.10 are the aggregate urban-WiFi coverage areas. In this case it

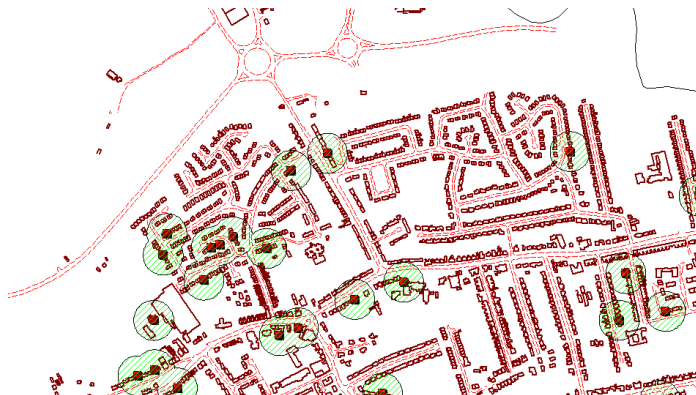


Figure 5.10: The random deployment of WLAN APs in an urban area with an adoption rate of 1%.

turns out that a 1% adoption rate leads to around 4% of town area coverage while 12.2% of the houses are covered by urban-WiFi deployment. This exercise is carried out for different adoption rates for towns with different household densities and the final statistics are gathered. This helps to understand the coverage and number of APs needed for a particular town.

Different services have different cutoff levels for pathloss tolerance, and grid cells with pathloss values exceeding this threshold are marked in a different color. However, a circular coverage is just an ideal scenario as the coverage would be affected by house geometry, walls, furniture, AP location, neighborhood houses, etc. The previous coverage map has a significant error margin, hence instead of plotting circular coverage the environmental parameters are taken into account. The town area is divided into a $5\text{m} \times 5\text{m}$ size raster grid. Based on the above-discussed RF model a pathloss profile cutting through houses, streets is created from each grid cell to its corresponding AP. Based on this profile, pathloss values for each grid cell are calculated. Furthermore, minimum pathloss values are chosen for grid cells in overlapping WLAN coverage areas. This exercise creates a pathloss map at a town level that can be used for further analysis. For instance to determine service and terminal requirements or to assess the percentage of a town area where a particular service will work or not (alternatively a particular location can be chosen instead of town area). Figure 5.11 shows a color coded path loss map for the town. The

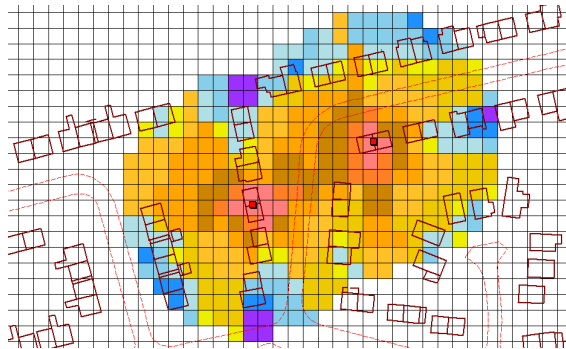


Figure 5.11: Coverage Map in more detail where the colors denote the pathloss values.

yellow-orange colored grid cells signify low pathloss areas whereas the blue/purple colored grid cells signify higher pathloss regions. This may be due to high number of walls or greater distance between the grid cell and urban-WiFi AP.

Next, statistics are generated regarding the percentage reduction in coverage of respectively town areas and house areas because of environmental parameters and the outcome is compared with the previous ideal circular coverage. In this case, for a predefined (pathloss) cutoff threshold of 105 dB, there is reduction of 5.4% in house coverage and a 1.07% reduction in town area coverage as compared to ideal scenario. The new results of 3% town area coverage and 6.74% house area coverage are more realistic and corrects the figures for services with a maximum tolerance of 105 dB. WLANs and other devices in the neighborhood may contribute as interference if they overlap with the client channels and this may bring down the system performance. There could be areas that are not able to provide adequate SNR margins because of ACI and CCI caused by nearby WLANs. For CCI the interfering signals are summed

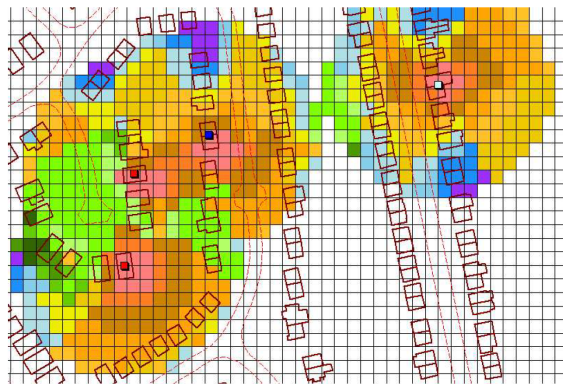


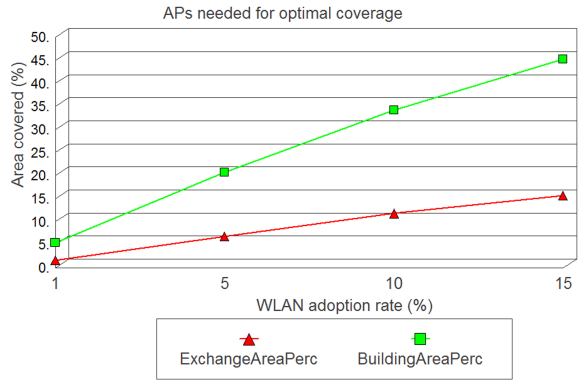
Figure 5.12: Coverage Map including the effects of interference (the affected areas are shown in green colour).

up and accounted as interference in the link budget calculations. For ACI, a weight factor is multiplied to the interfering signal. This factor depends on how far the adjacent channel is from the grid cell channel. Interference is modeled and shown as green regions in Figure 5.12. Here, the activated houses are marked with blue, green, red squares representing channels 1, 6, 11 with other shades used for adjacent channels. The interference leads to a further reduction of 0.7% in house coverage and 0.3% in town area. For a higher WLAN adoption rate the reduction in coverage and capacity due to interference is higher. In a similar fashion other interferers can be modeled such as Bluetooth or microwaves. Additionally, note that the focus is on interference from APs placed inside houses, however, nowadays mobile hotspots (APs) are also very common due to its build-in functionality on smartphones for tethering; interference from mobile hotspots is not included in this model.

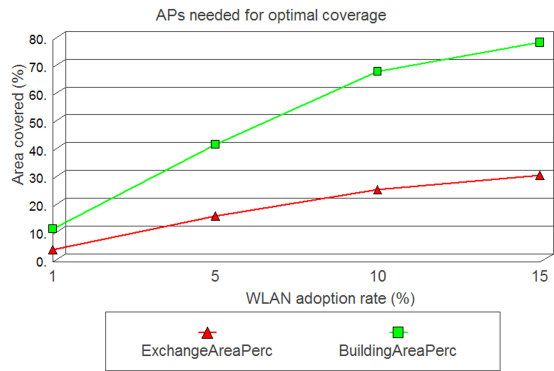
The localized coverage studies and experimental measurements combined with the demographic data can be used to view the likely WiFi coverage in urban areas across the whole country. The aggregate analysis is considerably accurate and provides insight about the expected UR-WiFi topology. In line with this Figure 5.13 shows the town area and house area coverage for different adoption rates for respectively 802.11g and 802.11 pre-n. It shows for instance a reasonable house coverage of around 75% and a town coverage of around of 30% achieved with a WLAN adoption rate of just 15% for 802.11 pre-n. Based on these results, towns can be ranked and selected for further economic analysis. These localized studies can be extrapolated across the whole country to obtain a considerably accurate UR-WiFi topology.

5.5 Conclusion

For a controlled environment a measurement setup is employed to assess the interference of different sources. This setup allows to analyze interference mechanisms in more detail at various levels of the OSI model, not found in literature. Traditional packet sniffers only focus on throughput and packet error rate, whereas the presented tool allows to analyze the received packets types and



(a) 802.11g rolled out.



(b) 802.11 pre-n rolled out.

Figure 5.13: APs needed for optimal coverage. The red curve represents the percentage of area coverage and the green curve the percentage of buildings covered.

subfields; a more sophisticated approach to analyze interference mechanisms. In addition, the study provides answers to some of the key technical questions related to public WLANs and the performance of 802.11 to different types of interference sources in urban environments. It provides a good understanding of problems related to coverage, capacity and interference and gave a positive feedback on the BT UR-WiFi project and on the economic feasibility questions that were posed. In line with this, the launch of BT’s large-scale Wi-Fi network took place in 2007 (see [2]).

Chapter 6

Collaborative Sensing to Enhance TV White-Space Database Performance in Shadow Fading Environments

6.1 Introduction

In recent years there has been a high level of interest in the UHF/VHF frequencies that have been reserved for TV broadcasts (UHF in the UK, VHF in the US) to use them on an opportunistic basis by so-called Cognitive Radios (CR) [13, 17]. The CR methodology works by searching for unused areas of the airwaves - also termed as white spaces - that exist in the radio spectrum. The increased interest in UHF/VHF bands is because of the switchover from analogue to digital TV, referred to as the Digital Switch Over (DSO), which opened up large portions of the UHF/VHF spectrum on a geographical basis for cognitive access [124, 125, 126]. This enabled technologies such as IEEE 802.11af (also known as super-Wi-Fi or White-Fi), ECMA 392 and IEEE 802.22 to access the vacant portions of the UHF/VHF bands using CR [16, 24, 25]. In addition, digital TV assures a higher spectrum efficiency compared to the analogue networks. Moreover, the dynamic access of the UHF/VHF can be very beneficial while recent studies [24, 26, 124] revealed that on average around 150 MHz of interleaved spectrum might be available.

Conditional upon avoiding harmful interference to the licensed users of the UHF/VHF-bands the secondary use is free for devices equipped with CR, also termed as White-Space Devices (WSDs). Note that in most countries the licensed users or primary users are Digital Terrestrial Television (DTT) services and wireless microphone users. However, the above-mentioned interference to licensed users turns out to be a major problem which is mainly due to shadow fading [127]. This is caused by secondary WSDs located in shadowed regions of nearby obstacles (e.g. high buildings, hills, etc) so that primary signals cannot be detected at the WSDs. Consequently, the secondary WSDs sense the channel as free, i.e. a white

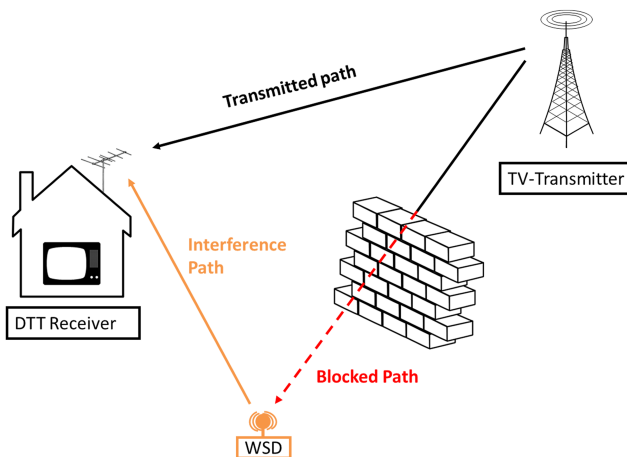


Figure 6.1: Due to terrain effect, e.g. an obstructing building, there is no TV reception at the WSD (secondary user). In other words, the WSD-user faces shadow fading because of the nearby building. As a consequence, the WSD-user detects the TV-channel as free and authorizes itself to start a transmission which in turn could cause interference to nearby DTT receivers (i.e. the primary users).

space is mistakenly detected, and transmissions are initiated at the secondary WSD users. These transmissions may cause interference upon nearby primary users; this problem [128, 129, 130] is also referred to as the hidden node problem [24] and is depicted in Figure 6.1 for the DTT case.

In this chapter the main topic is to avoid the hidden-node problem by using a hybrid approach (see Figure 6.2): cooperative sensing by secondary WSDs that operate with assistance from a geolocation database to enhance the dynamic spectrum access of secondary 802.11af users in the UHF/VHF bands. The possible benefit of a hybrid approach has been suggested recently in for example *Compatibility Challenges for Broadcast Networks and White Space Devices*, BBC Research White Paper, report number WHP 182, January 2010 [131]. Furthermore, the focus is on the emerging 802.11af standard while the application is on short-range wireless communication for which 802.11af appears better suited compared to other CR standards [25, 132] such as 802.22 (rural broadband access).

The rest of this chapter is organized as follows. First, the related work is presented in Section 6.2 followed up by the theoretical framework on collaborative sensing and detection in Section 6.3. Next, using this framework the proposed scheme is described in Section 6.4. A verification of the proposed scheme is carried out in Section 6.5 by enlightening a specific practical use case; this entails both simulation and measurements. Furthermore, in Section 6.6 results of the proposed scheme are presented. Finally, Section 6.7 contains the conclusions and future work.

6.2 Related Work

In literature mainly three methods are discussed to ensure that WSDs do not cause interference to primary users: beacons, a geolocation combined with access to white space database, and (cooperative) sensing. In what follows the latter two methods are highlighted. The beaconing method is omitted because it requires a complete new infrastructure to be set up whilst at the same time the hidden-node problem remains unsolved [24].

6.2.1 Geolocation Database

First, solving the above issue by operating with assistance from a geolocation database works while the database can provide information to the secondary users about the available channels and white spaces [126, 131, 133, 134, 135, 136]. This is possible as the geolocation database contains respectively terrain specific data, the exact locations of the DTT transmitters, and the corresponding TV-channels for a specific area. This is valuable while the possible harmful interference to DTT receivers is a strong function of the DTT coverage quality in a certain geographical area where the DTT receiver is located. However, there are drawbacks on the geolocation white space database approach. This is because of the geolocation database running extensive simulations based on various empirical propagation models such as Okumara-Hata [137], ITU-R P.1546-4 [138, 139] to estimate the quality of TV reception in a particular location. The propagation predictions however are of coarse nature due to limitations of propagation models in characterizing buildings/terrain fluctuations, diffraction, vegetation/foilage effects, etc. Key is that these propagation models are empirical, which poses difficulties to model terrain effects properly [140, 141]. Due to this a pure geolocation database solution for the shadowing problem does not suffice.

6.2.2 Cooperative Sensing

To improve spectrum sensing the collaboration between WSD users has been proposed among others in [129, 142, 143], demonstrating that collaboration may improve secondary spectrum access significantly. Regarding cooperative sensing two approaches can be distinguished: decentralized and centralized. The latter uses a central band manager or fusion center to collect the sensing data; in what follows, the focus is on the centralized approach.

Regarding fusion, a division can be made broadly into two categories: hard decision and soft data fusion strategies. Using soft-information, each CR reports to the fusion center its raw sensed signal measurement or a function of it (e.g. the SNR). Next, based on the delivered signal measurements a weighted decision is made at the fusion center on the presence of a primary user. Under these circumstances, the simplest methods of combining are Equal Gain Combining (EGC) and Selection Combining (SC) [144, 145, 146]. In the case of EGC identical weights are assigned to all CR users, whereas for SC the sensor with the highest SNR is selected. Results show that EGC performs one order of magnitude better compared to SC, while the latter includes only one sensor. Furthermore, the best soft combining technique is known as Maximal-Ratio Combining (MRC) which provides

a better performance while also channel state information is incorporated (e.g. the fading-channel gain). By doing so, the sensing information from different sensing nodes are weighted and fused based on the collected SNR values [147, 148, 149]. However, at the fusion center the MRC algorithm still assigns substantial weights to sensing nodes with low SNR values which means that shadowed CR users are taken into computation which provides a negative contribution to the fusion decision.

Hard decision combining is an approach where a sensor reports its binary state information to the fusion center. Among the hard decision strategies the OR and AND rule attract most of the attention, since these rules are easily implementable and lack complexity. It has been stated in [150, 151, 152] that good performance results can be achieved with hard decision combining when the estimated SNR values are delivered to the fusion center and taken into computation. However, it is also pointed out in [150] that for the AWGN channel the lower SNR values cause degradation of sensing performance and that consequently the sensing performance is not always improved upon when the number of sensors increases. Therefore it is argued in [150] to only include the sensors with the highest SNRs into cooperation while the unselected sensors remain unused. This means that in contrast to the MRC soft combining rule strictly zero-valued weights are assigned to the lower SNR values. A drawback of most of the above-presented SNR-based weighting schemes is that the impact of the spatial distribution is not well addressed.

Note that in general the soft combining fusion rules can provide the best detection performance. However, as stated in [150] the hard decision fusion rules are more appropriate to analyze and evaluate the sensing performance while the individual users threshold can be easily derived given a fixed targeted probability of false alarm P_f or detection P_d .

6.3 Theory: Performance and Analysis

At the energy detector a decision is made on the presence of a primary signal which is solely based on the measured received energy relative to the noise power level. Doing so, the sampled received signal - denoted by $y(n)$ - has two hypotheses under the assumption of a pure AWGN channel:

$$H_1 : \quad y(n) = s(n) + u(n) \tag{6.1}$$

$$H_0 : \quad y(n) = u(n) \tag{6.2}$$

where $s(n)$ denotes the primary user's signal which is assumed to be an i.i.d. random process with mean zero and variance σ_s^2 . Note that the latter equals the received signal power as follows $\sigma_s^2 = P_{rx}$. In a similar way, $u(n)$ refers to the i.i.d. system noise process which has zero mean and variance σ_n^2 . Here hypothesis H_1 means that the primary user is active; the other way around, hypothesis H_0 refers to an inactive primary user. At the energy detector the average received power is determined by integrating the m received samples. Note that m can also be viewed as the time-bandwidth product a.k.a. the sensing time. The output of the integrator is defined now as:

$$T(y) = \frac{1}{m} \sum_{n=1}^m |y(n)|^2 \tag{6.3}$$

This yields the test statistic $T(y)$ which a random variable distributed according to a non-central and chi-square distributions under respectively hypothesis H_0 and H_1 each with $2 \cdot m$ degrees of freedom. Using a predefined threshold λ a decision is made at the energy detector whether a channel is occupied or vacant. To illustrate the meaning of $T(Y)$ central limit theory is applied, i.e. for large m the mean output of the integrator $\mu = E[T(y)]$ corresponds to respectively $\mu_0 = \sigma_n^2$ under H_0 and to $\mu_1 = \sigma_s^2 + \sigma_n^2$ under H_1 . Note that once the noise power statistics σ_n^2 are known at the detector the instantaneous SNR $\gamma = \frac{\sigma_s^2}{\sigma_n^2}$ can be derived. Next, the probabilities of detection P_d and false alarm P_f can be derived at the receiver given a chosen threshold and under the condition of known SNR:

$$P_d = P \{T(Y) > \lambda | H_1\} = Q_m \left(\sqrt{2m\gamma}, \sqrt{\lambda} \right) \quad (6.4)$$

$$P_f = P \{T(Y) > \lambda | H_0\} = \frac{\Gamma(m, \lambda/2)}{\Gamma(m)} \triangleq G_m(\lambda) \quad (6.5)$$

where $\Gamma(a, b) = \int_b^\infty t^{a-1} \exp^{-t} dt$ is the incomplete gamma function and $Q_m(a, b)$ is the generalized Marcum Q-function which is defined as follows:

$$Q_m(a, b) = \int_b^\infty \frac{x^m}{a^{m-1}} e^{-\frac{x^2+a^2}{2}} I_{m-1}(ax) dx \quad (6.6)$$

where $I_{m-1}(\cdot)$ is the $(m-1)$ th modified Bessel function of the first kind. Note that P_f , as in line with the expectations, is independent of SNR, i.e. only relates to the variance of the noise distribution. Furthermore, in order to set the stage for primary user detection we provide the expression with respect to probability of detection P_d . Hence, by combining equations (6.4) and (6.5) the P_d can be formulated as function of P_f through,

$$P_d = Q_m \left(\sqrt{2m\gamma}, \sqrt{G_m^{-1}(P_f)} \right) \quad (6.7)$$

Regarding spectrum sensing, the implication of Equation (6.7) is the following. At the individual CR-user, a chosen threshold λ defines the P_f ; the channel is AWGN and during sensing the m consecutive received samples serve as input for the energy detector where the probability of primary user detection P_d is computed concordantly. The other way around, the P_f can be defined as function of P_d .

6.3.1 Log-normal Shadowing

In what follows, we study the receiver performance under shadow fading for which the attenuation, expressed in decibels, is represented by the zero mean Gaussian random variable X with standard deviation σ_{dB} :

$$X \sim N(0, \sigma_{dB}) \quad (6.8)$$

where in case of no fading this variable is set to 0. Furthermore, by projecting X back to the linear-domain the channel gain may be modeled by the log-normal random variable e^X . This allows to model the instantaneous SNR γ under shadow fading as a log-normal random variable with a mean value of $\bar{\gamma} = 0.1 \cdot \log(10) \cdot \bar{\gamma}_{dB}$ and

which is characterized by its dB spread $\sigma = 0.1 \cdot \log(10) \cdot \sigma_{dB}$. Therefore, the PDF of the log-normal distributed random variable γ due to shadowing can be defined as:

$$f_{\gamma}(x, \bar{\gamma}, \sigma) = \frac{1}{x\sigma\sqrt{2\pi}} e^{-\frac{(\log x - \bar{\gamma})^2}{2\sigma^2}} \quad (6.9)$$

While the SNR varies instantaneously due to shadowing, the probability of detection is required to be conditioned on the instantaneous SNR γ ; the average probability of detection under shadow fading (which, with an abuse of notation, is also referred to as P_d) may be computed by averaging over the shadow fading statistics:

$$\begin{aligned} P_d &= \int_{\gamma} Q_m\left(\sqrt{2mx}, \sqrt{\lambda}\right) f_{\gamma}(x, \bar{\gamma}, \sigma) dx \\ &= \int_{\gamma} Q_m\left(\sqrt{2mx}, \sqrt{G_m^{-1}(P_f)}\right) f_{\gamma}(x, \bar{\gamma}, \sigma) dx \end{aligned} \quad (6.10)$$

Note that substituting Equation (6.9) into Equation (6.10) does not yield a close-form analytical expression, this in contrast to for instance Rayleigh (fast) fading; as a consequence the expression in Equation (6.10) is required to be evaluated numerically.

6.3.2 Collaborative Sensing

The final decision is made at the geolocation database, where fusion of individual user data takes place in order to compute the network probability of detection and false alarm - which are with an abuse of notation - denoted by P_d and P_f . In the sequel the individual probability of detection and false alarm are denoted by respectively $P_{d,i}$ and $P_{f,i}$ for the i^{th} CR-user. In what follows, the OR and AND rules are highlighted while these fusion rules - in combination with channel estimation - are known to attain good sensing performance and are considered more suitable to analyze the detection performance than soft decision fusion rules (see Section 6.2). Regarding the OR-rule, the P_d is computed through:

$$P_d = 1 - \prod_{i=1}^n (1 - P_{d,i}) \quad (6.11)$$

Here, the above-provided OR-rule implies that a primary user is detected when at least one of the n CR-users indicates a primary user to be present. Note that in a similar way the expression for P_f can be derived. For the AND-rule it is the other way around, i.e. the CR-network declares a primary user to be present when all n users indicate its presence:

$$P_d = \prod_i^n P_{d,i} \quad (6.12)$$

Similarly, the equation for P_f can be set up. Furthermore, the network P_d can be expressed in terms of the network P_f and the other way around. Doing so, it is possible to provide the network performance under respectively Constant Detection Rate (CDR) and Constant False Alarm Rate (CFAR) requirements. This means that respectively the probability of detection and false alarm are fixed at a targeted

network value denoted by \bar{P}_d and \bar{P}_f . In line with this the targeted probabilities for the individual CR-user can be derived, i.e. $\bar{P}_{f,i}$ and $\bar{P}_{d,i}$. For the OR-rule this implies the following:

$$\bar{P}_{f,i} = 1 - \sqrt[n]{1 - \bar{P}_f}, \text{ for } i = 1, \dots, n \quad (6.13)$$

and for the AND-rule,

$$\bar{P}_{f,i} = \sqrt[n]{\bar{P}_f}, \text{ for } i = 1, \dots, n \quad (6.14)$$

While the focus is on primary user detection, the P_d under CFAR is defined which is expressed as function of \bar{P}_f by substituting Equation (6.13) into Equation (6.10) (which now defines the individual user detection probability). Next, by substitution of Equation (6.10) into Equation (6.12) the network probability of detection is defined under CFAR:

$$P_d = \prod_{i=1}^n \left(\int_{\gamma} Q_m(\sqrt{2mx}, \sqrt{G_m^{-1}(\sqrt[n]{\bar{P}_f})}) f_{\gamma}(x) dx \right) \quad (6.15)$$

where consequently the network probability of missed detection ($P_m = 1 - P_d$) can be derived concordantly. Notice that in a similar way the expression for the OR-rule can be computed. The other way around, under CDR the expressions for both of the fusion rules can be provided; for the sake of brevity these are omitted.

6.4 Model

6.4.1 Generic Model

The proposed model uses a database-assisted collaborative spectrum sensing framework to improve coexistence between 802.11af secondary users and licensed (DTT) users in the UHF/VHF bands. In what follows, for brevity the focus is on coexistence with primary DTT users. However, note that the model is also applicable to the case of wireless microphone detection. In Figure 6.2 the scenario is depicted regarding the proposed general model for the DTT situation. According to this model the secondary systems have CR capabilities to detect the presence of nearby DTT primary users and are installed to provide 802.11af access in the UHF/VHF band. Furthermore, the secondary users are assumed to be distributed randomly over a certain geographical area and are connected to the geolocation database under the master-slave architecture via the fixed-line. This means that one specific secondary user with the request for 802.11af channel access is designated as master device while the remaining devices operating within the master's coverage radius are called slave devices. In this study we make no distinction between the two; master or slave and treat them transparently. The number of WSDs available, denoted by the set V , relates to the size of the geographical coverage area centered around the master WSD. Note that the coverage area size is defined at the database and that an optimal coverage size exists. This means that on one hand the coverage area should not be excessively large leading to unwanted detection of remote DTT stations; on the other hand, for a small coverage area all the consulted WSDs might be shadowed by the same obstacle.

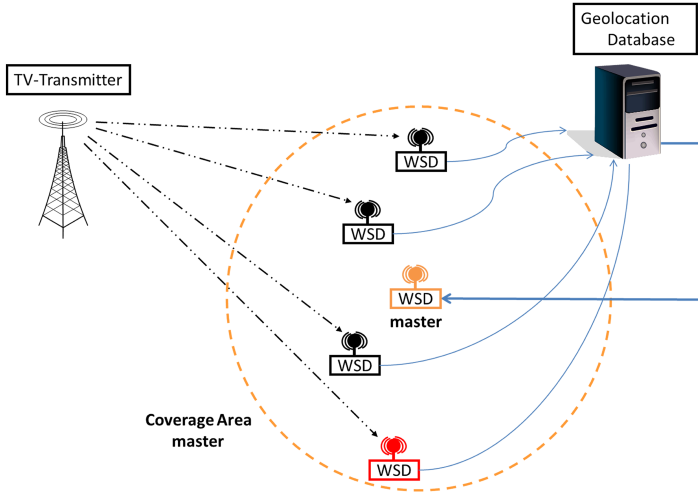


Figure 6.2: The CR network to detect the presence of DTT transmitted signals. The WSDs are connected to the geolocation database using a fixed connection (thin blue line). The coverage area of the master WSD is depicted, and the final decision is communicated from database to master device over a fixed feedback channel (solid blue line); the DTT signal's propagation paths are depicted as dashed black lines. Here the red-colored WSD is located too far away from the DTT station and is therefore not used for sensing.

Regarding the individual WSDs, each device assesses the SNR based on its m sensed samples and uploads this value to the database. This is possible while the receiver noise power σ_n^2 is known at each WSD. As indicated in for example [153] the σ_n^2 can be obtained *a priori* from experimental measurements when the primary system is turned off or from some previous experience. This means that the SNR can be derived through,

$$\gamma_i = \frac{(P_{rx,i} - \sigma_n^2)}{\sigma_n^2} \quad \forall i \in V \quad (6.16)$$

where linear data is used (after conversion from logarithmic to linear). The decision making process at the geolocation database is based on collected spectrum SNR samples obtained from the secondary devices. Doing so, at the fusion center **a subset of $k \leq n$ CR-users is selected with the highest SNR values denoted by U** ; this is carried out for all subset sizes, i.e. $k = 1 \cdots n$. Consequently the following holds: $\{U \subseteq V; |U| = k\}$. Next, based on these SNRs the network probabilities of detection and false alarm can be computed at the database using the fusion rules, i.e. the OR and the AND rule (see Section 6.3). For this purpose the equations for the fusion rules (e.g. see Equation (6.15) for the AND rule) are slightly modified to be applicable in practice. This means for instance that the integral is replaced by summation. This gives for the AND-rule the following regarding the network probability of detection:

$$P_d = \prod_{i=1}^k \left(Q_m(\sqrt{2m\gamma_i}, \sqrt{G_m^{-1}(\sqrt[k]{\bar{P}_f})}) \right) \quad (6.17)$$

as based on the k WSDs with the highest SNR values, i.e. $\forall i \in U$. Now, based

on these probabilities the decision is made at the fusion center whether the master device is granted channel access or not.

6.5 Model Validation

6.5.1 Use Case: Sudbury TV-Station

In this case the Sudbury TV-band transmitter station in the UK is chosen; the specifications are listed in Table 6.1. The TV-antennas can be assumed to be on top of the houses (around 10m); however, in the sequel an average Rx antenna height of 4m is assumed in order to be in line with the measurements for which a 10m antenna height was not feasible/allowed. As the TV-antennas are at the roof tops the fast fading effects (i.e. multi-path reflections) are negligible; note that this also holds for the above-mentioned Rx antenna height used for simulations/measurements. However, due to terrain obstacles, the main type of fading to be experienced is shadowing (i.e. slow fading). Notice that the measurement site is in the vicinity of Ipswich (UK). This particular area is selected since the site is classified as the edge-of-the-coverage-cell as according to the ITU-R P.1546-4 path-loss model depicted in Figure 6.3 where the propagation curves are in line with [138, 139]. Note that the edge-of-the-coverage-cell relates to the minimum required signal power level needed for detection which is defined by the receiver sensitivity, in this case -77 dBm; this in turn yields for the edge-of-the-coverage-cell an expected SNR of $\gamma_{dB} \leq 0$ or below.

6.5.2 Simulation

In this section the simulation model is described for the Sudbury specific-case based on the proposed scheme presented in Section 6.3. However, the simulation model can be adjusted in order to be applicable for any case (e.g. TV-transmitter, geographical area, etc). Basically, the simulation consist of the following building blocks:

- The CR-network contains of n users randomly distributed within a small circular area with radius $R = 250$ m (i.e. an intersection distance of 500m). This chosen to agree with ITU-R P.1546-4 where an area side of 500m is used

Table 6.1: The Sudbury transmitter specifications where the effective height takes into account the actual height of the transmit antenna w.r.t. the terrain heights.

Specifications		
Transmitter	ERP	100 kW
	Eff. Height	205 m
	Frequency	682 MHz
	Polarization	Omni directional
	Bandwidth	8 MHz

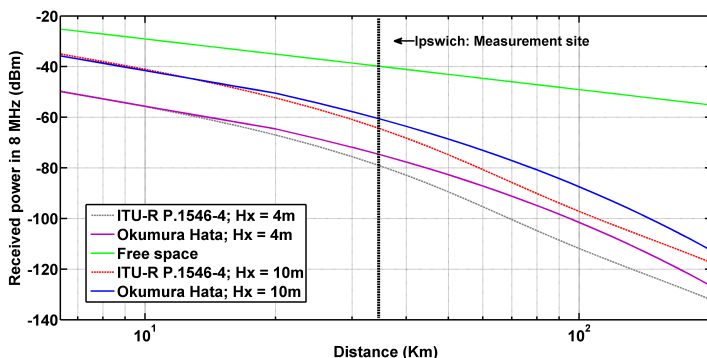


Figure 6.3: The received power prediction of the Sudbury TV broadcast signal on the 682 MHz channel in the UHF band (8 MHz bandwidth) according to different pathloss models: free space, Okumura Hata, and ITU-R P.1546-4; for the latter two models the pathloss is derived based on receiving antenna height of respectively 4m and 10m.

for which parameters such as location variability and percentage location are defined. Furthermore, the center of the CR-network corresponds to the master-CR device location.

- The radio channel is modeled using a path-loss model with on top a stochastic shadowing (slow) fading model. Doing so, this yields for each CR-user the received power P_{rx} ; using the receiver sensitivity the SNR can be derived concordantly.
- The number of users in the CR-network is allowed to be small which in turn however yields a small sample dataset for statistics. To cope with this the simulation accounts for $L = 100$ runs to obtain a reliable average value of P_d .
- Minimal requirements are imposed regarding the sensing detection settings, i.e. the number of sensing samples [128] and the network probability of false alarm.

The parameters used for simulation are listed in Table 6.2 regarding the topology and the propagation environment. Note that three parameters are colored in red to indicate that these are not known beforehand. Moreover, a lot more of terrain-specific information is needed to estimate these parameters. However, this comes at the expense of disproportionately more processing power and the availability of high resolution terrain and building information. For this reason the values of these parameters are obtained directly from the measurements and are fed back to the simulation; this can be derived for each selected geographical area. Next, the description of the simulation model is split up in two parts (i.e. Propagation Modeling and Sensing & Fusion) and is described in more depth below.

Simulation of Propagation Modeling

The ITU-R P.1546-4 model is used to compute the received field strength E as function of distance from the TV-transmitter. Note that in general E relates to the

Table 6.2: The simulation parameters w.r.t. the Sudbury transmitter case. Here, the minimum separation distance refers to the spatial distance between buildings (i.e. distance between WSDs). Three parameters are not known beforehand (colored in red) i.e. the fading deviation, the location variability and the CR-network size; the values of these parameters are obtained from measurements.

Simulation		
Topology	CR-users nr.	Measurements
	Number of Areas	3
	T_x - R_x	34 km
	Radius	250m
	Min. Separation dist.	10m
Propagation	Path-loss	ITU-R P.1546-4 (Land)
	Fading	Shadowing
	Correlation	i.i.d. channels
	Percentage location	Measurements
	Location variability	Measurements
Receiver	Sensing samples	10
	Network P_f	10^{-4}
	Antenna height	4m
	Sensitivity	-77 dBm

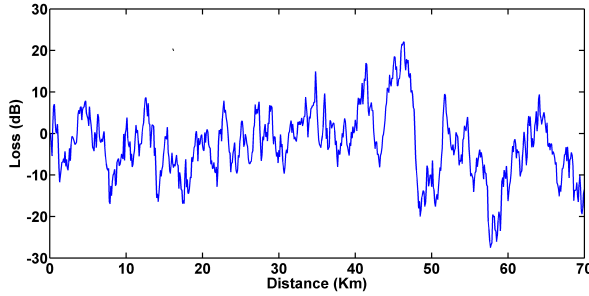
received power P_{rx} through,

$$P_{rx} = 139.3 - E + 20 \log_{10}(f) \quad (6.18)$$

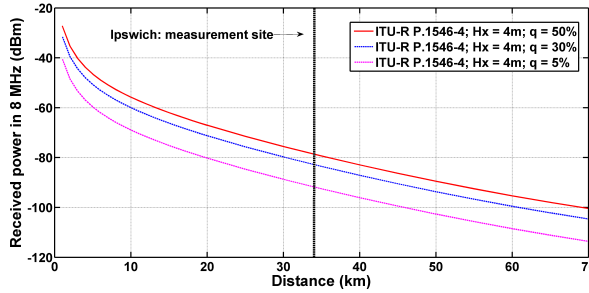
However stochastic signal deviations, i.e. shadowing effects due to terrain differences, are not covered by the listed path-loss models. These variations are commonly modeled by a log-normal distributed random variable, mean-centered around the path-loss values. The stochastic modeled loss due to shadowing/slow fading is shown in Figure 6.4(a) for illustration purposes. Furthermore, two parameters play an important role in characterizing shadowing, i.e., 1) location variability, 2) percentage location.

The definitions according to the ITU-R P.1546-4 model for these two parameters are as follows [138]. First, the location variability is defined as the variability of field strength over a small area, typically represented by a square with a side of 500m to 1 km. Note that the location variability corresponds to the standard deviation of the shadowing distribution in decibels (σ_{dB}). Secondly, the percentage location represents $q\%$ of locations within the predefined small area for which the received field strength values exceed the median received field strength. Due to these two parameters the propagation model needs to be redefined. By doing so, $E_{ITU}(q)$ now denotes the received field strength according to the ITU-R P.1546-4 model propagation and incorporates location variability σ_{dB} and percentage location q . This gives for the received field strength:

$$E_{ITU}(q) = E_{ITU}(\text{median}) + Q_i(q/100) \cdot \sigma_{dB} \quad (6.19)$$



(a) Slow fading (shadowing) fluctuations of the received power as function of distance for a location variability of $\sigma_{dB} = 9$ dB. Here, the pathloss is not incorporated.



(b) Percentage location: in $q\%$ of locations the received signal power exceeds the median signal power within any defined area of 500m x 500m.

Figure 6.4: Shadowing: location variability and percentage location.

where $E_{ITU}(\text{median})$ represents the median field strength according to ITU-R P.1546-4. Furthermore, $Q_i(x)$ denotes the inverse Q-function which is defined as:

$$Q_i = \frac{1}{\sqrt{2\pi}} \int_t^\infty \exp^{-\frac{t^2}{2}} dt \tag{6.20}$$

Note that $E_{ITU}(q) = E_{ITU}(\text{median})$ holds in case of $q = 50\%$ percentage location. In addition, the received power P_{ITU} can be derived by substituting the result of Equation (6.19) into Equation (6.18). Along this line, Figure 6.4(b) illustrates the importance of percentage location in propagation modeling where the ITU-R P.1546-4 standard is used.

Simulation of Sensing and Fusion

For each local sensor the average received power can be derived using the ITU-R P.1546-4 model [138], i.e. denoted by P_{ITU} , which is deterministic and thus fixed for a given location. Also the random variable X takes a constant value while it represents the slow fading component which means that the loss due to shadowing remains constant during the sensing interval of m successive samples [153]. The receiver noise $u(n)$ is modeled as a zero-mean Gaussian random variable with variance σ_n^2

defined by the receiver sensitivity; this gives for each sensor $i \in V$ the received power in the defined sensing interval through:

$$P_{rx,i} = P_{ITU}(d, \sigma_{dB}, q) + X(0, \sigma_{dB}) + \frac{1}{m} \sum_{n=0}^m u(n) \quad (6.21)$$

Based on $P_{rx,i}$ the SNR can be derived for each sensor which is reported to the fusion center. Here, the network P_d can be computed for each subset size (all sorted from highest SNR downwards). However, this is for one particular random topology, i.e. one simulation run. In order to obtain a good sample average the simulation runs a total of $L = 100$ times, where for each run a new random sensor network topology is rolled out within the fixed coverage area. Doing so, the sample average can be expressed as $\bar{P}_d = \frac{1}{L} \sum_j^L P_d(j)$ which is written out below for the AND-rule:

$$\bar{P}_d = \frac{1}{L} \sum_{j=1}^L \prod_{i=1}^k (Q_m(\sqrt{2m\gamma_i}, \sqrt{G_m^{-1}(\sqrt[k]{\bar{P}_f})})) \quad (6.22)$$

In a similar way the detection probabilities for the OR-rule can be derived but has been omitted for the sake of brevity.

6.5.3 Field Measurements

In this section the field measurements are presented which are carried out to compare with the simulation model. For this purpose the measurements follow the simulation settings as listed in Table 6.2 when possible. In addition, for each area the terrain specific parameters are derived which in turn are fed back to the simulation model: 1) the location variability (i.e. the fading deviation σ_{dB}), 2) the location percentage (q), and 3) the number of measurement locations (i.e. CR-users).



Figure 6.5: Measurement van and Yagi antenna.

More detailed information w.r.t. the measurements are specified below:

- Rohde and Schwarz FSH8 spectrum analyzer (100 kHz - 8 GHz).
- Signal power measured over 8 MHz bandwidth.
- Antenna height 4m. Recall that a typical house-roof antenna height is around 10m, however for mobile measurements this height is not allowed by regulatory rules.
- Antenna type Yagi; horizontal polarization and pointed into direction of the TV-transmitter.
- Average distance from TV-transmitter (i.e. Tx-Rx): around 34 km.
- Portable measurement equipment: a van with outdoor antenna (see Figure 6.5).
- Per location: $m = 10$ readings on regular intervals, i.e. the received signal samples.

The measurements are carried out in three different types of neighboring areas which are located at the edge-of-the-coverage-cell as depicted in Figure 6.3 by Ipswich measurement site. The three areas are listed below:

1. Area 1 (Blue colored rectangle): industrial area which includes buildings with higher dimensions.
2. Area 2 (Green colored rectangle): high density of detached houses (Marthlesham Heath, northern part).

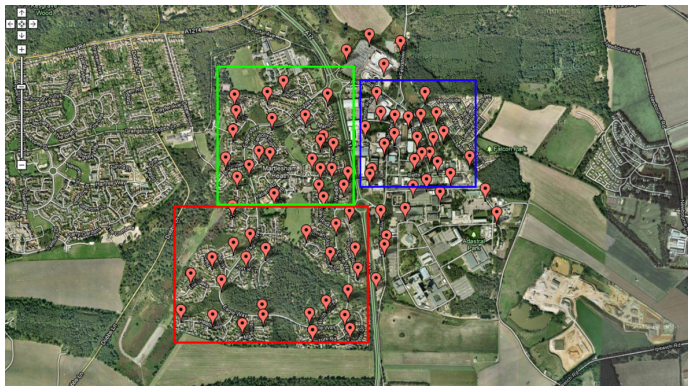


Figure 6.6: The measurement site zoomed in. The three different types of areas are framed by the colored rectangles, i.e. area 1 (blue), area 2 (green), area 3 (red). The measurement locations are shown as red markers. From the satellite photo the more open zone of area 3 is visible, once compared to the other two areas. Note that the upper part of the photo corresponds to the north; the Sudbury TV-transmitter is located west of the measurement site.

3. Area 3 (Red colored rectangle): a relatively open area with mainly detached houses, i.e. more open area around the houses (Marthlesham Heath, southern part).

The three different types of areas are shown (denoted by their colors) in Figure 6.6. For all locations within a particular area the received power levels are recorded. Based on these values the location variability σ_{dB} and percentage location variability q can be derived, which in turn characterize the area of interest. For each area the parameters are listed in Table 6.3. Note that the location variability is computed relative to the ITU-R P.1546-4 predicted field strength $E_{ITU}(median)$. The obtained values are in line with the extensive set of measurements [141] where the location variability is assessed for an area of size 500m x 500m. They found location variability values of around 3 dB \pm 1 dB. However, note that in broadcast planning (e.g. geolocation databases and ITU-R P.1546-4) the 5.5 dB value is retained for all types of areas in response to requests from broadcasters.

Table 6.3: The location variability, the percentage location, the number of measurement locations, and the average distance from the Sudbury TV-transmitter are displayed for each area.

	Location Variability	Percentage Location	Number of Locations	Average distance
Area 1	1.4 dB	10.0%	20	34.7 km
Area 2	2.37 dB	27.0%	23	33.8 km
Area 3	2.28 dB	53.2%	26	33.8 km

6.6 Results

In this section the results are presented of the proposed scheme for different fusion rules under shadowing. This in order to 1) validate whether or not the simulation-based results are in line with the measurement-based results, 2) to compare the results with the pure geolocation results to show the performance gain. Finally, the validation outcome is used to examine the proposed model in a wider context.

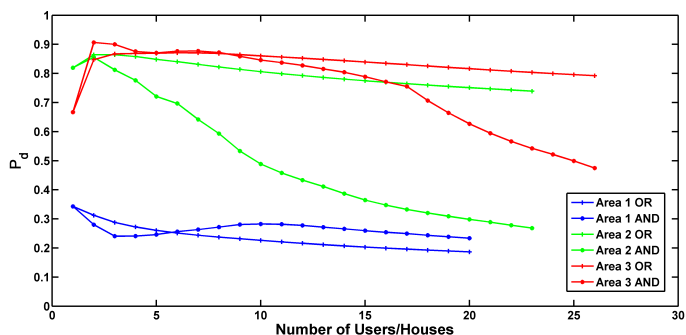
6.6.1 Model Validation: Performance

A performance evaluation of the validation model is carried out and the results are depicted in Figure 6.7(a) and Figure 6.7(b) for respectively the simulation-based and field measurement-based data input.

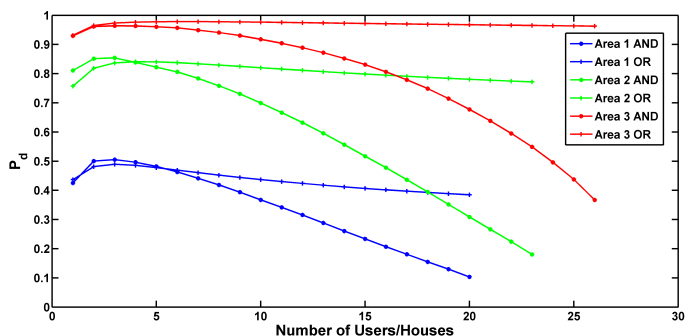
In general, the results show that adding more users for cooperation under shadowing does not necessarily improve detection performance, as adding many low SNR values may degrade detection performance [150]. In particular, the results show that the measurement-based output fairly matches the simulation-based output while a small margin is visible between the curves.

However, a perfect match is not possible due to the detailed terrain-specific properties that need to be incorporated into the simulation, i.e. the height of the buildings, the position of the buildings etc. The key observations are as follows:

- The ITU-R P.1546-4 propagation model provides a good estimate of the average DTT signal power, i.e. confirmed by the measurement results.
- The performance gain of using the database-assisted collaborative sensing scheme over the pure database method can be up till 52.50% in detection probability.
- The performance gain when using a subset instead of all CR users for fusion. For the AND rule this can be up to an additional 58.73% in detection probability.
- The optimal number of CR users for fusion, i.e typically the 3 CR users with the highest SNRs in networks of 20-26 CR users in total.



(a) The performance according to the measurements.



(b) The performance according to the simulations.

Figure 6.7: Probability of TV-station detection versus the different subset sizes $k \leq n$, where the subset contains the users with the highest SNR. For area 1 ($n=20$), area 2 ($n=23$) and area 3 ($n=26$). For the AND and OR fusion rules the performance is shown. Here, the fixed network P_f is set to 10^{-4} where the number of sensing samples equals $m = 10$.

Table 6.4: The probabilities of DTT detection for respectively the optimum number of users and all users collaborating. Here $P_f = 10^{-4}$ and $m = 10$. As a comparison, the DTT location probabilities as according to the geolocation database approach are listed.

	Area 1	Area 2	Area 3
OR (Optimum)	34.29%	86.42%	87.11%
OR (All)	18.67%	73.92%	79.21%
AND (Optimum)	34.29%	85.55%	90.64%
AND (All)	23.37%	26.82%	47.47%
Database Only	35.13%	41.36%	38.14%

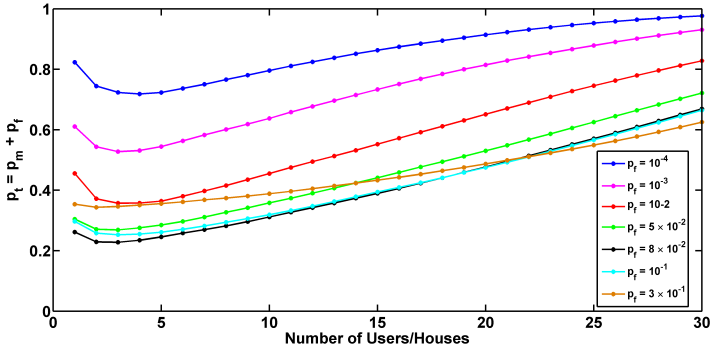
- The OR-rule gives the best performance when compared with the AND rule: shows a larger range of subset sizes for which a relatively high level of P_d can be attained.

The performance of the database-assisted cooperative sensing approach (based on the measurement data input) is compared with the pure geolocation database prediction. For the latter the ITU-R P.1546-4 propagation model is adopted to run on the database with a location variability of $\sigma_{dB} = 5.5$ dB as outlined in [138, 140, 141]. Furthermore, the coverage quality of DTT service is measured by the location probability in a small area (pixel), i.e., the probability with which the median wanted signal level is appropriately greater than a minimum required value (see [132, 134]). The outcome is presented in Table 6.4 and shows the gain of the proposed scheme compared with the pure geolocation database. Due to this gain the proposed model could be considered for use to run on geolocation databases instead, which may lead to a refined fading margin and an improvement in accuracy of DTT prediction.

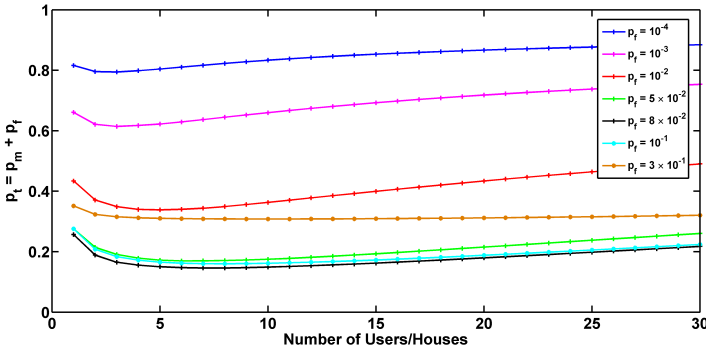
6.6.2 Extension of the Simulation Model

The comparison of the simulation model with the measurements allows to extend the simulation model to different areas and CR-network sizes. This could be of use for future CR sensing applications where the simulation model could pre-compute the optimal number of cooperating users for a certain area for instance. However, another performance metric is needed in order to derive the optimal number of users in general. This means that the total error probability P_t is of higher relevancy, i.e. the $P_t = P_m + P_f$. Next, a simulation is set up in order to derive both the preferred hard decision fusion rule (i.e. OR vs AND) and the optimal subset of CR-users for which the minimal error can be achieved.

For this purpose a sample CR-network and area are chosen with the following parameters: a percentage location of 10%, a location variability of 1.4 dB (for a circular area with radius 100m), distance $T_x-R_x = 40$ km and CR-network size $n = 30$. The results are plotted in Figure 6.8(a) and Figure 6.8(b) for respectively AND and OR fusion rules. In this case the minimum P_t is achieved with $P_f = 8 \times 10^{-2}$ for both fusion rules. However, the OR rule performs better than the AND rule, i.e. $P_t = 0.16$ versus $P_t = 0.22$. Regarding the optimal number of collaborating users, for the OR-rule and AND rule this corresponds to respectively $k = 6$ and $k = 2$ users. In



(a) AND fusion rule.



(b) OR fusion rule

Figure 6.8: The total probability error $P_t = P_m + P_f$ depicted for two fusion rules using $m=10$ sensing samples. Each curve depicts P_t as function of the number of CR-users for a fixed P_f ; this is carried out for several P_f values in order to find the minimum P_t . In this case $P_f = 8 \times 10^{-2}$ provides the minimal error.

addition, the range of low P_t values is relatively large for the OR-rule, this in contrast with the AND rule. The results are in line with the outcome presented in [154] where a comparison is made between the two rules for signal detection in the Wi-Fi band.

6.7 Conclusion and Future Work

A novel hybrid method is presented to ensure that WSDs do not cause interference to primary users in shadow fading environments (hidden node problem) so that 802.11af systems can coexist properly with the licensed DTT systems. This method is based on a cooperative sensing network combined with geolocation access to a white space database.

First, we have demonstrated the advantage of using the proposed database-assisted collaborative sensing scheme over the pure geolocation database approach. For a relatively small networks (20-30 users), and minimal network

requirements (a CR network $P_f = 10^{-4}$ and $m = 10$ sensing samples per CR), the gain can be up to an additional 52.50% in detection probability at the edge-of-the-coverage-cell (i.e. average SNR ≤ 0 dB).

Secondly, we showed that the proposed scheme gives a performance gain compared with the situation where *all* users of the CR-network collaborate, i.e. results show a gain of up to an additional 58.73% in detection probability. Furthermore, the optimal size of the sensing network is determined and a comparison is made between low-complexity fusion-rules: AND vs OR; the results show that the OR rules performs best.

Thirdly, at the geolocation database the developed simulation model can be used to pre-compute the primary user detection probability for a particular grid cell while the simulation incorporates the full range of modeling from propagation/shadowing parameters to detection metrics. The simulation model has been verified by means of field measurements showing fairly similar results which validates the application of simulations for modeling propagation and shadowing. Once the actual CR-network is rolled the actual sensing data can be used instead which in turn can be fed back to the geolocation database.

In the future the proposed scheme could improve the accuracy of the (Ofcom) DTT geolocation database in allocating spectrum for WSD devices and may refine the fading margin in the geolocation databases. The latter is valuable while geolocation databases currently operate with a location variability of 5.5 dB for all grid cells.

Chapter 7

Outlook

This thesis covers several topics concerning coexistence and spectrum sensing issues for 802.11 systems that can be used for cognitive radio applications. In what follows, the several topics are addressed by answering the main research questions posed in Chapter 1 to conclude the thesis and recommendations will be provided concordantly. The questions are formulated below and will be answered one by one.

How do the radio spectrum observation results obtained from the mobile monitoring network compare for different type of areas, i.e., rural versus urban?

The mobile monitoring results showed a large variation in received power levels which differs from area to area. Here, the monitoring equipment sensed the received power levels by means of energy detection and a frequency sweep has been carried out every 2 seconds at a resolution of around 78 kHz in the frequency band of interest (in this case the GSM bands). In general the measured spectrum occupancy has been significantly higher in urban areas compared to rural areas which has been the case for all GSM operators taken into account. As a quantitative measure the field strength value is used that separates the lower 10 percent of sensed field strength values from the higher 90 percent and that this is a measure for the level of mobile network usage. It turned out that this field strength value is always significantly larger for urban spectrum observations compared to the rural case and that the difference can be up till 9 dB for a particular operator.

What is the impact of the AGC on the performance of mobile spectrum monitoring and how can it be removed best?

First, the influence of Automatic Gain Control has been determined, in a controlled environment with known input parameters, by means of calibration measurements. The calibration measurements show the effect of AGC on the monitoring results where the noise floor lifts up as function of the imposed step-wise input signal strength to match the dynamic range of the following-up ADC. Along this line, due to the lifted noise floor levels energy detection becomes more difficult while the threshold, needed for detection, directly relates to the noise floor level which in turn can yield an unreliable prediction of spectrum occupancy. In order to remove the AGC distortion a novel approach has been proposed by means of matrix factorization techniques to separate AGC noise contributions from the monitoring data to be applied on block-wise spectrum data samples only. A

comparison of two candidate matrix factorization techniques was carried out, that means, Singular Value Decomposition and Non Linear Matrix Factorization. Both techniques have been applied to mobile spectrum monitoring data, recorded in an urban environment, in the frequency range of the 2.4 GHz ISM band; NMF turned out to be the best suitable technique for AGC noise removal. In addition, a verification of AGC removal has been carried out using the calibration data which validates the use of NMF as AGC removal technique on the urban mobile monitoring spectrum data. By doing so, results show that the AGC can lead to an overestimation of spectrum usage by 60% in the 2.4 GHz ISM for mobile spectrum monitoring in urban areas.

How is the QoS degradation due to overlapping Wi-Fi networks and what are the occurring mechanisms? First, the interference between overlapping WLAN systems operating on the same channel has been investigated. The selected WLAN systems include the amendments as according to 802.11e and the setup has been located in a controlled environment without any influences from external devices. The impact of interference has been assessed by monitoring the performance at the lowest two layers of the OSI model simultaneously. For this purpose a specifically developed packet sniffing software tool has been used in combination with spectrum analyzer equipment. The results show the severe impact of overlapping WLANs denoted by respectively the main network and the interfering network. The packet rate between server and client in the main network faces a significant decay as when the second network becomes active. In particular, a very high level of RTS/CTS and block ACKs has been recorded coming from the interferer network which causes the strong decrease in the number of data packets transmitted in the main network. Here, the high level of RTS/CTS packets may indicate that the interferer network has identified the main network as a hidden-node. Furthermore, an interference network at distances of either 1m or 5m from the main network demonstrates similar mechanisms and results. The outcome of the measurements in a controlled environment were used to examine the observed mechanisms in a wider context. Doing so, live measurements have been carried out in different environments, i.e., office space, college room, and in the city center. Especially the college room environment, with up till 100 students present and working on laptop devices, showed lots of congestion. The monitoring results illustrate that only a small portion is actual data traffic (less than 21%) and also indicate that a significant number of packets is classified as control packets (e.g. RTS/CTS). This is in line with the experimental results of the controlled environment, showing that RTS/CTS significantly degrades the performance when two networks are in range of each other. In addition, also Block ACKs have been identified as a good indicator of congestion in WLAN environments.

What are the mechanisms that indicate and/or cause performance degradation of 802.11 systems in the 2.4 GHz ISM band for different interference sources i.e. microwave ovens, A/V transmitters, and Bluetooth devices?

Regarding 802.11, the behavior of the PHY and MAC link layer mechanisms under different interference conditions has been investigated using a software tool specifically designed for this purpose. Here the investigated interference conditions refer to the impact of non-802.11 technologies, active in the 2.4 GHz ISM band, with focus on the above-mentioned types of sources. Doing so, the experimental

results show severe impact of A/V transmitters which causes significant overall QoS degradation of Wi-Fi communication in contrast to microwave and Bluetooth interference. Along this line, the A/V transmitters interference causes a strong increase in the number of retry data packets at the MAC link layer which leads to doubling in the total number of data packets transmitted. Eventually, an A/V transmitter in short range of the 802.11 system causes a connection breakdown. At the PHY layer, the A/V transmitter can be identified by narrow-band high power artifacts in the spectrum. Further, both microwave and Bluetooth interference can be recognized at the MAC link layer level by a significant increase in RTS/CTS traffic and a low level of retries ($< 10\%$). At the PHY layer, the microwave oven is visible as a lifted wide-band signal levels whereas Bluetooth can be identified by scattered activity throughout the 2.4 GHz ISM band due to its inherent frequency hopping mechanism.

What is the gain in detection performance of using white-space database-assisted collaborative CR-based sensing when compared with a method that uses geolocation access to a white-space database only?

The proposed hybrid scheme combines cooperative sensing with geolocation access to a central white-space database in order to improve on primary user detection (e.g. TV broadcasting stations) for secondary exploitation of the frequency spectrum in the UHF/VHF bands. For this purpose the optimum number of collaborating CR users is assessed and an evaluation is provided of sensor fusion algorithms that may run on such a database. The optimization has been carried out under the assumption of SNR-based data being uploaded from cognitive sensing devices to a central geolocation database and under the assumption of shadow fading influences (e.g. building, hills) being experienced at the individual cognitive devices. Both channel simulations and measurements were performed to assess the impact of shadow fading and to model it properly. In general it turned out that taking all cognitive users into cooperation does not provide the best detection performance. Note that typically in shadow fading environments it is very likely that some cognitive sensing devices may be blocked by nearby buildings or other obstacles and subsequently cannot detect the TV broadcasting signal of interest. Consequently, the SNR values sensed by these cognitive devices have a negative contribution to the fusion process. Hence, a selection of an optimal set of cognitive users for cooperation at the fusion center (database) leads to an improvement in detection performance. Furthermore, the optimal set turned out to correspond with a particular set of users having the highest average SNR values. The results show that in networks of around 25 cognitive users, in typical grid cell areas (e.g. 500m \times 500m), the number of optimal users for fusion is around 3 users with the highest SNR. Moreover, results show that the OR-fusion rule can be preferred over the AND-fusion rule.

Using the above optimization the gain in detection performance of the database-assisted approach over the pure geolocation approach can be significantly large. The pure geolocation approach refers to a database capable of providing information to the cognitive users about the available channels and white-spaces based on the geographic information provided (i.e. the GPS coordinates of the cognitive user). The geolocation database can provide the data while it has access to respectively the terrain specific data, the exact locations of the DTT transmitters,

and the corresponding TV-channels for a specific area. To estimate the quality of TV reception in a particular location the database runs extensive simulations based on various empirical propagation models such as Okumara-Hata. Now, the gain of using the proposed database-assisted collaborative sensing scheme over the pure geolocation database approach can be up to an additional 52.50% in detection probability at the edge-of-the-coverage-cell (i.e. average SNR ≤ 0 dB). This is the case for a relatively small sensing networks (i.e. 20-30 users), and minimal network requirements (a network probability of false alarm of $P_f = 10^{-4}$ and $m = 10$ sensing samples per cognitive radio user).

7.1 Recommendations

- The mobile spectrum monitoring measurements showed that the spectrum occupancy varies significantly in different geographical areas and inherently illustrates the importance of including spatial power variations. It would be interesting for future research to investigate the distribution of the in-band spatial power variation in more depth using curve-fitting methods in order to see which distribution, and scale parameters, would fit best. It appears from the monitoring results that, as expected, the spectrum is more heavily used in urban areas compared to rural areas. Hence, it would be interesting to look more into issues like the economical viability of opportunistic radio, i.e., you have more opportunity in rural, but most demand for spectrum in urban areas.
- The AGC removal techniques were applied to off-line available spectrum block data but it would be interesting to look into the opportunities of mapping these AGC removal algorithms to hardware platforms to enable real-time application. Further, besides the 2.4 GHz ISM band, we consider it interesting to apply the proposed techniques to other frequency bands as well.
- It turns out that 802.11 interference mechanisms are complex and often unexplored in practical situations. Therefore the following topics are considered interesting for further research. First, it is interesting to look at the mechanisms causing interference between WLAN clients and to compare products from different WLAN vendors with each other. Secondly, open questions remain regarding the interaction between 802.11 overlapping WLANs, e.g. the high amount of Block ACKs, and the 20/40 MHz protection mode operation. Moreover, additional research could aim at many WLAN networks on the same channel, and interfering WLAN networks on adjacent overlapping WLAN channels. Thirdly, it is interesting to investigate how the packet rate on the MAC link layer and the spectrum utilization relate to each other and whether an analytical expression can be provided. The analysis may take into account the different packet sizes that are possible (e.g. an ACK packet is in general significantly smaller than a data content packet). Finally, to improve on the current 802.11 standard we recommend adjustments w.r.t. to the RTS/CTS protocol in order to cope with the high amount of RTS/CTS packets once two APs are in range of each other and adjustments to reduce the control overhead mechanisms (i.e. less than 21% has been classified as data packets in the classroom live recordings). In line

with this, we recommend further inspection of the CSMA/CA protocol so that neighboring APs could share the channel more fairly including improvements on the back-off procedure.

- The impact of different interference sources on 802.11 systems has been investigated. Three specific sources were selected for research, i.e., microwave, A/V transmitter, and Bluetooth communication. However, more non-802.11 systems are active in the unlicensed 2.4 GHz ISM band and could be investigated using the same monitoring setup, i.e. among others, Zigbee, cordless phones, wireless sensor networks, etc. Summarizing, it turns out that the interference impact of non-802.11 systems can be considerably high upon Wi-Fi communication. For this reason, we recommend to consider the use of other frequency bands for 802.11 communication to avoid the congestion issues in the crowded unlicensed ISM band.
- The proposed hybrid scheme, which combines collaborative sensing with geolocation access to a white-space database, may improve the accuracy of the (Ofcom) DTT geolocation database in allocating spectrum for WSD devices and also may refine the fading margins. The latter is valuable while the geolocation databases currently operate with a location variability of 5.5 dB for all grid cells.

Bibliography

- [1] Wi-Fi Alliance. "<http://www.wi-fi.org/>."
- [2] BT Group plc, "BT and FON launch the world's largest Wi-Fi community," Press Release, Oct. 2007.
- [3] S. Kawade, J. W. H. van Bloem, V. S. Abhayawardhana, D. Wisely. "Sharing your urban residential WiFi (UR-WiFi)," in *63rd IEEE Vehicular Technology Conference, 2006. VTC 2006-Spring*, pp. 162–166, May 2006.
- [4] BT Group plc, "BT Wi-fi launches new Windows Phone app as hotspot numbers pass 7.5 million," Press Release, http://www.btwifi.com/news/news_20121113.jsp, Jan. 2013.
- [5] BT Group plc, "BT Openzone and BT Fon rebrands to BT Wi-Fi," Press Release, http://www.btwifi.com/news/news_20120618.jsp, June 2012.
- [6] comScore, "Digital omnivores: how tablets, smartphones and connected devices are changing U.S. digital media consumption habits," White Paper, Oct. 2011.
- [7] Wi-Fi Alliance, "Wi-Fi CERTIFIED passpoint: a new program from the Wi-Fi Alliance to enable seamless Wi-Fi access in hotspots," White Paper, Feb. 2012.
- [8] Informa Telecoms & Systems, "Understanding today's smartphone user: demystifying data usage trends on cellular & Wi-Fi networks," White Paper, Jan. 2012.
- [9] Wireless Broadband Alliance (WBA), Informa Telecoms & Systems. "Global developments in public Wi-Fi," in *WBA Industry Report*, Nov. 2011.
- [10] Accuris Networks, "Why Wi-Fi offload and roaming are key to meeting growing data demands," White Paper, Feb. 2012.
- [11] Cisco Systems, "Cisco Visual Networking Index: forecast and methodology, 2011-2016," White Paper, Feb. 2012.
- [12] A.J. Wagstaff, "Estimating the utilisation of key licence-exempt spectrum bands," Technical Report Issue 3, Mass Consultants Ltd, April 2009.
- [13] J. Mitola III and G. Maguire Jr., "Cognitive radio: making software radios more personal," in *IEEE Personal Communications*, vol. 6, no. 4, pp. 13–18, Aug. 1999.

- [14] J. Mitola III, "Cognitive radio: an integrated agent architecture for Software defined radio," in *Doctoral Dissertation*, KTH, Stockholm, Sweden, May 2000.
- [15] I. F. Akyildiz, W.-Y. Lee, M. C. Vuran, and S. Mohanty, "NeXt generation/dynamic spectrum access/cognitive radio wireless networks: a survey," in *Computer Networks Journal (Elsevier)*, vol. 50, pp. 2127–2159, 2006.
- [16] A. Wyglinski, M. Nekovee, and Y. Hou, *Cognitive radio communications and networks: principles and practice*, ser. Academic Press, 2010.
- [17] S. Haykin, "Cognitive radio: brain-empowered wireless communications," in *IEEE J.Sel. A. Commun.*, vol. 23, no. 2, pp. 201–220, Sep. 2006.
- [18] Federal Communications Commission, "Notice of proposed rule making and order: facilitating opportunities for flexible, efficient, and reliable spectrum use employing cognitive radio technologies," in *ET Docket No. 03-108*, Feb. 2005.
- [19] S. Pollin, M. Timmers, and L. van der Perre, *Software defined radios: from smart(er) to cognitive*, ser. Signals and Communication Technology, Springer, 2011.
- [20] M. Sherman, A. N. Mody, R. Martinez, C. Rodriguez, and R. Reddy, "IEEE standards supporting cognitive radio and networks, dynamic spectrum access, and coexistence," in *IEEE Communications Magazine*, vol. 46, no. 7, pp. 72–79, 2008.
- [21] J. O. Neel, L. A. Dasilva, R. P. Gilles, A. B. Mackenzie, and J. O. Neel, "Analysis and design of cognitive radio networks and distributed radio resource management algorithms," Tech. Rep., 2006.
- [22] L. Berlemann and S. Mangold, *Cognitive Radio and Dynamic Spectrum Access*. John Wiley & Sons, 2009.
- [23] F. Granelli, P. Pawelczak, R. V. Prasad, K. P. Subbalakshmi, R. Chandramouli, J. A. Hoffmeyer, and H. S. Berger, "Standardization and research in cognitive and dynamic spectrum access networks: IEEE SCC41 efforts and other activities," in *Comm. Mag.*, vol. 48, no. 1, pp. 71–79, Jan. 2010.
- [24] M. Nekovee, "A survey of cognitive radio access to TV white spaces," in *International Journal of Digital Multimedia Broadcasting*, vol. 2010, 11 pages, April 2010.
- [25] J. Urn, S.-H. Hwang, and B. J. Jeong, "A comparison of PHY layer on the ECMA-392 and IEEE 802.11af standards," in *7th International ICST Conference on Cognitive Radio Oriented Wireless Networks and Communications (CROWNCOM)*, 2012, pp. 313–319, June 2012.
- [26] S. Kawade and M. Nekovee, "Wireless options for high data-rate indoor users: cognitive access to TV white space," in *First UK-India International Workshop on Cognitive Wireless Systems (UKIWCWS)*, 2009, pp. 1–6, Dec. 2009.
- [27] D. Lekomcev, R. Marsalek, "Comparison of 802.11af and 802.22 standards - physical layer and cognitive functionality," in *Elektor Revue*, vol. 3, no. 2, pp. 12–18, June 2012.

- [28] R. Schiphorst and C. H. Slump. "A monitoring network for spectrum governance," in *Frequenz journal*, vol. 64, pp. 236-239, Nov. 2010.
- [29] W. Baumol and D. Robyn. "Toward an evolutionary regime for spectrum governance: licensing or unrestricted entry?," relax Brookings Institution Press, 2006.
- [30] L. Yang, L. Cao, and H. Zheng. "Physical interference driven dynamic spectrum management," in *3rd IEEE Symposium on New Frontiers in Dynamic Spectrum Access Networks (DySPAN) 2008*, pp. 1–12, Oct. 2008.
- [31] O. Ileri, D. Samardzija, and N. Mandayam. "Dynamic property rights spectrum access: flexible ownership based spectrum management," in *2nd IEEE International Symposium on New Frontiers in Dynamic Spectrum Access Networks (DySPAN) 2007*, pp. 254–265, April 2007.
- [32] L. Mastroeni and M. Naldi. "Option-based dynamic management of wireless spectrum," in *Next Generation Internet Networks, 2009. NGI '09*, pp. 1–8, July 2009.
- [33] J. Bae, E. Beigman, R. Berry, M. Honig, H. Shen, R. Vohra, and H. Zhou. "Spectrum markets for wireless services," in *3rd IEEE Symposium on New Frontiers in Dynamic Spectrum Access Networks (DySPAN) 2008*, pp. 1–10, Oct. 2008.
- [34] S. Sengupta, M. Chatterjee, and S. Ganguly. "An economic framework for spectrum allocation and service pricing with competitive wireless service providers," in *2nd IEEE International Symposium on New Frontiers in Dynamic Spectrum Access Networks (DySPAN) 2007*, pp. 89–98, April 2007.
- [35] S. Gandhi, C. Buragohain, L. Cao, H. Zheng, and S. Suri. "A general framework for wireless spectrum auctions," in *2nd IEEE International Symposium on New Frontiers in Dynamic Spectrum Access Networks (DySPAN) 2007*, pp. 22–33, April 2007.
- [36] Cambridge Radio Frequency Services. "<http://www.crfs.co.uk/>."
- [37] M. Islam, C. Koh, S. Oh, X. Qing, Y. Lai, C. Wang, Y.-C. Liang, B. Toh, F. Chin, G. Tan, and W. Toh. "Spectrum survey in Singapore: occupancy measurements and analyses," in *3rd International Conference on Cognitive Radio Oriented Wireless Networks and Communications (CROWNCOM) 2008*, pp. 1–7, May 2008.
- [38] M. Lopez-Benitez, A. Umbert, and F. Casadevall. "Evaluation of spectrum occupancy in Spain for cognitive radio applications," in *IEEE 69th Vehicular Technology Conference Spring*, pp. 1–5, April 2009.
- [39] M. Wellens, J. Wu, and P. Mahonen. "Evaluation of spectrum occupancy in indoor and outdoor scenario in the context of cognitive radio," in *2nd International Conference on Cognitive Radio Oriented Wireless Networks and Communications (CROWNCOM) 2007*, pp. 420–427, Aug. 2007.

- [40] F. Sanders. "Broadband spectrum surveys in Denver, CO, San Diego, CA, and Los Angeles, CA: methodology, analysis, and comparative results," in *IEEE International Symposium on Electromagnetic Compatibility 1998*, vol. 2, pp. 988–993, Aug. 1998.
- [41] S. Ellingson. "Spectral occupancy at VHF: implications for frequency-agile cognitive radios," in *IEEE 62nd Vehicular Technology Conference 2005, VTC-2005-Fall*, vol. 2, pp. 1379–1382, Sept. 2005.
- [42] R. Chiang, G. Rowe, and K. Sowerby. "A quantitative analysis of spectral occupancy measurements for cognitive radio," in *IEEE 65th Vehicular Technology Conference 2007, VTC2007-Spring*, pp. 3016–3020, April 2007.
- [43] J. W. H. van Bloem, R. Schiphorst, and C. H. Slump. "Initial results of a new mobile spectrum occupancy monitoring network," in *17th IEEE Symposium on Communications and Vehicular Technology in the Benelux*, pp. 64–69, Nov. 2010.
- [44] "Capture of spectrum utilisation information using moving vehicles. "CRFS, Tech. Rep. Ofcom Tender No: 32/2008, 2009.
- [45] T. W. Anderson. *An introduction to multivariate statistical analysis*, 2nd ed., Wiley series in probability and mathematical statistics. John Wiley & Sons, 1984.
- [46] F. Castells, P. Laguna, L. Sörnmo, A. Bollmann, and J. M. Roig. "Principal component analysis in ECG signal processing," in *EURASIP Journal on Applied Signal Processing*, vol. 2007, no. 1, pp. 98–98, Jan. 2007.
- [47] A. Shalash. "An automatic gain control topology for CMOS digital radio receiver," in *IEEE International Symposium on Circuits and Systems (ISCAS) 2009*, pp. 2033–2036, May 2009.
- [48] H. Zhang, G. Wang, and M. Lu. "Analysis and implementation of digital automatic gain control for DAB baseband decoder," *IEEE Transactions on Consumer Electronics*, vol. 57, no. 2, pp. 327–334, May 2011.
- [49] W. Victor and M. Brockman. "The application of linear servo theory to the design of AGC loops," in *Proceedings of the IRE*, vol. 48, no. 2, pp. 234–238, Feb. 1960.
- [50] D. Mercy, "A review of automatic gain control theory," in *Radio and Electronic Engineer*, vol. 51, no. 11.12, pp. 579–590, Nov.-Dec. 1981.
- [51] D. Green. "Global stability analysis of automatic gain control circuits," in *IEEE Transactions on Circuits and Systems*, vol. 30, no. 2, pp. 78–83, 1983.
- [52] E. Tacconi and C. Christiansen. "A wide range and high speed automatic gain control," in *Proceedings of the 1993 Particle Accelerator Conference*, vol.3, pp. 2139–2141, May 1993.
- [53] L. Popken and W. Kriedte. "Statistical description of non-coherent automatic gain control," in *Singapore ICCS/ISITA '92. 'Communications on the Move'*, pp. 133–136, vol.1, Nov 1992.

- [54] J. Smith, *Modern Communications Circuits*. McGraw-Hil, ch. 5, 1986.
- [55] R. Harjani. "A low-power CMOS VGA for 50 Mb/s disk drive read channels," in *IEEE Transactions on Circuits and Systems II: analog and Digital Signal Processing*, vol. 42, no. 6, pp. 370–376, June 1995.
- [56] R. Gomez and A. Abidi. "A 50-MHz CMOS variable gain amplifier for magnetic data storage systems," in *IEEE Journal of Solid-State Circuits*, vol. 27, no. 6, pp. 935–939, June 1992.
- [57] B. Vejlgaard, P. Mogensen, and J. Knudsen. "Performance analysis for UMTS downlink receiver with practical aspects," in *IEEE VTS 50th Vehicular Technology Conference 1999, VTC 1999 - Fall*, vol. 2, pp. 998–1002, 1999.
- [58] A. Sonnenschein and P. Fishman. "Radiometric detection of spread-spectrum signals in noise of uncertain power," in *IEEE Transactions on Aerospace and Electronic Systems*, vol. 28, no. 3, pp. 654–660, July 1992.
- [59] R. Tandra and A. Sahai. "Fundamental limits on detection in low SNR under noise uncertainty," in *International Conference on Wireless Networks, Communications and Mobile Computing*, vol. 1, pp. 464–469, June 2005. .
- [60] D. Cabric, A. Tkachenko, and R. Brodersen. "Spectrum sensing measurements of pilot, energy, and collaborative detection," in *IEEE Military Communications Conference, MILCOM 2006*, pp. 1–7, Oct. 2006.
- [61] W. Gardner. "Exploitation of spectral redundancy in cyclostationary signals," in *IEEE Signal Processing Magazine*, vol. 8, no. 2, pp. 14–36, April 1991.
- [62] Radiocommunication Bureau. *HANDBOOK Spectrum Monitoring*. International Telecommunication Union, 2002.
- [63] M. S. Oude Alink, A. B. J. Kokkeler, E. A. M. Klumperink, G. J. M Smit, and B. Nauta. "Lowering the SNR Wall for Energy Detection Using Cross-Correlation," in *IEEE Transactions on Vehicular Technology*, vol. 60, no. 8, pp. 3748–3757, 2011.
- [64] Y. Zeng and Y.-C. Liang. "Eigenvalue-based spectrum sensing algorithms for cognitive radio," in *IEEE Transactions on Communications*, vol. 57, no. 6, pp. 1784–1793, June 2009.
- [65] M. Olivieri, G. Barnett, A. Lackpour, A. Davis, and P. Ngo. "A scalable dynamic spectrum allocation system with interference mitigation for teams of spectrally agile software defined radios," in *First IEEE International Symposium on New Frontiers in Dynamic Spectrum Access Networks (DySPAN), 2005*, pp. 170–179, Nov. 2005.
- [66] A. J. Hendrikse, L. Spreeuwiers, and R. Veldhuis. "A bootstrap approach to eigenvalue correction," in *Ninth IEEE International Conference on Data Mining, 2009, ICDM '09*, pp. 818–823, Dec. 2009.

- [67] K. Hermus, P. Wambacq, and H. van Hamme. "A review of signal subspace speech enhancement and its application to noise robust speech recognition," in *EURASIP Journal on Applied Signal Processing*, vol. 2007, no. 1, pp. 195–195, Jan. 2007.
- [68] S. Aviyente, E. M. Bernat, S. M. Malone, and W. G. Iacono. "Time-frequency data reduction for event related potentials: combining principal component analysis and matching pursuit," in *EURASIP Journal on Advances in Signal Processing*, vol. 2010, pp. 1–13, June. 2010.
- [69] D. Lee and H. Seung. "Learning the parts of objects by non-negative matrix factorization," in *Nature*, vol. 401, no. 6755, pp. 788–791, Oct. 1999.
- [70] F. Weninger, B. Schuller, A. Batliner, S. Steidl, and D. Seppi. "Recognition of nonprototypical emotions in reverberated and noisy speech by nonnegative matrix factorization," in *EURASIP Journal on Advances in Signal Processing*, vol. 2011, 16 pages, Jan. 2011.
- [71] W. Wang, Y. Luo, J. A. Chambers, and S. Sanei. "Note onset detection via nonnegative factorization of magnitude spectrum," in *EURASIP Journal on Advances in Signal Processing*, vol. 2008, pp. 1–15, 2008.
- [72] J. W. H. van Bloem, A. J. Hendrikse, R. Schiphorst, and C. H. Slump. "An eigenvalue approach to enhance energy detection in a mobile spectrum monitoring network," in *5th IEEE International Conference on Signal Processing and Communication Systems*, pp. 346–351, Dec. 2011.
- [73] D. D. Lee and H. S. Seung. "Algorithms for non-negative matrix factorization," in *Advances in Neural Information Processing*. MIT Press, pp. 556–562, 2000.
- [74] M. W. Berry, M. Browne, A. N. Langville, V. P. Pauca, and R. J. Plemmons. "Algorithms and applications for approximate nonnegative matrix factorization," in *Computational Statistics and Data Analysis*, pp. 155–173, 2006.
- [75] Z. Yang, H. Zhang, Z. Yuan, and E. Oja. "Kullback-Leibler divergence for nonnegative matrix factorization," in *Artificial Neural Networks and Machine Learning - ICANN 2011*, ser. Lecture Notes in Computer Science, vol. 6791, Springer Berlin / Heidelberg, pp. 250–257, 2011.
- [76] O. Okun and H. Priisalu. "Fast nonnegative matrix factorization and its application for protein fold recognition," in *EURASIP Journal on Applied Signal Processing*, vol. 2006, pp. 649–656, Jan. 2006.
- [77] A. Lindgren, A. Almquist, and O. Schelén. Evaluation of quality of service schemes for IEEE 802.11 wireless LANs. in *Local Computer Networks, 2001. Proceedings. LCN 2001. 26th Annual IEEE Conference on*, pp. 348–351, 2001.
- [78] A. Lindgren, A. Almquist, and O. Schelén. Quality of service schemes for IEEE 802.11 wireless LANs – An evaluation, in *Mobile Networks and Applications (MONET)*, vol. 8, pp. 223–235, 2003.

- [79] S. Mukherjee, X. Peng, and Q. Gao. QoS performances of IEEE 802.11 EDCA and DCF: a testbed approach, in *5th International Conference on Wireless Communications, Networking and Mobile Computing, 2009, WiCOM '09*, pp. 1–5, Sept. 2009.
- [80] S. Mangold, S. Choi, P. May, O. Klein, G. Hiertz, L. Stibor. IEEE 802.11e wireless LAN for Quality of Service, in *Proc. European Wireless 02*, vol. 1, pp. 32–39, Feb. 2002.
- [81] S. Choi, J. Prado, S Shankar N, and S. Mangold. IEEE 802.11e contention-based channel access (EDCF) performance evaluation, in *IEEE International Conference on Communications, 2003. ICC '03*, vol. 2, pp. 1151–1156, May 2003.
- [82] Qiang Ni. Performance analysis and enhancements for IEEE 802.11e wireless networks, in *IEEE Network*, vol. 19, no. 4, pp. 21–27, July-Aug. 2005.
- [83] J. Sydor. Coral: a Wi-Fi based cognitive radio development platform, in *7th International Symposium on Wireless Communication Systems (ISWCS), 2010*, pp. 1022–1025, Sept. 2010.
- [84] A. Mishra, V. Shrivastava, S. Banerjee, and W. Arbaugh. Partially overlapped channels not considered harmful, in *Proceedings of the joint international conference on Measurement and modeling of computer systems, SIGMETRICS '06/Performance '06*, pp. 63–74, 2006.
- [85] E. G. Villegas, E. Lopez-Aguilera, R. Vidal, and J. Paradells, Effect of adjacent-channel interference in IEEE 802.11 WLANs, in *2nd International Conference on Cognitive Radio Oriented Wireless Networks and Communications (CROWNCOM), 2007*, pp. 118–125, Aug. 2007.
- [86] J. Hu, G. Min, W. Jia, and M.E. Woodward, “Admission Control in the IEEE 802.11e WLANs based on analytical modelling and game theory,” in *IEEE Global Telecommunications Conference (GLOBECOM), 2009*, pp. 1–6, Dec. 2009.
- [87] S. Mangold, J. Habetha, S. Choi, and C. Ngo. Coexistence and interworking of IEEE 802.11a and ETSI BRAN HiperLAN/2 in multihop scenarios, in *3rd IEEE Workshop on Wireless Local Area Networks*, 9 pages, Sept. 2001.
- [88] A. P. Jardosh, K. N. Ramachandran, K. C. Almeroth, and E. M. Belding-royer. Understanding congestion in IEEE 802.11b wireless networks, in *Proceedings of the 2005 Internet Measurement Conference*, pp. 279–292, 2005.
- [89] A. P. Jardosh, K. N. Ramachandran, K. C. Almeroth, and E. M. Belding-Royer. Understanding link-layer behavior in highly congested IEEE 802.11b wireless networks, in *Proceedings of the 2005 ACM SIGCOMM workshop on Experimental approaches to wireless network design and analysis, E-WIND '05*, pp. 11–16, 2005.
- [90] K. Puttaswamy, H. Lundgren, K. Almeroth, A. Sharma, R. Raghavenda and E. Belding-R. Experimental characterization of interference in a 802.11g wireless mesh network, Technical report, Univ. California Santa Barbara, Dec. 2005.

- [91] S. Khurana, A. Kahol, and A.P. Jayasumana. Effect of hidden terminals on the performance of IEEE 802.11 MAC protocol, in *23rd Annual Conference on Local Computer Networks, 1998, LCN '98, Proceedings*, pp. 12–20, Oct. 1998.
- [92] S. Mangold. IEEE 802.11e: coexistence of overlapping basic service sets (invited paper), in *Proceedings of Mobile Venue'02*, pp. 131–135, May 2002.
- [93] S. Mangold, L. Berlemann, and G. Hiertz. QoS support as utility for coexisting wireless LANs, in *International Workshop on IP Based Cellular Networks, IPCN'02*, 6 pages, Apr 2002.
- [94] S. Mangold, S. Choi, P. May, and G. Hiertz. IEEE 802.11e - fair resource sharing between overlapping basic service sets, in *Proceedings of the PIMRC 2002*, pp. 166–171, 2002.
- [95] K. Kosek, M. Natkaniec, L. Vollero, and A. R. Pach. An analysis of star topology IEEE 802.11e networks in the presence of hidden nodes, in *International Conference on Information Networking, ICOIN 2008*, pp. 1–5, Jan. 2008.
- [96] IEEE standard for information technology-telecommunications and information exchange between systems-local and metropolitan area networks-specific requirements - part 11: Wireless LAN Medium Access Control (MAC) and Physical Layer (PHY) specifications. *IEEE Std 802.11-2007 (Revision of IEEE Std 802.11-1999)*, pp. C1–1184, 2007.
- [97] G. Bianchi. Performance analysis of the IEEE 802.11 distributed coordination function, in *IEEE Journal on Selected Areas in Communications*, vol. 18, no. 3, pp. 535–547, March 2000.
- [98] IEEE Std 802.11e/D13.0, draft supplement to standard for telecommunications and information exchange between systems-LAN/MAN specific requirements. part 11: Wireless Medium Access Control (MAC) and Physical Layer (PHY) specifications: Medium access control (MAC) enhancements for quality of service (QoS), *IEEE Std P802.11e/D13.0*, April 2005.
- [99] N. Passas, D. Skyrianoglou, and P. Mouziouras. Prioritized support of different traffic classes in IEEE 802.11e wireless LANs, in *Comput. Commun.*, vol. 29, pp. 2867–2880, Sept. 2006.
- [100] A. E. Xhafa, A. Batra, A. Zaks. On the 20/40 MHz Coexistence of Overlapping BSSs in WLANs, in *Journal of Networks*, vol. 7, no. 3, pp. 56–63, July 2008.
- [101] G. Bianchi, I. Tinnirello, and L. Scalia. Understanding 802.11e contention-based prioritization mechanisms and their coexistence with legacy 802.11 stations, in *IEEE Network*, vol. 19, no. 4, pp. 28–34, July-Aug. 2005.
- [102] A. Salhotra, R. Narasimhan, and R. Kopikare. Evaluation of contention free bursting in IEEE 802.11e wireless LANs, in *IEEE Wireless Communications and Networking Conference, 2005*, vol. 1, pp. 107–112, March 2005.

- [103] E. Kim and Y. Suh. ATXOP: an adaptive TXOP based on the data rate to guarantee fairness for IEEE 802.11e wireless LANs, in *IEEE 60th Vehicular Technology Conference 2004, VTC2004-Fall*, vol. 4, pp. 2678–2682, Sept. 2004.
- [104] Y. Choi, B. Lee, J. Pak, I. Lee, H. Lee, J. Yoon, and K. Han. An adaptive TXOP allocation in IEEE 802.11e WLANs, in *Proceedings of the 6th WSEAS International Conference on Electronics, Hardware, Wireless and Optical Communications*, pp. 187–192, 2007.
- [105] T. Suzuki, A. Noguchi, and S. Tasaka. Effect of TXOP-bursting and transmission error on application-level and user-level QoS in audio-video transmission with IEEE 802.11e EDCA, in *IEEE 17th International Symposium on Personal, Indoor and Mobile Radio Communications, 2006*, pp. 1–7, Sept. 2006.
- [106] J. Majkowski and F. Casadevall Palacio. Dynamic TXOP configuration for QoS enhancement in IEEE 802.11e wireless LAN, in *International Conference on Software in Telecommunications and Computer Networks, SoftCOM 2006*, pp. 66–70, Oct. 2006.
- [107] D. J. Thunte, B. Newlin, and M. Acharya. Jamming vulnerabilities of IEEE 802.11e, in *IEEE Military Communications Conference, MILCOM 2007*, pp. 1–7, Oct. 2007.
- [108] H. Lee, I. Tinnirello, J. Yu, and S. Choi. Throughput and delay analysis of IEEE 802.11e block ACK with channel errors, in *2nd International Conference on Communication Systems Software and Middleware (COMSWARE), 2007*, pp. 1–7, Jan. 2007.
- [109] G. R. Hiertz, L. Stibor, J. Habetha, E. Weiss, and S. Mangold. Throughput and delay performance of IEEE 802.11e wireless LAN with block acknowledgments, in *11th European Wireless Conference 2005 - Next Generation Wireless and Mobile Communications and Services (European Wireless)*, pp. 1–7, April 2005.
- [110] I. Papapanagiotou, G. S. Paschos, and M. Devetsikiotis. A comparison performance analysis of QoS WLANs: approaches with enhanced features, in *Adv. in MM*, vol. 2007, no. 1, 13 pages, April 2007.
- [111] I. Harjula, J. Pinola, and J. Prokkola. “Performance of IEEE 802.11 based WLAN devices under various jamming signals,” in *Military Communications Conference, 2011 - MILCOM 2011*, pp. 2129–2135, Nov. 2011.
- [112] Task Group 2 (TG2). “<http://www.ieee802.org/15/pub/TG2.html>.”
- [113] G. V. Dyck, N. Golmie, R. E. V. Dyck, A. Soltanian, A. Tonnerre, and O. Rebala. “Interference evaluation of Bluetooth and IEEE 802.11b systems,” in *ACM Wireless Networks 2003*, vol. 9, pp. 202–211, 2003.
- [114] C. Chiasserini and R. Rao. “Coexistence mechanisms for interference mitigation in the 2.4-GHz ISM band,” in *IEEE Transactions on Wireless Communications*, vol. 2, no. 5, pp. 964–975, Sept. 2003.

- [115] R. Gummadi, D. Wetherall, B. Greenstein, and S. Seshan, "Understanding and mitigating the impact of RF interference on 802.11 networks," in *Proc. of Sigcomm07*, pp. 385–396, 2007.
- [116] N. Golmie, N. Chevrollier, and O. Rebala. "Bluetooth and WLAN coexistence: challenges and solutions," in *IEEE Wireless Communications*, vol. 10, no. 6, pp. 22–29, Dec. 2003.
- [117] T. Taher, M. Misurac, J. LoCicero, and D. Ucci. "Microwave oven signal interference mitigation for Wi-Fi communication systems," in *5th IEEE Consumer Communications and Networking Conference, CCNC 2008*, pp. 67–68, Jan. 2008.
- [118] G. Li, S. Srikanteswara, and C. Maciocco. "Interference mitigation for WLAN devices using spectrum sensing," in *5th IEEE Consumer Communications and Networking Conference, CCNC 2008*, pp. 958–962, Jan. 2008.
- [119] A. Kamerman and N. Erkocevic. "Microwave oven interference on wireless LANs operating in the 2.4 GHz ISM band," in *The 8th IEEE International Symposium on Personal, Indoor and Mobile Radio Communications*, vol. 3, pp. 1221–1227, Sept. 1997.
- [120] K. Pietikainen, A. Silvennoinen, M. Hall, and S.G. Haggman. "IEEE 802.11g tolerance to narrowband jamming," in *IEEE Military Communications Conference (MILCOM), 2005*, vol. 3, pp. 1825–1830, Oct. 2005.
- [121] "Universal Mobile Telecommunications System (UMTS) Base Station (BS) classification." in tech. rep., 3GPP ETSI TR 25.951 version 6.2.0.
- [122] M. Lott and I. Forkel. "A Multi-Wall-and-Floor Model for Indoor Radio Propagation," in ETSI TR 125 951 V6.2.0, May 2001.
- [123] MapInfo Professional. "[http://www.mapinfo.com/.](http://www.mapinfo.com/)"
- [124] Ofcom, "Statement on cognitive access to interleaved spectrum," July 2009.
- [125] FCC, "Additional spectrum for unlicensed devices below 900MHz and in the 3GHz band," ET Docket 02-380, Dec. 2002.
- [126] M. Nekovee and D. Wisely, "Cognitive radio networks in TV white spaces," in *Cognitive Communications: distributed Artificial Intelligence (DAI), Regulatory Policy and Economics, Implementation*, D. Grace and H. Zhang, Eds. John Wiley & Sons, Ltd, pp. 319–357, 2012.
- [127] A. Rabbachin, T. Q. Quek, H. Shin, and M. Z. Win, "Cognitive network interference," in *IEEE J.Sel. A. Commun.*, vol. 29, no. 2, pp. 480–493, Feb. 2011.
- [128] A. Ghasemi and E. Sousa, "Collaborative spectrum sensing for opportunistic access in fading environments," in *First IEEE International Symposium on New Frontiers in Dynamic Spectrum Access Networks (DySPAN), 2005*, pp. 131–136, Nov. 2005.

- [129] G. Ganesan and Y. Li, "Cooperative spectrum sensing in cognitive radio networks," in *First IEEE International Symposium on New Frontiers in Dynamic Spectrum Access Networks (DySPAN), 2005*, pp. 137–143, Nov. 2005.
- [130] Y. Selen and J. Kronander, "Cooperative detection of programme making special event devices in realistic fading environments," in *IEEE Symposium on New Frontiers in Dynamic Spectrum, 2010*, pp. 1–9, April 2010.
- [131] M. Waddell, "Compatibility challenges for broadcast networks and white space devices," BBC Research White Paper WHP 182, Jan. 2010.
- [132] N. Dumont, R. Watson, and S. Pennock, "Propagation modelling for white space geo-location databases," in *6th European Conference on Antennas and Propagation (EUCAP), 2012*, pp. 2175–2179, March 2012.
- [133] Ofcom, "Implementing geolocation," Nov. 2010.
- [134] H. Karimi, "Geolocation databases for white space devices in the UHF TV bands: specification of maximum permitted emission levels," in *IEEE Symposium on New Frontiers in Dynamic Spectrum Access Networks (DySPAN), 2011*, pp. 443–454, May 2011.
- [135] M. Nekovee, "Quantifying the availability of TV white spaces for cognitive radio operation in the UK," in *IEEE International Conference on Communications Workshops, 2009*, pp. 1–5, June 2009.
- [136] Ofcom, "Digital dividend: geolocation for cognitive access," Nov. 2009.
- [137] M. Hata, "Empirical formula for propagation loss in land mobile radio services," in *IEEE Transactions on Vehicular Technology*, vol. 29, no. 3, pp. 317–325, Aug. 1980.
- [138] ITU-R, "Recommendation ITU-R P.1546-4: method for point-to-area predictions for terrestrial services in the frequency range 30 MHz to 3000 MHz," Oct. 2009.
- [139] J. van de Beek, J. Riihijarvi, A. Achtzehn, and P. Mahonen, "UHF white space in Europe - a quantitative study into the potential of the 470 - 790 MHz band," in *IEEE Symposium on New Frontiers in Dynamic Spectrum Access Networks (DySPAN), 2011*, pp. 1–9, May 2011.
- [140] I. Pullen, "DTT coverage predictions – how they are made and tested," in *Digital News*, vol. 11, no. 9, pp. 14–15, July 1999.
- [141] Ofcom, "The co-existence of LTE and DTT services at UHF: a field trial," Tech. Rep., July 2011.
- [142] M. Gandetto and C. Regazzoni, "Spectrum sensing: a distributed approach for cognitive terminals," in *IEEE J.Sel. A. Commun.*, vol. 25, no. 3, pp. 546–557, April 2007.
- [143] S. Mishra, A. Sahai, and R. Brodersen, "Cooperative sensing among cognitive radios," in *IEEE International Conference on Communications 2006, ICC '06*, vol. 4, pp. 1658–1663, June 2006.

- [144] F. F. Digham, M.-S. Alouini, and M. K. Simon, "On the energy detection of unknown signals over fading channels," in *IEEE Transactions on Communications*, vol. 55, no. 1, pp. 21–24, Jan. 2007.
- [145] Y.-L. Foo, "Performance of cooperative spectrum sensing under Rician and Nakagami fading," in *Wireless Personal Communications*, pp. 1–11, July 2012.
- [146] T. Yucek and H. Arslan, "A survey of spectrum sensing algorithms for cognitive radio applications," in *IEEE Communications Surveys Tutorials*, vol. 11, no. 1, pp. 116–130, first quarter 2009.
- [147] M. Bin Shahid and J. Kamruzzaman, "Weighted soft decision for cooperative sensing in cognitive radio networks," in *16th IEEE International Conference on Networks 2008, ICON 2008*, pp. 1–6, Dec. 2008.
- [148] J. Ma, G. Zhao, and Y. Li, "Soft combination and detection for cooperative spectrum sensing in cognitive radio networks," in *Trans. Wireless. Comm.*, vol. 7, no. 11, pp. 4502–4507, Nov. 2008.
- [149] E. Visotsky, S. Kuffner, and R. Peterson, "On collaborative detection of TV transmissions in support of dynamic spectrum sharing," in *First IEEE International Symposium on New Frontiers in Dynamic Spectrum Access Networks (DySPAN) 2005*, pp. 338–345, Nov. 2005.
- [150] E. Peh and Y.-C. Liang, "Optimization for cooperative sensing in cognitive radio networks," in *IEEE Wireless Communications and Networking Conference (WCNC) 2007*, pp. 27–32, March 2007.
- [151] P. Qihang, Z. Kun, W. Jun, and L. Shaoqian, "A distributed spectrum sensing scheme based on credibility and evidence theory in cognitive radio context," in *IEEE 17th International Symposium on Personal, Indoor and Mobile Radio Communications, 2006*, pp. 1–5, Sept. 2006.
- [152] H. Wang, G. Noh, D. Kim, S. Kim, and D. Hong, "Advanced sensing techniques of energy detection in cognitive radios," in *IEEE Journal of Communications and Networks*, vol. 12, no. 1, pp. 19–29, Feb. 2010.
- [153] Z. Quan, S. Cui, and A. Sayed, "Optimal linear cooperation for spectrum sensing in cognitive radio networks," in *IEEE Journal of Selected Topics in Signal Processing*, vol. 2, no. 1, pp. 28–40, Feb. 2008.
- [154] L. Bixio, M. Ottonello, M. Raffetto, C. Regazzoni, and C. Armani, "A comparison among cooperative spectrum sensing approaches for cognitive radios," in *2nd International Workshop on Cognitive Information Processing (CIP), 2010*, pp. 168–173, June 2010.

List of Publications

Journals

- [1] J. W. H. van Bloem, R. Schiphorst, T. Kluwer, C. H. Slump. "Spectrum Utilization and Congestion of IEEE 802.11 Networks in the 2.4 GHz ISM Band," in *Journal of Green Engineering Special Issue on Cognitive Radio*, vol. 2, no. 4, July 2012.
- [2] J. W. H. van Bloem, R. Schiphorst, C. H. Slump. "Removing Non-Stationary Noise in Spectrum Sensing Using Matrix Factorization," in *EURASIP Journal on Advances in Signal Processing*, vol. 2013, April 2013.
- [3] J. W. H. van Bloem, S. Kawade, R. Schiphorst. "Collaborative Sensing to Enhance TV White-Space Database Performance in Shadow Fading Environments," *submitted*.

Book Chapters

- [4] J. W. H. van Bloem, S. Kawade. "Database-Assisted Collaborative Sensing," in *Quasar Deliverable 2.5*, chapter 3, July 2012.

Conference Proceedings

- [5] J. W. H. van Bloem, R. Schiphorst, T. Kluwer, C. H. Slump. "Interference Measurements in IEEE 802.11 Communication Links Due to different Types of Interference Sources," in *Proceedings of the 8th International Conference on Wireless Communications, Networking, and Mobile Computing (WiCOM'12)*, vol. 2, Sept. 2012.
- [6] J. W. H. van Bloem, A. J. Hendrikse, R. Schiphorst, and C. H. Slump. "An eigenvalue approach to enhance energy detection in a mobile spectrum monitoring network," in *5th IEEE International Conference on Signal Processing and Communication Systems*, pp. 346–351, Dec. 2011.
- [7] J. W. H. van Bloem, R. Schiphorst, and C. H. Slump. "Initial results of a new mobile spectrum occupancy monitoring network," in *17th IEEE Symposium on Communications and Vehicular Technology in the Benelux*, pp. 64–69, Nov. 2010.

- [8] J. W. H. van Bloem, R. J. Boucherie, J. Goseling, M. de Graaf, G. J. Heijenk, J. C. W. van Ommeren, R. Schiphorst. "Effective Scheduling for Coded Distributed Storage in Wireless Sensor Networks," in: *Proceedings of the 31st Symposium on Information Theory in the Benelux*, May 2010.
- [9] J. W. H. van Bloem, R. J. Boucherie, J. Goseling, G. Heijenk, J. C. W. van Ommeren, R. Schiphorst. "Distributed Storage in Wireless Sensor Networks with Network Coding," in *Workshop on the Pervasive Application of Wireless Technologies*, Nov. 2009.
- [10] S. Kawade, J. W. H. van Bloem, V. S. Abhayawardhana, D. Wisely. "Sharing your Urban Residential WiFi (UR-WiFi)," in *63rd IEEE Vehicular Technology Conference, 2006. VTC 2006-Spring*, pp. 162–166, May. 2006.

Press Releases

- [11] University of Twente, "Research at the university of Twente: Wi-Fi will soon reach its limits," Press Release, June 8 2012, http://www.utwente.nl/en/archive/2012/06/research_at_the_university_of_twente_wi-fi_will_soon_reach_its_limits.doc.

Reports

- [12] J. W. H. van Bloem, S. Kawade, R. Schiphorst. "Collaborative Sensing and Data fusion approach for CR systems (phase 2)," in *Technical Report COST-STSM-IC0905-9942, European Union COST-TERRA*, April. 2012.
- [13] J. W. H. van Bloem, S. Kawade, R. Schiphorst. "Collaborative Sensing and Data fusion approach for CR systems (phase 1)," in *Technical Report COST-STSM-IC0905-9121, European Union COST-TERRA*, Jan. 2012.
- [14] J. W. H. van Bloem, R. Schiphorst. "Measuring the service level in the 2.4 GHz ISM band," in: *Technical Report TR-CTIT-11-27, Centre for Telematics and Information Technology, University of Twente, Enschede*, Dec. 2011, ISSN 1381-3625.

Acronyms

ACI Adjacent Channel Interference

ACK Acknowledgment

AFH Adaptive Frequency Hopping

ADC Analog-to-Digital Converter

A/D Analogue-to-Digital

AGC Automatic Gain Control

AIFS Arbitration Interframe Space

AP Access Point

API Application Programming Interface

A/V Audio/Video

AWGN Additive White Gaussian Noise

BC Back-off Counter

BT British Telecommunications

CAGR Combined Annual Growth Rate

CCA Clear Channel Assessment

CCI Co-Channel Interference

CDF Cumulative Density Function

CDR Constant Detection Rate

CFAR Constant False Alarm Rate

CMOS Complementary Metal Oxide Semiconductor

CR Cognitive Radio

CSMA Carrier Sense Multiple Access

CSMA/CA Carrier Sense Multiple Access with Collision Avoidance

CTS Clear to Send

CW Contention Window

DCF Distributed Coordination Function

DFS Dynamic Frequency Selection

DCS Dynamic Channel Selection

DIFS DCF Interframe Space

DME Distance Measuring Equipment

DSA Dynamic Spectrum Access

DSO Digital Switch Over

DTT Digital Terrestrial TV

DVD Digital Versatile Disc

EDCA Enhanced Distributed Channel Access

EDCF Enhanced Distributed Coordination Function

ERP Effective Radiated Power

FCC Federal Communications Commission

FHSS Frequency Hopping Spread Spectrum

FTP File Transfer Protocol

GPS Global Positioning System

GSM Global System for Mobile communications

GUI Graphical User Interface

HC Hybrid Controller

IEEE Institute of Electrical and Electronics Engineers

ITS Intelligent Transportation Systems

IF Intermediate Frequency

ITS Intelligent Transportation Systems

ITU International Telecommunication Union

ITU-R ITU Radiocommunication sector

KL Kullback-Leibler

ISM Industrial, Scientific and Medical

LTE Long Term Evolution

MAC Medium Access Control
MIMO Multiple Input Multiple Output
MWF Multi-Wall-Floor
NMF Non-negative Matrix Factorization
Ofcom the Office of communications
OFDM Orthogonal Frequency Division Multiplexing
OSI Open System Interconnection
PC Power Control
PCA Principal Component Analysis
PCF Point Coordination Function
PDA Personal Digital Assistant
PDF Probability Density Function
PER Packet Error Rate
PHY PHYsical Layer
RTS Request To Send
RF Radio Frequency
QoS Quality of Service
ROC Receiver Operating Characteristics
SAS Signals and Systems
SIFS Short Interframe Space
SVD Singular Value Decomposition
SJR Signal-to-Jammer Ratio
SNR Signal-to-Noise Ratio
TCP Transmission Control Protocol
TDMA Time Division Multiple Access
TG2 Task Group 2
TXOP Transmission Opportunity
TV TeleVision
TVWS TV White Space
UDP User Datagram Protocol

UHF Ultra High Frequency

UMTS Universal Mobile Telecommunications System

UK United Kingdom

UR-WiFi URban Wi-Fi

USB Universal Serial Bus

VCR Video Cassette Recorder

VGA Variable Gain Amplifier

VHF Very High Frequency

WLAN Wireless Local Area Network

WSD White Space Device

Acknowledgments

First I would like to thank my promotor professor Kees Slump for giving me the opportunity to conduct my PhD research at the Signals and Systems group. I am grateful for the pleasant understanding, encouragements and for the support on the research.

In particular I would like to express my gratitude to my daily supervisor Roel Schiphorst who always found time to give support and advise in a friendly atmosphere and without whom this research could not have been carried out. I am very thankful for his help, insights and guidance on the research content but also for his commitment in setting up and arranging projects in favor of my PhD work.

I am also very grateful to Santosh Kawade for arranging my stay in the United Kingdom at British Telecom and for being a very good host. It has been a pleasant collaboration and I owe him many thanks for providing me this opportunity and for his research vision and support.

I also would like to thank the members of the graduation committee, prof.dr.ir. A.J. Moutaah, dr.ir. M. Nekovee, prof.dr.ir. P.J.M. Havinga, prof.dr.ir. S.M. Heemstra de Groot, prof.dr.ir. B. Nauta, and prof.dr.ir. G.J.M. Smit for reading and evaluating this dissertation. In addition, I would like to thank my (former) colleagues at the University of Twente for the pleasant collaboration and the fruitful discussions. Especially my thanks go to Anne Hendrikse for his valuable suggestions on the research, to Sandra Westhoff for the administrative support, and to Geert-Jan Laanstra and Henny Kuipers for the technical assistance. Also thanks to Loek Colussi, Taco Kluwer, Helmut Leonhard and Ben Witvliet from Agentschap Telecom for the support on the research.

I also would like to express my gratitude to my colleagues at British Telecom, Colin Harold and Andrew Garrett for their support on the field experiments and to Keith Briggs for his research insights. Besides, I would like to kindly acknowledge the funding support from the European Union COST-TERRA projects accommodating my visit in the United Kingdom.

Next, I am happy to thank all my friends that were around in Enschede, Raalte and Ipswich, and in particular Arjan Schutte who I know since high school.

However, nothing would have been possible without the constant support from my family. Especially I would like to thank my father Wim and mother Ellie, my sister Marjolein and her friend Jos Boeije, and my brothers Matthijs and Maarten for their unconditional support, inspiration, believe and committed help.

*Jan-Willem van Bloem
Enschede, April 2013*

Curriculum Vitae

Personalialia

Fullname	Johan Willem Hermanus van Bloem
Date of Birth	29 December, 1982
Place of Birth	Almelo, the Netherlands
Gender	Male

Profile

Jan-Willem van Bloem has received his M.Sc. in Electrical Engineering from the University of Twente in 2007. He participated in the BT-FON project from October 2005 till February 2006 at British Telecom (UK) during his internship. From 2008 till July 2010 he worked as a researcher in a multidisciplinary project on coding and wireless sensor networks at the University of Twente. From July 2010 onwards he followed a PhD trajectory at the Signals and Systems Group of the University of Twente. As part of this trajectory he conducted research commissioned by the Radio Communication Agency Netherlands to investigate the quality of service of technologies in the ISM band and the GSM band. Also as part of this trajectory he was employed as researcher at British Telecom from October 2011 till May 2012 to work on white-space database assisted collaborative sensing in the TV bands. In addition, he worked on a part-time basis as R&D engineer for Bluemark Innovations from April 2011 till October 2011.